University of Southampton

The effect of posture on the regional deposition of an inhaled aerosol

Matthew James Quint, Grad Dip Phys, MCSP

Thesis submitted for the degree of Master of Philosophy

School of Health Professions and Rehabilitation Sciences,
Faculty of Medicine and Biological Sciences

October 2003

University of Southampton

Abstract

School of Health Professions and Rehabilitation Sciences,
Faculty of Medicine and Biological Sciences

Master of Philosophy

The effect of posture on the regional deposition of an inhaled aerosol

by
Matthew James Quint

Inhaled drugs continue to provide the foundation for treating airways disease in acute and chronic conditions, allowing the delivery of active agents directly to the site of the disease with minimal systemic absorption. The role of particle size and respiratory manoeuvre on deposition are appreciated but the impact that posture may have is not. Current understanding of respiratory physiology states changes in posture result in the ventilation gradients within the lung. This thinking is based on two-dimensional (2D) imaging which has the obvious limitation of projecting a three-dimensional (3D) structure in 2D. In recent years these restrictions have been overcome, particularly in the field of aerosol science, with the use of Single Photon Emission Computed Tomography (SPECT). This provides 3D information on the distribution of the isotopes and is aligned with the anatomical structures using Magnetic Resonance Imaging (MRI). From this background the hypothesis that the position in which an individual inhales an aerosol has an effect on its regional deposition within the lung was formulated. To test this, ten healthy subjects were recruited to a randomised, cross over, clinical trail. Each individual inhaled a nebulised suspension of human serum albumin (HSA) radiolabelled with ^{99m}Tc on three separate occasions in three different positions (sitting, supine lying and right side lying). The aerosol was delivered in a controlled manner using a closed nebuliser circuit that regulated the subjects' respiratory pattern. The total and regional pulmonary deposition of the aerosol was assessed using planar 2D imaging and SPECT aligned with MRI. Both data sets demonstrated that posture had a significant effect on the regional deposition of an inhaled aerosol. The SPECT data set was analysed in terms of the central to peripheral distribution in a series of shells and in terms of the lung segments. The anatomical model highlighted uneven distribution of the aerosol within the lungs that changed dramatically with posture. This may have implications for the delivery of drugs to the lung.

Acknowledgements

There are many people without whom I would have never completed this work. Both of my supervisors, Joy Conway and Tony Postle have provided me with much inspiration and guidance over the duration of this study. They have nurtured, nagged, cajoled, comforted and pushed with the sole aim of making me realise what I could achieve.

John Fleming and Livia Bolt have not only acted as consultant physicists but also provided excellent sounding boards for some of my more obscure thoughts!

The Radiology staff of Nuclear Medicine department, Julian Williams in particular, have been invaluable in assisting with the imaging. Without them there would be no images to look at.

The departments of Physiotherapy and Respiratory Medicine at Portsmouth need to be thanked for releasing me to complete this work.

This work has been dependant on funding from the Physiotherapy Research Foundation. Thanks need to go to Profile Human Systems for advice and the use of equipment.

For Carol my wife and my strength,

For Thomas my son and joy,

For Charlotte my daughter and hope for the future.

It's a long way to the top.....

(Young & Young 1976)

Chapter 1

The Interaction of aerosols with the lung.

1.0 Introduction

Inhaled drugs continue to provide the foundation for the treatment of airways disease in acute and chronic conditions. The use of this route for administrations gives the ability to deliver active agents directly to the site of the disease with minimal systemic absorption. A rapid clinical response can be achieved as the barriers to bioavailability, such as poor gastrointestinal absorption and metabolism by the liver, can be bypassed. However, a lack of understanding of the mechanisms underlying the deposition of inhaled agents results in an unclear or inconsistent dose and delivery to the lung.

It is accepted that only 5 - 20% of an aerosolised drug will reach the lungs [1] but there is no clear understanding of how it is distributed throughout the lungs. The regional distribution has been investigated by a variety of techniques to compare the central to peripheral regions, but this approach assumes that the lung has a uniform structure from bronchus to alveolus. There is minimal work published which investigates the distribution of inhaled agents on a lobar or segmental basis.

There remains considerable debate as to whether peripheral as opposed to central deposition of a drug increases its efficacy. To a degree this is dependent on the agent to be delivered. Clearly in diseases of the alveoli and terminal airways it is an advantage to deposit the drug peripherally. For example Alpha-1 Antitrypsin would be targeted towards the alveolar region [2] but with other inhaled agents, bronchodilators for example, there remains some ambiguity over the location of receptor sites within the lungs. This has implications for the drug delivery.

The study of particle deposition in the lung has largely been restricted to inhaled radio-aerosol combined with two-dimensional (2D) imaging via static gamma cameras. This is still considered the "gold standard" for assessment of intra-pulmonary aerosol deposition. Two-dimensional imaging is quick with acquisition times

of 30-100 seconds. This is a great advantage as it minimises the errors that may occur as a result of mucocillary clearance or absorption and will also reduce any movement artefact. Attenuation correction can normally be achieved in the same visit with the use of a one of four techniques.

- Body thickness: is based upon the measurements of the thickness and a number of assumptions about how different tissues attenuate gamma-rays.
- Transmission scanning: involves measuring transmitted radiation through the area under investigation.
- Perfusion technique: injection of a known amount of radiopharmaceutical that becomes lodged in the capillaries of the lung.
- Sealed source: a source containing a known amount of activity held in the mouth. [3]

While some of these procedures will mean additional exposure to ionising radiation, the dose remains comparatively low. So this technique is quick and relatively inexpensive using a low dose of radiation. It has well validated attenuation correction, and generates reproducable results. Indeed much of the current understanding of particle behaviour within the airways is based on 2D imaging. As such, the value of three-dimensional (3D) imaging has been questioned. For many research questions it is an entirely valid view.

The major weakness of gamma camera imaging is the poor airway and parenchymal resolution [4]. Two Dimensional imaging can give the total deposition within the lung and provide some indication of the gross distribution of the aerosol by the application of regions of interest to the images acquired. But it is inevitable some of the activity that appears in the "central" zone will in fact be in the peripheral lung. A crude example of the lack of discrimination of this approach is demonstrated in figure 1.0. The first image

(1.0a) is of a posterior to anterior chest x-ray (essentially a planar view) of a gentleman with a 9mm gunshot round in his chest. The second image (1.0b) has had regions of interest applied to define central and peripheral regions of the lung with the round on the border of the central zone. The final image (1.0c) is a lateral view, which demonstrates that the round was, in fact, just beneath the skin between the scapulae and not within the thorax at all. This underlines that a 2D projection of a 3D structure does not allow accurate discrimination of the areas within the thorax.

To gain a more valid indication of the regional (i.e. central to peripheral) or geographical distribution of the aerosol (namely consistent with the lung architecture of lobes and segments) would require a 3D technique.

The recent advent of 3D techniques such as Single Photon Emission Computed Tomography aligned with Magnetic Resonance Imaging or Positron Emission Tomography resolve this problem. These techniques are not widely used, as the image acquisition and analysis is more time consuming and complex than simple 2D imaging. It has been suggested that while 3D techniques theoretically provide improved image resolution, suitable images could be obtained by the more simple 2D techniques for total dose and response to pharmacological agents, mucocillary clearance and large airway behaviour [4]. However, the same author goes on to suggest that the value of 3D techniques will be in imaging the lung parenchyma and small airways. As such, with the advent of these novel imaging techniques, the opportunity now exists to improve our understanding of the regional deposition of inhaled particles, distinguishing central versus peripheral deposition and identifying the distribution to specific lobes or segments.

While both SPECT and PET can provide can provide multiplanar (coronal, transaxial and sagital) information there are considerable differences between the two techniques. SPECT uses multiple head gamma cameras and so is reliant on gamma emitting radioisotopes such as ^{99m}Tc in the form of pertechnate that are

associated with the delivered formulation rather than incorporated directly into it. Therefore with comparatively long imaging times, there is the potential for a disassociation of the two resulting in an error in the measurement of drug deposition [5].

Figure 1.0

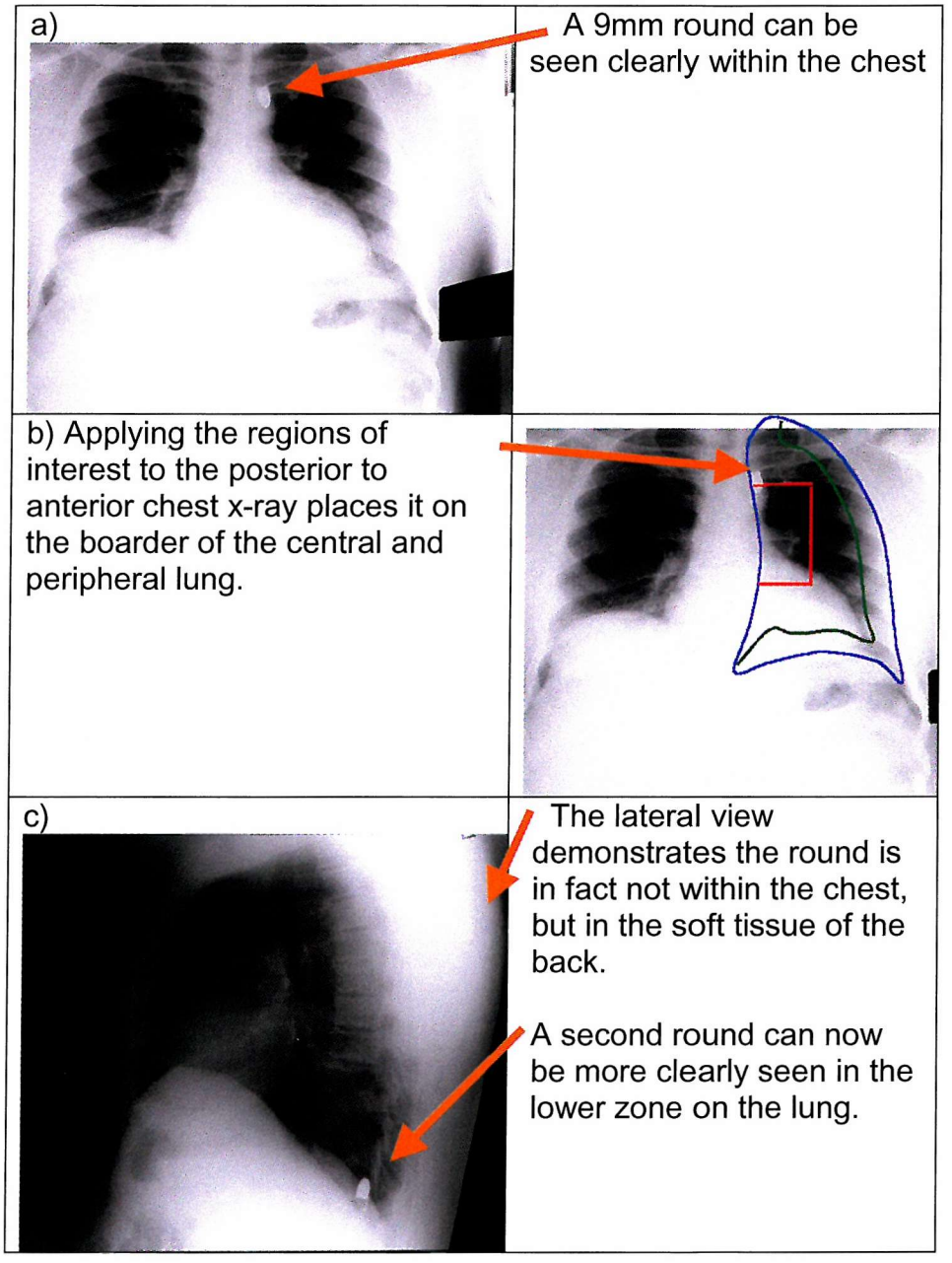

In contrast, PET uses positron-emitting isotopes (^{18}Florine or ^{11}Carbon in the case of aerosol deposition) that are directly incorporated into the molecule to be studied. The technique relies on the coincidence detection of gamma rays of a specific energy

that result from the annihilation of the positron with its antiparticle, the negatively charged electron. A scanners consisting of multiple rings of detectors are used to detect gamma rays emitted from within the subject. This measurement defines the line along which the event occurred and thus the location of the labelled molecule [5]. PET provides greater spatial resolution than SPECT and attenuation correction that can be achieved by the use of a PET transmission scan, rather than an additional MRI scan [6]. While these advantages make it an attractive option, unfortunately, it is not a simple procedure. Incorporating the PET radioisotopes into the compound to be delivered involves complex radiopharmacy and quality control. The personnel with these skills are not widely available. In addition, a cyclotron is required to generate the isotope, as is specific imaging equipment. Due to the short half-life of the isotopes generated, ideally these should be located in close proximity and are not widely available primarily due to cost. Therefore in this study, the simplicity of the radiolabelling techniques and availability of gamma cameras made SPECT a more viable option than PET.

The object of this thesis is to investigate one aspect of aerosol deposition, namely the effect of changes in body position in healthy subjects, on the regional distribution of the inhaled aerosol. This requires an understanding of lung anatomy and physiology in addition to some insight to aerosol behaviour and the limitations of the imaging techniques used.

1.1.1 Use of positioning as a treatment

The use of changes in body position as a treatment for lung disease is well established as a simple intervention, which can have effects on both physiological and pathological processes. One of the earliest examples results from an understanding of the structure of the large airways, which has been used to formulate positions that can assist the drainage of excess secretions from the specific

lobes or segments of the lung [7] [8]. More recently posture has been used to improve lung volume, in particular post operatively, where volume is reduced by anaesthetic and pain [9]. This approach manipulates the distribution of ventilation and perfusion throughout the lungs, which is not distributed evenly and is influenced by gravity. For example, in the normal erect adult both ventilation and perfusion are preferentially distributed to the lower zones on the lung. The engorged lower zones of the lung are heavier and this increased weight generates a vertical pressure gradient via the pleura, with more negative pleural pressure at the apex of the lung. This pressure gradient will, in turn mean that the apical sections of the lung are more distended than the lower zones and will have a higher volume but a lower compliance. That is to say that the lung tissue will be "stiffer".

Lung compliance is the relationship between lung volume and airway pressure. This relationship can be plotted on a curve (see Fig 1.1.1). Those lung units at the apex with the higher volume will be on the flatter upper portion of the curve and for a given change in pressure will have a much smaller change in volume. Conversely, those lung units towards the base of the lung will be on the steeper portion of the curve and will have much larger changes in volume for the same change in pressure. Therefore, there will be more change in volume at the base and so more ventilation. A change in posture will change this gradient and thus the ventilation within the lung.

The preferential ventilation of the dependent zones does not always occur in the young, elderly or obese as a result of the reduced recoil of the chest wall. In these groups the upper zones of the lung lie on the steep portion of the compliance curve and as such are better ventilated. This was demonstrated by Hurewitz *et al* [10]. In a small group, they found, as expected, in normal subjects increased ventilation in dependent lung units but in a group of obese subjects the upper zones received better ventilation

Figure 1.1.1

The pressure volume or Compliance curve

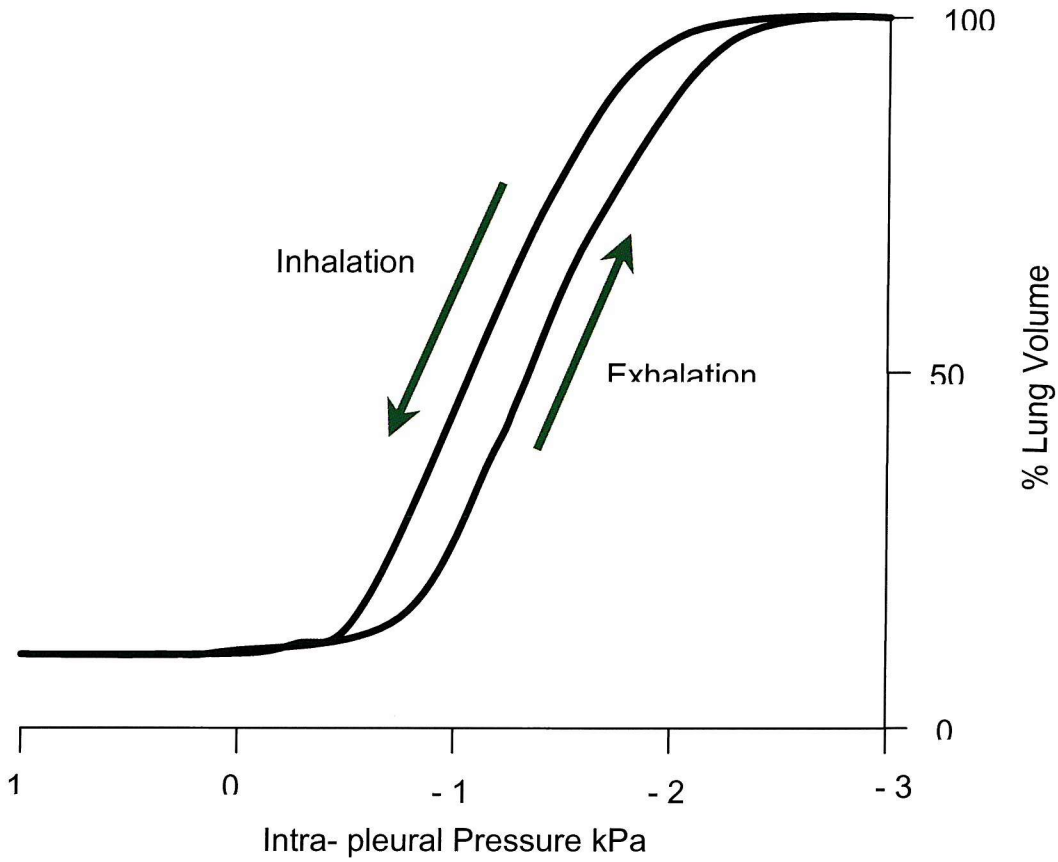

The effect of gravity is not restricted to compliance. Structures inside and around the thorax will move with changes of posture and compress different sections of the lung. Figure 1.1.2 illustrates this process. It consists of two coronal cuts taken from a high-resolution computer tomography (CT) study of a male patient. Both cuts were taken at the same anatomical level but in slice (a) the patient was positioned supine and in slice (b) he was prone. A comparison between the two slices shows the structures within the mediastinum, shifting posteriorly in the supine position, compressing the posterior lung units, whereas in the prone position those same structures are resting against the anterior chest wall with the surrounding lung compressed.

Figure 1.1.2

Two slices from a high resolution CT of a patient taken at the same level in supine (a.) and prone (b.) positions.

a. Patient in a supine position

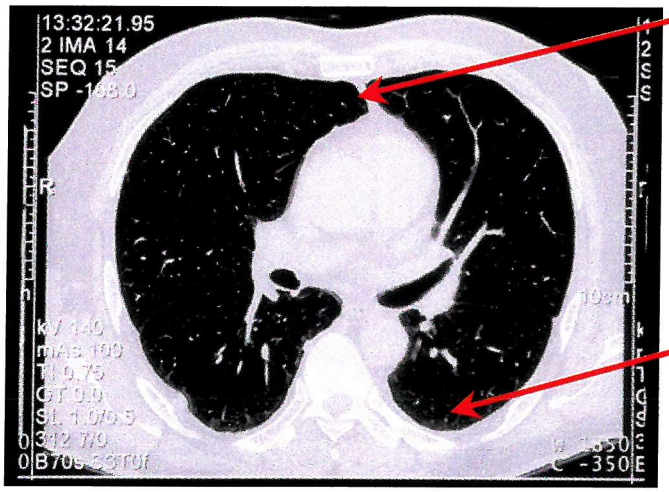

The heart has moved away from the anterior chest wall and surrounding lung tissue is not compressed.

Dependant areas of the lung are compressed by the weight of the lung and other structures above.

b. Patient in a prone position.

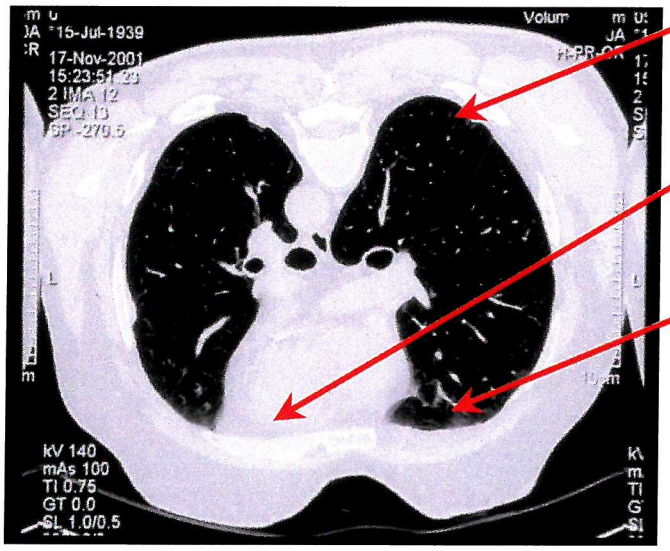

Previously compressed area of the lung is now open.

The heart is resting against the anterior chest wall.

The anterior region of the lung is now compressed.

The shifting of structures in and around the thorax has a direct effect on the muscles driving the respiratory pump, primarily the diaphragm, either by changing the loading on the muscles or their length. For example, in the supine position the abdominal contents will shift towards the head, increasing the resistance to contraction, whereas lying on one side will allow the viscera to shift forwards and unload the muscles. As the load on a relaxed muscle increases, so does its length. The force of contraction of skeletal

muscle is not uniform through its range. It is most efficient in mid-range and least efficient at the extremes of either full elongation or contraction. Therefore, the varying degrees of stretching of muscle fibres by shifting viscera will result in varying degrees of efficiency.

1.1.2 Importance of inhaled drugs

An understanding of factors which effect the distribution of the deposition of inhaled particles or aerosols within the lung is highly important in the field of inhalation toxicology in addition to medicine. Particle deposition experiments and modelling have shown that deposition is enhanced at airway bifurcation, relative to tubular airway segments [11] [12-15]. It has been suggested that this may contribute to pathology within the airways, which may be related to localized doses of irritants.

1.1.2.1 Drug delivery to the lung

There are three principal routes through which treatments can be delivered to the lungs; oral, injection, be it intra venous, muscular or sub-cutaneous and inhalation. Each has its own distinct advantages and disadvantages.

The oral route is safe, convenient and the most economical method. Unfortunately the absorption of the drug is dependent on a variety of unpredictable factors and therefore the onset of action is often slow. These factors include the ingestion of food, the rate of gastric emptying and breakdown of the drug by the action of digestive enzymes or the low pH in the stomach. Once absorbed by the gut the drug is then transported via the hepatic portal vein to the liver. The liver is the major organ of drug metabolism and as such a proportion of many drugs are likely to be broken down or excreted. This results in less drug being available for further systemic delivery, a process known as "First Pass Metabolism". To compensate for this a higher initial dose of drug is required.

Injection offers several advantages over the oral route. Absorption is quicker and more predictable as this route avoids the

variability of the gut with absorption directly into the systemic circulation. Its primary disadvantage is the need for specific training combined with sterile equipment and solutions. This is essential if the delivery is to be safe. Once injected there is no means of either slowing or stopping the absorption of the drug. As such, much care is required to avoid any adverse reactions. In addition patients also complain of pain and discomfort from repeated stabs.

The use of the inhaled route to deliver a therapeutic agent to the lungs results in the drug going directly to its site of action. This avoids first pass metabolism altogether and is therefore more efficient. Indeed, it has been shown that to achieve an equivalent anti-inflammatory effect of a dose of inhaled corticosteriod, eight times the dose would be required via the oral route [16]. This process is well demonstrated in the case of inhaled bronchodilators. These are normally effective at inhaled doses of only a few hundred micrograms with maximal effect occurring within 15 minutes and minimal side effects. These drugs are partially deactivated by the liver and so, if delivered via the oral route, higher doses will be required to achieve the same clinical effect.

1.1.2.2 The lung as a route for systemic drug delivery.

Over recent years developing technology has allowed the manufacture of a wide variety of bioengineered proteins such as hormones. These compounds have a relatively large molecular size and are easily metabolised by enzymes and cannot be administered via the oral route. As a result most proteins are delivered via injection. As has already been discussed, this route is not a simple one with some disadvantages, which can lead to low levels of patient compliance. Because of its large surface area, low level of enzyme activity and avoidance of first pass metabolism the inhaled route is increasingly being investigated as a portal for delivery of these proteins. The example of insulin illustrates the development of this approach well.

Insulin is widely used to control plasma glucose levels in patients with diabetes via a sub-cutaneous injection three times or more per day [17]. It has been demonstrated to remain biologically active after inhalation and has been successfully used to normalise plasma glucose levels [18]. While these are exciting developments, the pulmonary absorption of insulin is profoundly affected by its regional deposition within the lung (namely central versus peripheral) and there is limited understanding of its pharmacokinetics within the lung [19]. Therefore, more work needs to be completed before this can provide a viable alternative to subcutaneous injections.

1.2 Anatomy of the lungs

Having reviewed the rationale behind drug delivery to the lung and its use to deliver systemic drugs, it is necessary to review the anatomy of the lungs before moving on to consider the factors that influence the deposition of inhaled agents within the lung. The description which follows is intended to provide this and provide a background to the later sections of the thesis. For a full description, the reader is directed to standard anatomy texts. It is of note that within normal clinical practice, individuals are encouraged to inhale agents to be delivered to the lungs through their mouth. This approach was followed within the experimental design described later in this thesis with the subjects inhaling the aerosol through a mouthpiece while wearing a nose clip. As such there will be no description of the nasal anatomy.

1.2.1 Larynx

Once past the bend of the oropharynx, the first significant obstacle to the passage of an aerosol is the larynx. This is a structure composed of bone, muscle, cartilage and ligaments, which extends from the root of the tongue to the trachea. It has three roles; as an organ of phonation, a sphincter protecting the airway and a conduit for air into the respiratory tract. In the adult male, the

larynx is larger and lower than the female, located opposite the third to sixth cervical vertebrae.

The cavity of the larynx is divided into three sections by two pairs of mucous membranes. The upper pair are thick pink membranes called the *vestibular folds* or false vocal cords. These combine with the epiglottis and vocal cords in protection of the airway. The lower two are involved in the production of the voice and are known as *vocal folds* or vocal cords. These are sharp white layers of mucous membrane (see Fig. 1.2.1a). The fissure between these two pairs of folds is commonly referred to as the *glottis*.

During quiet respiration, the vocal folds form a triangular opening into the trachea with its apex on the anterior aspect and the base to the posterior. During a forced inspiratory manoeuvre, the opening will increase in size as the vocal folds are actively abducted whereas it will decrease to the point of closure during speech or swallowing on active adduction of the vocal folds. This narrowing of the airway does impact on the airflow into the lung, which will be described in section 1.4.1.

1.2.2 Upper / conducting airways

The large airways are a branching structure of tubes constructed from cartilage, smooth muscle and soft tissue membranes extending from the base of the larynx. The trachea descends down and divides at the carina into the left and right main stem bronchi (Fig1.2.1b.). These in turn, further divide into secondary bronchi (Fig1.2.1c.), each supplying a whole lobe and then tertiary bronchi, which supply bronchopulmonary segments. Weibel [20] published one of the more accepted detailed morphological studies of this structure. This symmetrical model consists of 23 dichotomous branches originating from the trachea with the first 16 branches forming the conducting airways (see Fig 1.2.2). Obviously, in life the bronchial tree is not symmetrical, and has branches of varying angles, lengths and diameters. This is well

demonstrated in Fig. 1.2.3, which is a photograph of a cast taken from the bronchial tree of a human cadaver. This asymmetry will influence gas mixing in the lung. Even taking these inconsistencies into account, this model is of some value in understanding the anatomy of the airways and will be referred to later on in this chapter.

The walls of the large airways are composed of 3 layers; the mucosa, the sub-mucosa and the adventitia. The mucosa in the trachea is ciliated pseudostratified columnar epithelium resting on a basement membrane. This progresses to a simple columnar ciliated epithelium further down the bronchial tree. The sub-mucosa, primarily located between the cartilaginous rings, contains seromucus glands and some fat cells. The adventitia contains incomplete rings of cartilage within the trachea and main stem bronchi. As the airway generations progress distally, these become plates of cartilage and reduce in number until they disappear in the bronchioles[21]. A fibrous membrane encloses the cartilage that also contains smooth non striated muscle fibres. These fibres are longitudinal and transverse in nature. Contraction of the transverse fibres can reduce the lumen of the airway and there is some evidence that can result in occlusion of the airway where there is less cartilage[21].

Figure 1.2.1

A series of photographs taken via flexible bronchoscopy. a, the larynx, b, the trachea and c, a segmental bronchus, in this case the right upper lobe.

a

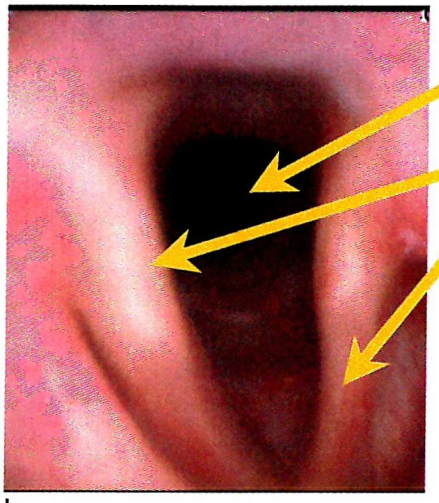

b

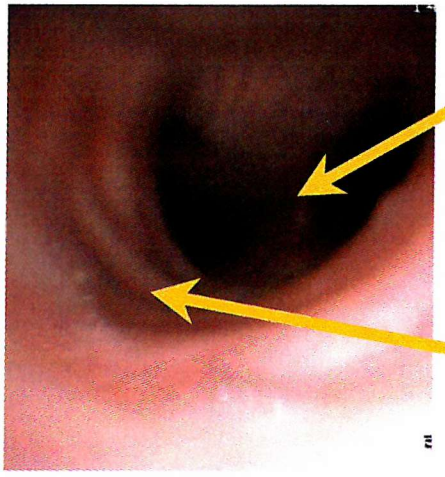

c

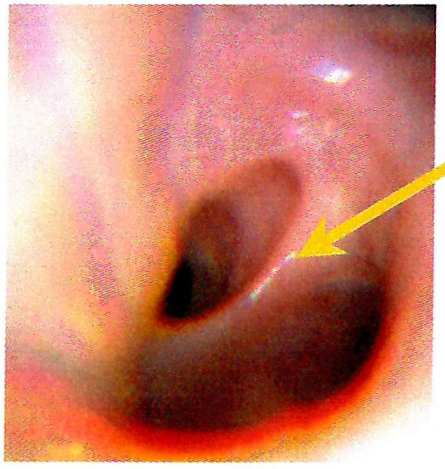

Figure 1.2.2

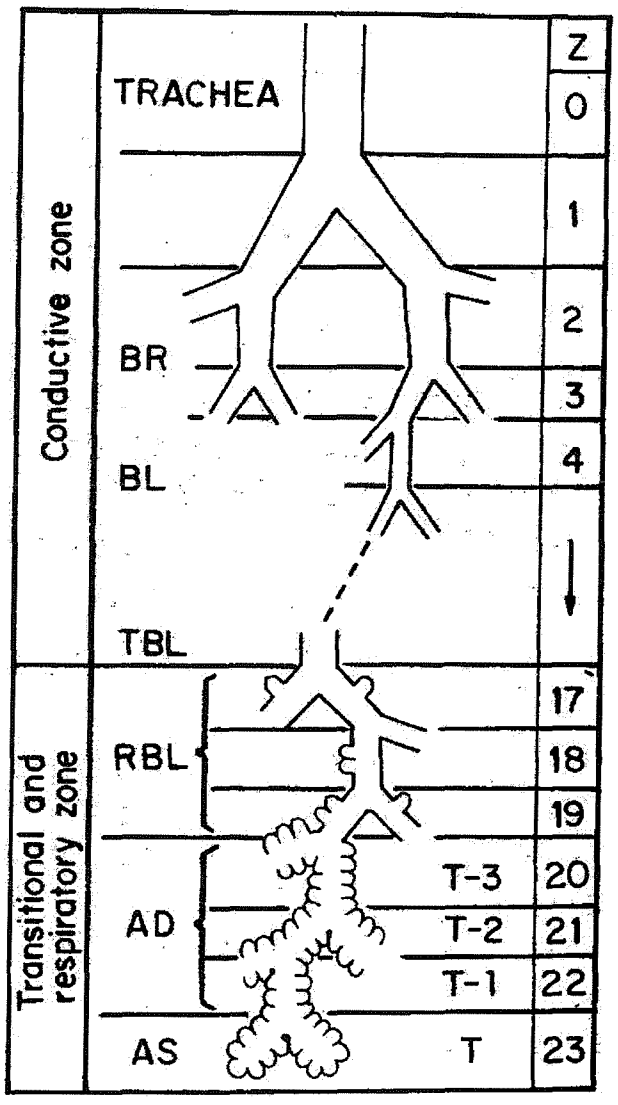

Model of airway branching, BR = bronchus; BL = bronchiole ; RBL = respiratory bronchiole; TBL = terminal bronchiole ; AD = alveolar duct ; AS = Alveolar Sac. Reproduced by permission from E.R. Weibel, In *Morphometry of the Human Lung.* Heidelberg, Springer- Verlag, 1963.

Figure 1.2.3

A photograph of a cast taken from the bronchial tree of a human cadaver lung. Each of the segments of the lung has coloured differently.

1.2.3 Lower airways

Further along the respiratory tract, the airways continue to divide until they are less than 1 mm in diameter. From this point

they are described as bronchioles. The epithelium also changes from ciliated columnar structure to a cubiodal nature. Within the walls of the airways, the cartilage disappears and the number of glands reduces and smooth muscle becomes the main feature of airway walls with some elastic fibres. The branching continues until terminal bronchioles divide into respiratory bronchioles. This marks the transition from the conducting airways to the gas exchanging portion of the lung.

1.2.4 Acinus

The Acinus is described as the terminal unit of the respiratory tract which extends from the terminal bronchiole and includes all air passages distil to this point. The terminal bronchioles further divide into respiratory bronchioles, which in turn give rise to alveolar ducts from which the alveolar sacs extend [22]

This thin walled epithelium is supported by connective tissue and is principally composed of a single layer of squamous cells called *type I pneumonocytes*. This can be as thin as 0.05 μm when combined with the basement membranes the normal barrier to diffusion in the human lung is 2.2 μm. In addition, rounded secretory cells or *type II pneumonocytes* are present. These produce a film of surfactant, which covers the surface of the acinus and the small airways. This material is widely accepted as being essential for normal alveolar expansion by reducing the surface tension.

While the alveolus with its rich blood supply may appear at first impression to be the principal gas exchange unit there is evidence to suggest that the acinus is in fact the functional unit. Different rates of gas filling in the acinus have been demonstrated to result in additional gas mixing beyond the terminal bronchioles [23].

1.3 Clearance mechanisms

The anatomy and physiology of the bronchial tree provides a significant barrier to particulates. It is this barrier, which, in health

protects the respiratory tract that provides a challenge to overcome when delivering an active agent to the lungs.

The gross anatomy as described in section 1.2 has a significant effect on airflow. The mechanisms involved in this process are described in more detail in section 1.5. In short, the turbulence generated by the divisions of the airways results in a marked impaction of the particulates on the airway walls and the increase in the cross-sectional more peripherally reduces the velocity of the airflow.

Within the large airways there are two principal defence mechanisms; cough and mucocilary clearance. A cough is the result of a forced expiratory manoeuvre producing a shearing stress on the mucus sheet, after a deep breath in and the build up of pressure against a closed glottis followed by a sharp release. It is relatively inefficient mechanism and only clears the central airways down to the sixth or seventh generation [24].

Mucocilary clearance is the result of the coordinated beating of a ciliated epithelium, which propels mucus and any trapped particles up the bronchial tree towards the epiglottis. Each ciliated cell has a diameter of 5μm and is covered with around 200 cilia. These are finger like projections of 5-6μm in length, tipped with three to seven short claws [25]. In health they are bathed in a low viscosity fluid or pericilary layer, which is slightly less deep than the extended length of a cilia. Above this layer lies a layer of high viscosity mucus. The coordinated beat of the cilia pushes the mucus layer forward. This action is slowest in the small airways (approximately 0.01 mm/min) and fastest in the trachea (approximately 1 cm/min [26]). Figure 1.3 shows a section of healthy trachea with its ciliated epithelium and mucus layer.

Figure 1.3

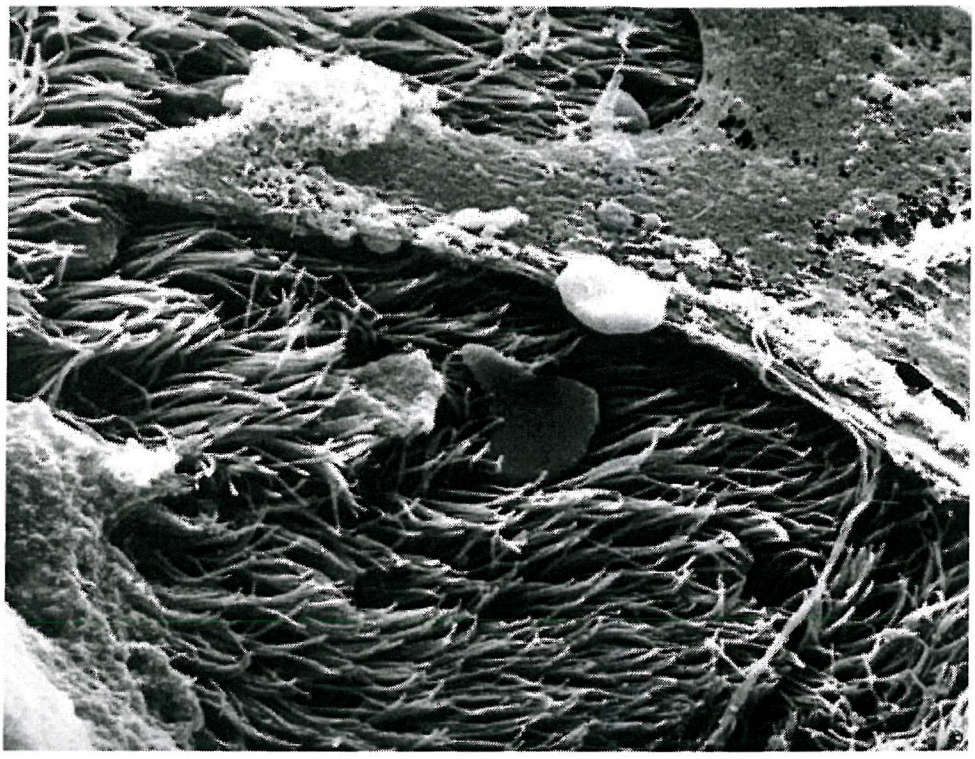

In the alveolar region, the majority of inhaled particles are cleared by macrophages through the process of phagocytosis. The macrophages then either transport the particles to ciliated airways to be cleared or into the alveolar interstitial space and on into the lymphatic system to be cleared from the lung.

1.4 Air flow

Air is transported down to the terminal bronchioles (generation 16) by bulk flow. After this point the velocity of the air becomes very small due to the exponential increase in airway cross-sectional area and movement of the air occurs by diffusion.

For air to be transported through the bronchial tree it must overcome the resistance offered by the pulmonary system, of which airway resistance is a key component. The relationship between airflow and airway resistance is not simple and therefore difficult to predict. To a large extent, it is due to complex airflow patterns of turbulent through to laminar airflow. It is the turbulent flow, which provides the most resistance. Laminar flow is streamlined and straight. This is the flow one would expect through a straight,

circular tube with no surface irregularities. Whereas turbulent flow is characterised by random velocity fluctuations and the formation of local eddies. The generation of turbulence is dependent on the relationship between the size of the airway, the viscosity and velocity of the air. This is the Reynolds number (Re) and can be calculated for an individual airway:

Equation 1

$$Re = 2rvd/n$$

Where d=density, v = average velocity, r = radius, n = viscosity.

Airflow will be laminar where the Re is less than 2000, turbulent where the Re is greater than 4000 and transitional at values between 2000 and 4000. Therefore, turbulence is most likely to occur when the gas velocity is high and the diameter is large such as in the generations 1-8 during maximal ventilation and is less likely in the small airways with lower flow rates [27].

1.4.1 Air flow through the larynx

As described in section1.2.1, the larynx forms a narrowed opening to the trachea. As the air negotiates the constriction of the glottis, it is accelerated in to a jet of gas. This will cause turbulent flow on the boundaries of that jet, resulting in mixing of gases and resistance to flow [28]. It should be noted that the laryngeal aperture varies in size throughout the respiratory cycle, in response to the flow rate of gases and depending on the active modulation by the laryngeal muscles. As such the level of resistance it provides will also change.

1.4.2 Upper / conducting airways

The assumption in the Reynolds equation (Equation 1) is that the walls of the large airways are smooth and regular is incorrect in the human trachea. In reality the cartilaginous rings result in irregularities on the surface which will cause additional disruptions

and encourage turbulent flow will occur. In experiments on airway casts turbulent flow was demonstrated at Reynolds numbers as low as 500 [29].

1.4.3 Lower airways

Conventional thinking states that the movement of gas in the terminal airways is dependent on the maintenance of diffusion gradients between inspired air and the gas in contact with the alveolar wall. However, recent publications [30, 31] based on modelling have suggested that there may be additional mixing of gases by a "stretch and fold" mechanism as the result of alveolar wall motion.

1.4.4 Expiratory flow

So far there has been the assumption that the airflow within the lungs is unidirectional and in a steady state. These assumptions are clearly wrong as the pressure gradients and flow change twice in each cycle. Expiratory flow will result in a very different pattern of airflow, which results in the coming together of two airstreams as opposed to a single stream being divided.

While this area has not been well investigated it is thought that the oscillatory nature of the respiratory cycle does not have a significant effect on the pressure-flow relations in the lung but can have important effects on gas mixing [23, 32]. In addition there is some evidence to indicate that the cardiac cycle has some influence on the pattern of ventilation [33].

1.5 Aerosols and their properties

Having described the anatomy of the lungs and the pattern of airflow within the airways, an explanation of the nature of aerosols and their application to the lungs follows.

Figure 1.5

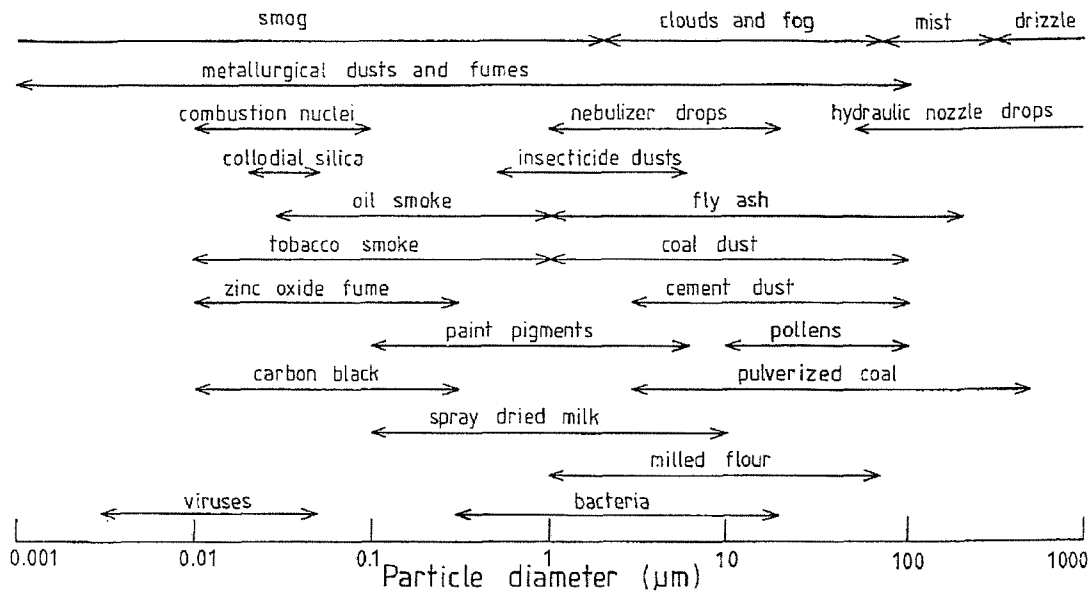

Particle size range for aerosols. Reproduced from I. Colbeck, *Introduction to Aerosol Science* In *Physical and Chemical Properties of Aerosols* 1998 [32]. with kind permission of Kluwer Academic

An aerosol is a dispersion of fine solid particles or liquid droplets in a gas. These are produced both in nature and by man intentionally and incidentally and have a wide range of particle sizes from 0.001μm to 100μm although 5 μm or less is the particle size used for drug delivery to the lungs. To illustrate this point, Figure 1.5 demonstrates a range of aerosol particle sizes from different sources [34].

It is very unusual for all the particles in an aerosol to be of the same size. This would be described as a *monodisperse* aerosol. A more normal situation would be a *heterodisperese* aerosol, containing a wide range of particle sizes. This presents a challenge of how to describe the size distribution. There can be discrepancies in the figures obtained according to whether distribution is plotted as the number of particles, or relative to their mass. Small particles may be very abundant but as mass is dependent on the cube of the

diameter, will only contribute a small proportion of the total mass [34]. As such, for the purpose of this thesis, the particles size distribution is based on the mass measurement. This distribution is not normal (Gaussian) and so is better described mathematically by a lognormal distribution. From this, the mass can then be plotted and the mass median aerodynamic diameter (MMAD) can be described i.e. the particle diameter above and below which 50% of the mass of the particles are distributed. The geometric standard deviation (GSD) can also be described. GSD is a dimensionless parameter, which is the ratio of the diameter at the 84^{th} or 16^{th} percentile to the MMAD [35]. Most therapeutic aerosols have a GSD greater than 1.2. A GSD of less than 1.2 would be a monodisperse aerosol.

1.5.1 Generation of aerosols for therapeutic delivery to the lungs.

There are a wide variety of methods to produce an aerosol for therapeutic delivery to the lungs. These can take the form of handheld devices such as dry powder inhalers (DPIs) or metered dose inhalers (MDIs). These are popular for use in the community, primarily because of their size and convenience. In the hospital setting nebulisation is frequently used to deliver liquid formulations. There are two categories of nebuliser, either ultrasonic or jet. More recently a variety of "novel liquid aerosol devices" have been developed. These new approaches or techniques to improve drug delivery are not currently in clinical use [36] and therefore will not be considered in this thesis, which will focus on the gas driven jet nebuliser.

Jet nebulisers use a high flow of gas forced through a small orifice known as a Venturi to generate an area of low pressure. This draws the fluid to be nebulised up a capillary tube where it is mixed with the gas to form an aerosol. Baffles remove larger droplets and the fluid is re-circulated back to the reservoir, while the smaller particles of a respirable range are carried forward in the

airstream to the patient. This process is demonstrated in Fig. 1.5.1. An aerosol generated in this manner is heterodisperese.

The output from a jet nebuliser is not uniform throughout the duration of the nebulisation process. Water evaporation will increase the concentration of the solution and reduce the temperature of the solution altering its viscosity vapour pressure and surface properties. This process will increase over time and affects the particle size generated. As the volume within the reservoir is reduced as a result of the nebulisation process the output is reduced up to a point where it can no longer be maintained. While the nebulisation process has been completed, there is likely to be some fluid remaining. This is termed as the residual volume and may be as much as 1 ml but will vary widely between different commercially available nebulisers, as will the particle size and total output [37, 38].

Figure 1.5.1

A schematic illustration of the working principals of a jet nebuliser in cross-section

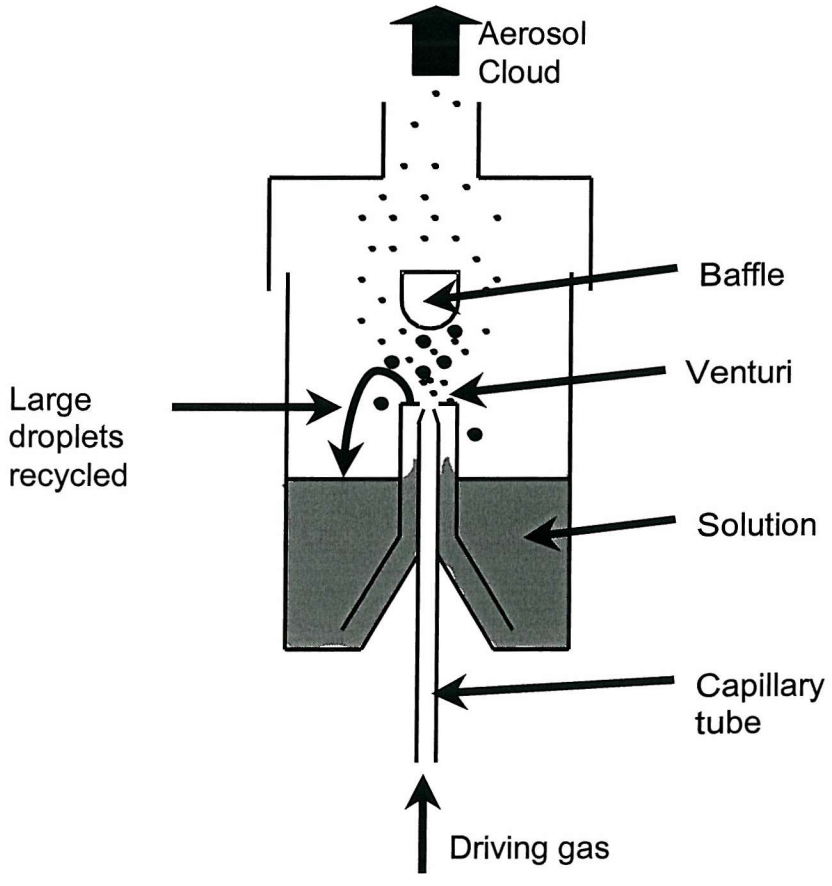

1.5.2 Physical processes controlling particle deposition in the lung

Having reviewed how aerosols are generated for delivery to the lung, the mechanisms that influence their deposition will now be discussed. There are three classes of variables that act upon an aerosol cloud to induce deposition within the airways. These are the characteristics of the aerosol, the ventilatory parameters and the morphology of the respiratory tract [39]. These variables need to be related to the mechanisms of inertial impaction, gravitational sedimentation and diffusion by which an aerosol will deposit within the airway.

1.5.3 Mechanisms of deposition

1.5.3.1 Inertial impaction

Impaction is a process that principally occurs in the oropharynx and at airway bifurcations. It is more important for larger particles (from 5 - 10μm [40]) and of the mechanisms described here, is responsible for the greatest deposition in terms of mass. This method of deposition relies on the inertia of the inhaled particle to carry it towards the wall of the airway when there is a change in the direction of airflow at the bifurcation or bend of the airway (see Fig 1.5.3). Stokes law is often applied to predict the likelihood of impaction of a given particle. This law states:

Equation 2

$$F=3\pi \eta v d$$

Where η = the viscosity of the air, v = the velocity of the particle, d = is the diameter of the particle

However, it is generally acknowledged that the prediction of impaction is complicated by other factors such as the differing flow resulting from airway geometry, turbulence and the presence of bronchoconstriction.

1.5.3.2 Gravitational sedimentation

As the smaller and slower moving particles travel into the lung, deposition can occur by gravitational sedimentation, i.e. the particles fall under the influence of gravity and sediment out onto the airway wall (see Fig 1.5.3). This generally occurs in the small and conducting airways and alveoli where the flow velocities are decreased and will be augmented by quiet breathing and breath-holding. During these breathing manoeuvres gravity has a greater chance of acting on the aerosol due to the increased residency time of the aerosol in the airways. The likelihood of this mechanism occurring therefore depends upon factors such as the velocity of the particle, the diameter of the airway and the angle of inclination with respect to the horizontal [41]. Particles greater than 0.5 μm are influenced by this mechanism.

1.5.3.3 Diffusion

Diffusion describes random motion due to interaction of the aerosol with air molecules (see Fig 1.5.3). This random motion encourages movement of aerosols from areas of high concentration along a diffusion gradient to areas of lower concentration in line with Fick's law [41]. This mechanism is of especial importance to small particles (smaller than 1.0 μm), which penetrate as far as the terminal bronchioles and alveolar region. Love and Muir [42] have suggested that a particle of between 0.5 and 1.0 μm inhaled with a tidal volume of 600 ml will penetrate to alveolar ducts but does not enter the alveoli other than by diffusion. This has recently been questioned in the literature [43, 44] with the suggestion that movement of the alveolar wall would also contribute to the deposition.

1.5.3.4 Other mechanisms

In addition to the mechanisms already described, interception and electrostatic forces can have an effect on an inhaled aerosol. Interception occurs when the physical diameter of a particle

exceeds that of the airway (see Fig 1.5.3). As therapeutic aerosols are significantly smaller than the diameters of the airways, this mechanism is not important.

Figure 1.5.3

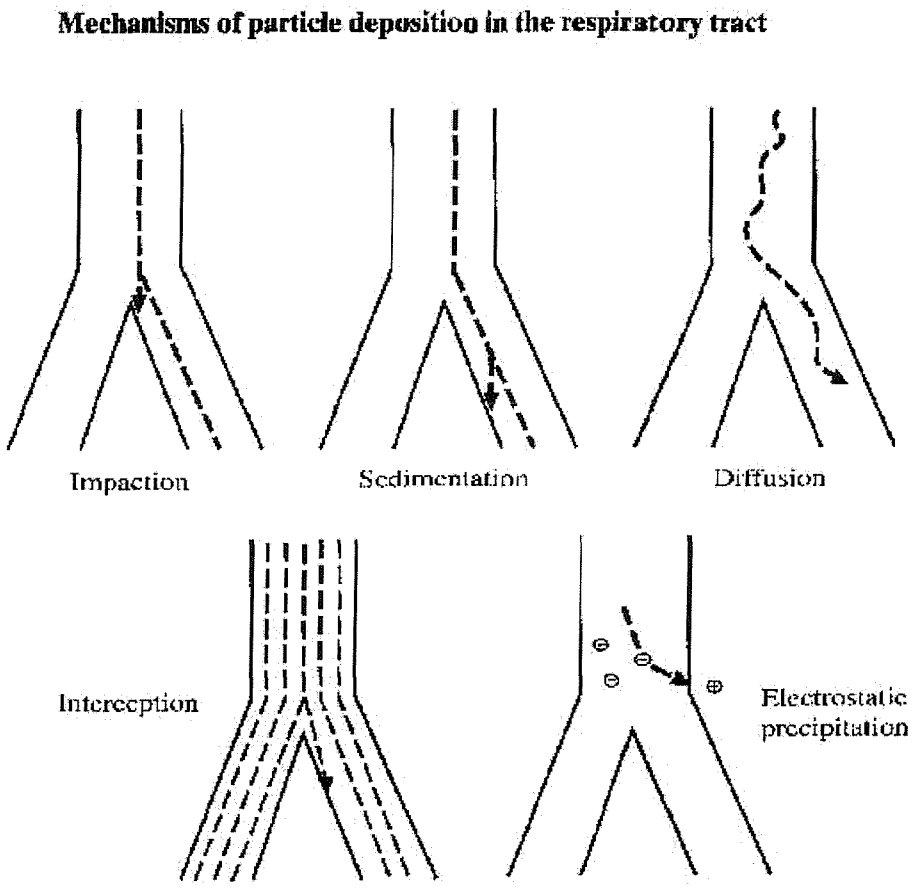

A schematic diagram to demonstrate the possible mechanisms of aerosol deposition within the airways. Reproduced by kind permission from Department of Committee on the Medical Effects of Air Pollutants, Non-Biological Particles And Health, HMSO 1995, [45]

A particle can possess an electrostatic charge, which may encourage its attraction to the wall of the airway (see Fig 1.5.3). This is only relevant to particles smaller than 1μm and is an important mechanism when aerosols are delivered via spacers or holding chambers when particles are attracted to the plastic walls of the spacer [46]. This can be clinically significant reducing the

amount of drug available to inhale but is not applicable to nebuliser delivery of aerosols.

1.5.4 Particle characteristics

1.5.4.1 Particle shape

The majority of the work cited thus far assumes that the particle inhaled is a smooth sphere. This is not always the case. Figure 1.5 demonstrates there are wide variety of aerosols from natural and industrial sources that have diverse shapes including fibres or complex aggregates composed of smaller particles. The irregular geometry and surface morphology of these particles can impact on their behaviour, requiring more complex analysis than is described in this thesis.

1.5.4.2 Particle size

Particle size is an important determinant of deposition of an aerosol within the lung. Inhaled particles below 5μm are generally described as being within the respirable range with larger particles impacting in the upper airway. A re-examination of Stokes law (from 1.5.3.1) reveals that one of the variables that will increase impaction of the particle is its diameter. It is also of note that momentum is a product of mass multiplied by velocity. Larger particles, assuming a similar density, will have a higher mass and therefore be more likely to deposit within the upper airways as a result of impaction and conversely the smaller particles with smaller mass are more likely to remain in the air stream to come under the influence of other mechanisms of deposition.

1.5.4.3 Hygroscopic growth

The term hygroscopic growth describes the increase in particle diameter that occurs as the result of association with water vapour [47]. The respiratory tract provides just such an environment. The nose and upper respiratory tract warm and humidify inspired air to

near body temperature and complete saturation by the time the air reaches the third airway generation [48]. If an aerosol is inhaled that is not a saturated droplet then it has the capacity to undergo hygroscopic growth, absorbing water from the respiratory tract until equilibrium is achieved [48]. Many pharmaceutical inhalation aerosols display hygroscopic behaviour in their passage through the airways, particularly aqueous aerosols. This increase in size can be significant, up to 4.5 times the original diameter with an obvious potential to effect the regional deposition within the lung [49]. The factors that determine hygroscopic growth are the temperature, humidity of the local environment, the osmolarity of the solute of the aerosol, the particle size, its residency time in the airway and cloud density [50]. An isotonic aerosol should remain stable throughout the respiratory tract whilst a hypertonic will take up water and grow but a hypotonic particle will lose water and shrink. Therefore an isotonic aerosol is preferable for drug delivery to the lung.

1.5.5 Breathing regime and velocity

The current recommendation is that nebulised drugs be delivered during normal tidal breathing to give optimum deposition [51]. In normal clinical practice, this is a sensible approach. There can be wide potential variations in the patient's respiratory pattern. Again, referring back to Stoke's Law one of the determinants of impaction was the velocity of the airflow. An increase in velocity would increase the impaction and therefore the central deposition. Conversely, a slower breath in will increase peripheral deposition. Anderson *et al* [52] demonstrated just this effect with healthy volunteers. As the inspiratory flow rate increased deposition in the oropharynx increased from 20% to 38%.

Slowing the inspiratory flow rate and increasing breath hold times will not only improve peripheral deposition by reducing impaction but will also aid sedimentation of the smaller particles in the peripheral lung. This results from the increased residency time

of the aerosol within the lung, increasing the likelihood of sedimentation occurring. Newman *et al* [53] found this to be the case with a group of patients with chronic lung disease inhaling from a Meter Dose Inhaler. A four second breath hold increased deposition in the alveolar region of the lungs.

It is of note that there is no current, accepted standard for the controlled delivery of radiolabelled aerosols to subjects. The consensus statement from the British Association for Lung Research suggests the use of a system ideally with visual feedback and also suggests the use of inductance plethysmography but suggests no specific system [3]. Within the literature, numerous systems have been developed. For example, Chan et al [50] investigated the regional deposition of hyper and hypotonic aerosols. This involved the subjects inhaling on two separate occasions in what was described as a "controlled manner". A total of four subjects were rejected from this study as they "could not control their breathing within the prescribed limits". This would suggest a system that imposed a rigid respiratory pattern on the subjects and did not reflect how they breathed normally. While they report the respiratory parameters of the subjects that showed that the variation within any one subject was within acceptable limits, it is unclear how this was achieved or whether FRC was taken into account. Brown *et al* [54], in a retrospective study, controlled subjects breathing pattern with a set tidal volume (0.5l) and rate (30 breaths / min). This approach does not reflect a normal respiratory pattern, nor does it address the issue of Functional Residual Capacity (FRC). O'Riordan [55], when investigating the deposition of pentamadine, had his subjects breath tidally for five minutes. This does reflect the clinical situation and allows for the variations between subjects but does not allow comparisons between visits, as this system did not record the respiratory pattern. In contrast, Chan *et al* [56] used a highly regulated respiratory pattern, breathing at a fixed tidal volume of 1l above FRC, with feedback provided for subjects to follow on an oscilloscope over the six

breaths of the delivery from a novel drug delivery system. While this breathing pattern, with a relatively large tidal volume does not reflect a normal breathing pattern, the subjects were given a practice session, thus reducing the effects of learning and FRC was considered. In part this variation in delivery systems is related to the different aims of the studies but with no accepted standard of delivery, it can make comparisons between studies difficult.

1.5.6 Anatomical influences

It has already been suggested that the architecture of the airways has an impact on the deposition of an aerosol with a particular increase associated with the bifurcations of airways. Any change in the airway morphology which effects airflow, be it as a result of disease or aging, will influence on the pattern of deposition.

Reduction of airway calibre as a result of bronchoconstriction in asthma has been shown to increase the deposition in the proximal airways relative to the peripheral [57, 58]. Yanai [59] demonstrated a similar process but with a more uneven pattern in patients with chronic obstructive pulmonary disease (COPD). This would be expected, as the changes bought about by the disease process will not be uniform throughout the lung, therefore there will be variation in the degree of airflow obstruction throughout the lung.

The presence of excess mucus is also likely to cause airflow obstruction and therefore have an effect on deposition. This process was investigated by Kim and Eldridge [60] using an in vitro airway model lined with various mucus simulants of differing rheological properties. They demonstrated an increase in deposition of 2-5 times in the mucus lined tubes compared to dry ones. The later *in vivo* work of Olseni *et al* [61] comparing the deposition pattern of healthy volunteers and patients with chronic bronchitis found an increase in the central deposition. This difference was in part attributed to the presence of mucus within the central airways.

After puberty there are differences in the thoracic anatomy of males and females. While the thorax of a male or a female of the same height will have the same vertical and lateral dimensions, the anterior to posterior dimensions will be smaller in the female. This results in smaller overall lung volumes. These differences produce different deposition patterns in males and females [62].

1.6.0 Perfusion

An understanding of pulmonary perfusion is of value in understanding the delivery of inhaled agents, particularly those that act systemically. As with ventilation, perfusion is effected by gravity. In the upright human lung the blood flow decreases from a maximum at the base to low levels in the apex. This gradient is affected by changes in posture and exercise. This raises the question of whether these changes in perfusion will have an influence on the pattern of deposition. On initial examination this statement is counterintuitive. A number of methods have been described within the literature that use a radiolabelled aerosol to provide the ventilation portion of a ventilation / perfusion (V/Q) scan [63, 64]. If perfusion were a key determinant of deposition this approach would be fundamentally flawed, as no mismatch of ventilation and perfusion would be found. This is not to say that there will be no effect from changes in perfusion. The distension of engorged blood vessels will contribute to changes in the compliance of lung tissue and therefore may have an influence on ventilation and deposition. Obviously this is an oversimplification of the interaction between ventilation and perfusion. A more detailed description is outside of the scope of this thesis. It is, however reasonable to assume that if an aerosol deposits in an area with poor perfusion it is less likely to be available to the systemic circulation. This statement is consistent with the findings of Laube *et al* [65] who demonstrated an improved response to inhaled insulin in type 2 diabetic patients when the aerosol was targeted towards the better perfused base of the lung.

1.7 Summary and the objectives of the thesis

The prediction of the regional intra-pulmonary deposition of an inhaled aerosol is influenced by a complex matrix of factors, which include the size of the inhaled particles, the presence of airflow obstruction and the respiratory manoeuvre of the patient or subject. The current understanding of the pattern of deposition of these inhaled agents is based on 2D, planar radioaerosol images, studies of the response to inhaled agents or indirect measures of particle retention. By far the majority of these studies have been performed in the upright position and no comparison has been made between different postures. As discussed earlier in this chapter, changes in posture can have an effect on both lung volumes and the pattern of ventilation. The hypothesis of this thesis was that the posture of an individual, at the time of inhalation of an aerosol, has an effect on the final destination of the aerosol within the lung.

The objective of this thesis was to apply the higher spatial resolution of 3D imaging techniques, namely SPECT aligned with MRI to a radioaerosol study of a group of subjects in different postures. It was hoped that this would allow the quantitative analysis of the regional intra-pulmonary deposition of an inhaled aerosol and allow a comparison between the postures used.

It was recognised that to achieve this would require collaboration with a group with an understanding of aerosol delivery, image acquisition and analysis. Such a group already exists in the form a partnership between the Department of Nuclear Medicine at Southampton University Hospitals NHS Trust and the Department of University Medicine in the University of Southampton. Therefore this work linked with this group.

To summarise, the objectives of this thesis are:

1. To assess the in vivo, three-dimensional (3D) intra-pulmonary regional deposition of an inhaled, radiolabelled aerosol using single photon emission computed tomography (SPECT) aligned with magnetic resonance imaging (MRI).
2. To establish if the intra-pulmonary deposition of an inhaled particle is affected by the postural position of a healthy subject.

Chapter 2 Methodology

2.1.0 Introduction

This chapter will provide an overview of the techniques used within the study. This includes a review of the reliability of the equipment used, the selection and screening of subjects prior to entry and finally the methods used to deliver the aerosol to the lungs and the imaging techniques used.

To test the hypothesis, a total of ten subjects were recruited and completed the imaging portion of the study. All were healthy male non-smokers aged between 22-38, who completed the screening as described in section 2.3 and gave their consent. They were entered into a three-limbed randomised crossover clinical trail, with each subject acting as their own control.

The subjects inhaled a nebulised suspension of radiolabelled Human Serum Albumin (HSA) on three separate occasions in three different positions in a random order. Only one position was used per visit and each subject took about four weeks to complete the study. The inhalation was carefully controlled using the system described in section 2.2. Technetium (^{99m}Tc) was used as a label as it is a gamma-emitter with a short half-life (6.04 hours). The positions used were; high sitting with hips and knees at 90°, supine lying with arms to the side and knees flexed for comfort, and right side lying with shoulder protracted for comfort and left knee flexed to 90°, supported by a pillow. Immediately after the inhalation of the radiolabelled HSA the subjects underwent a SPECT image acquisition. For this, the subjects were required to lie supine with both arms above their head for a period of sixteen minutes. The same position was used for the MRI scan. The protocols for all imaging are described in detail later in this section. Figure 2.0 demonstrates each subject's flow through the study.

This study was approved by the Joint Research Ethics Committee of Southampton University Hospitals NHS Trust and the Administration of Radioactive Substances Advisory Committee (ARSAC).

Figure 2.0

A flow diagram to summaries a subjects progress though the study

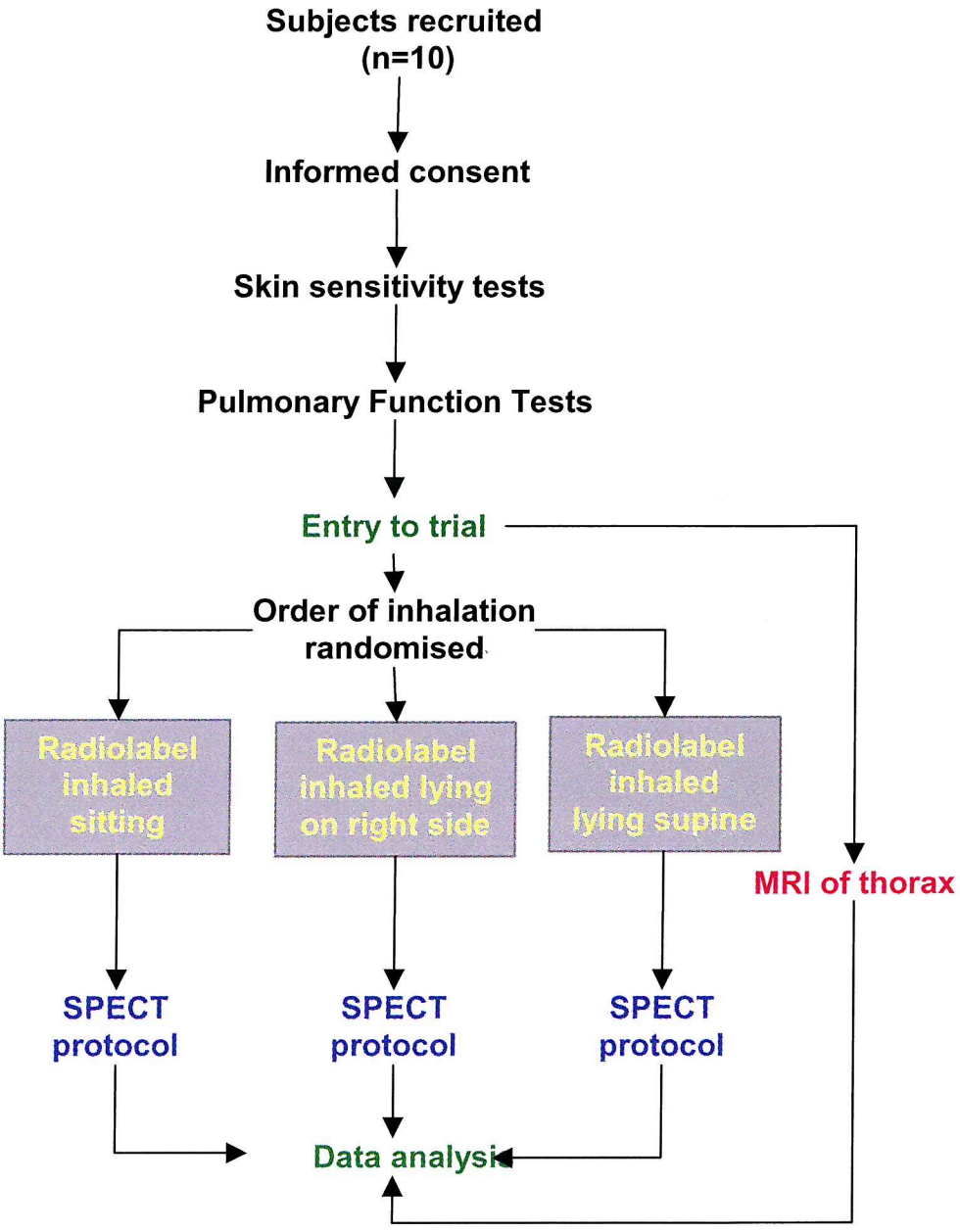

The main variables that dictate deposition in the lungs are the particle size, the respiratory manoeuvre and the presence of airflow obstruction. As such, these variables needed to be controlled.

When a wet aerosol is generated by a nebuliser, the particle size is determined by the equipment used. A smaller particle size has the advantage of giving deeper penetration into the peripheral airways. As such, the ideal nebuliser for this trial would be one that produced a small particle throughout the duration of the nebulisation, despite the addition of the HSA. These criteria were used to select the appropriate nebuliser.

A means to control the subject's respiratory pattern to allow a comparison between separate visits was developed in previous work [66]. This entailed breathing through a closed circuit, regulated by pneumotachographs attached to a computer, which worked well in the original study but required additional development to be appropriate to this study.

Exclusion of pathological airflow limitation was achieved by the use of strict entrance criteria. Only healthy male subjects with no history of airways disease or smoking were recruited. These individuals were screened by a battery of tests, which are described, prior to entry to the trial with limits placed on acceptability at screening and throughout the study.

It is recognised that there are differences in the deposition patterns of inhaled aerosols between men and women [62]. To avoid this only male subjects were used. In addition this eliminates any possibility of exposing a pregnant mother to ionising radiation. It is of note that breast tissue is particularly sensitive to radiation thus the use of male subjects minimises this additional risk. In addition, the nipples were used as soft tissue markers. These are more fixed in a male population and their use would have been viewed as unethical in a female population.

Only a small sample size was used in this study. The reasoning for this was two fold: one, it was anticipated that there

would be large differences in the deposition pattern between the postures, two: the minimum number of subjects should always be used to limit radiation dosage.

This chapter describes the development of the equipment to be used within the study and the subject's progress through the trial from recruitment to imaging.

In summary, this chapter is divided into four main sections.

- 2.2 describes the preparation work involved in establishing and validating the techniques to be used. This includes an overview of the lung function data collection used for the participants of the study.
- 2.3 describes the screening process used prior to entering subjects into the trial
- 2.4 describes the data collection and imaging that was used within the study
- 2.5 reports the techniques used to analyse to data obtained in 2.4.

2.2.0 Pre-clinical bench testing on the equipment.

Prior to starting any data collection it was necessary to characterise the equipment to be used within the trial, in order to ensure that it was adequate and appropriate for the purpose of the study. The areas addressed were as follows;

- Nebuliser output
- Pneumotachograph function
- Radiolabelling HSA
- Selection of activity levels for SPECT markers

2.2.1 Nebuliser output:

For the purposes of the imaging, which was to form the core of this trial, a precise dose of radioactivity was to be delivered to the lungs of the subjects. To achieve this, it was necessary to have an accurate understanding of the performance of the nebulising

equipment to be used as only a small amount of the dose of any agent instilled into the chamber of a nebuliser will actually reach the airways of the subject. Some of this will remain as a residue within the nebuliser, some will deposit in the upper airways and some will be lost to the atmosphere. These characteristics vary between different manufacturer's models and to a lesser degree the individual nebulisers

In this case the "Optimist" nebuliser (Medicaid Ltd, Pagham, West Sussex) was selected (Figure 2.1). This produces a small particle size of around 1.5- 2.5 μm which is likely to reach the small airways. It was also well known to the aerosol group having been characterised in detail previously [66]. As such it was felt that only a review of the particle size generated by the nebulisers was required to ensure consistent delivery.

There is some commercially available equipment that has been used to regulate the delivery of aerosols. Dosimeters have often been used for the controlled delivery of aerosols for airways challenges. Saari *et al* [67], used such equipment to good effect with a system that was patient triggered, displayed tidal volumes digitally and controlled flow rate by a flow indicator. This system did not, however, take FRC into account.

The Halolite (Profile Human Systems, Bognor, West Sussex UK), is a system that constantly monitors the respiratory pattern and adapts the delivery in response to any changes, only producing an aerosol on a portion of the inspiratory phase [68] and so achieving accurate delivery. Unfortunately, there is no facility to display the respiratory pattern nor does the system take the subject's lung function into account. In addition, this system was developed for use in a clinical setting, delivering drugs using an "open" system, venting waste gas and aerosol to the environment. The use of a radioisotope requires a closed system so all the activity can be accounted for and so this system was inadequate for use in this trial without significant modification.

In contrast, the AKITA (InAMed GmbH, Gauting, Germany) is a system that has been specifically designed for the controlled delivery of aerosols, including radioaerosols. It functions in a highly reproducible manner, based on the measured lung function parameters of the subject. Very high deposition rates, as high as 82%, of which some 57% is peripheral have been reported using this equipment [69] but it is reliant on a slow and maintained inspiratory manoeuvre. This would not reflect the normal pattern of breathing at tidal volume and so was not appropriate for this study nor was it available when this work was commenced.

2.2.1.1 Particle sizing,

There were two possible techniques to measure the particle size, either directly using laser diffraction or by evaluating the aerodynamic properties by cascade impaction. Both methods have their critics. Laser diffraction has been described as the method of choice for measuring the output from a wet nebuliser [70]. Its speed avoids the significant drying of aerosols that occurs with cascade impaction and would produce a result indicating a smaller particle size. But it does have critics who have suggested that evaporative loss of small particles within the plume may cause an apparent shift in distribution and therefore an apparently larger particle size [71] and it does not measure the entire aerosol stream, only a sample. In contrast, cascade impactors sample the entire aerosol stream but evaporative loss of an aerosol as it enters the cascade impactor may result in droplets passing further into the device giving the impression of a smaller particle size [38]. This effect is increased when a large volume cascade impactor is used and warm ambient air is used to draw the aerosol into the apparatus. A recent paper confirmed these findings [72], directly comparing the two techniques. The authors found no significant difference between the two techniques, although they did highlight the need for cool air to be used to entrain the aerosol into the

cascade impactor. If this were not used then the cascade impactor results would suggest a smaller particle size.

This argument has been put into the context of the European Committee for Normalization (CEN) protocols in a comparison of the two methods [73]. The authors concluded that the small differences between the techniques were not significant statistically and as such laser diffraction was acceptable in line with the European standard.

Figure. 2.1

The "Optimist" nebuliser (Medicaid Ltd, Pagham West Sussex)

These points were considered when selecting a method for particle sizing the aerosols used in this study there was no access to a cooling unit for use in combination with a cascade impactor. Therefore, laser diffraction was selected for this study as the more accurate of the two systems available.

A Malvern Instruments HLS 2600 particle sizer (Malvern Instruments Inc., Worcestershire, UK) was used as an accepted

method to measure the droplet size and distribution generated by the nebulisers. This device uses a 2 mega Watt, monochromatic helium / neon beam of laser light and works on a light scattering principal. Particles of different sizes will scatter light at different angles as a result of diffraction, with the angle of diffraction being inversely proportional to diameter. The scattered light is collected by a lens and is focused onto a multi-element photodiode detector. A computer program is used to reconstruct the particle size distribution as a percentage of mass contained in each of fifteen bands on a logarithmic scale between 1.2 and 118.4 μm diameter. From this data the cumulative mass distribution can be plotted and the following parameters measured:

- Mass Median Diameter (MMD) – the diameter such that half the aerosol mass is below and half above.
- Geometric Standard Deviation (GSD) – the ratio of 84.1% to 50% points on the cumulative plot.
- The percentage of the aerosol mass less than 5 μm.

These three indicies are accepted as expressions of aerosol distribution [74]. A GSD of greater than 1.22 is the classic definition of a heterodisperse or polydisperse aerosol. This technique does assume that the particles are spherical and of a uniform diameter. This is not an unreasonable assumption with a wet aerosol generated by a nebuliser.

The manufacturer had calibrated the particle sizer by the use of off-the-shelf standard samples of traceable microspheres. These materials are Polystyrene DVB Microspheres with a size range of 0.3um to 9um (Duke Scientific Corp, California, USA). An automatic compensation for background is incorporated into the equipment.

The size distribution of the aerosols produced were measured at the point of delivery to the subject. This corresponded to the mouthpiece of the radio-aerosol circuit. All nebulisers were clamped in the upright position. The emerging aerosol spray was

placed 2.5 cm from the laser beam and 6 cm from the collecting lens, the sample time was 3 seconds according to the manufacturers' guidelines and previously publish protocols [72]. A summary of these results is presented in 3.2.1.

2.2.2 Development of the breathing circuit and pneumotachograph validation

Previous work [66] had developed a system for the accurate and controlled delivery of the radio aerosol to an individual. This recognised that the respiratory manoeuvre was extremely important, having a significant effect on the regional deposition of an aerosol. The breathing circuit ensured that the aerosol delivery was controlled, could be monitored and matched to any subsequent visits. The system used a self regulated breathing pattern as it was felt that this would best mimic the clinical situation and it is thought that nebulisers achieve optimum deposition during tidal breathing [51, 75].

Figure. 2.2.1

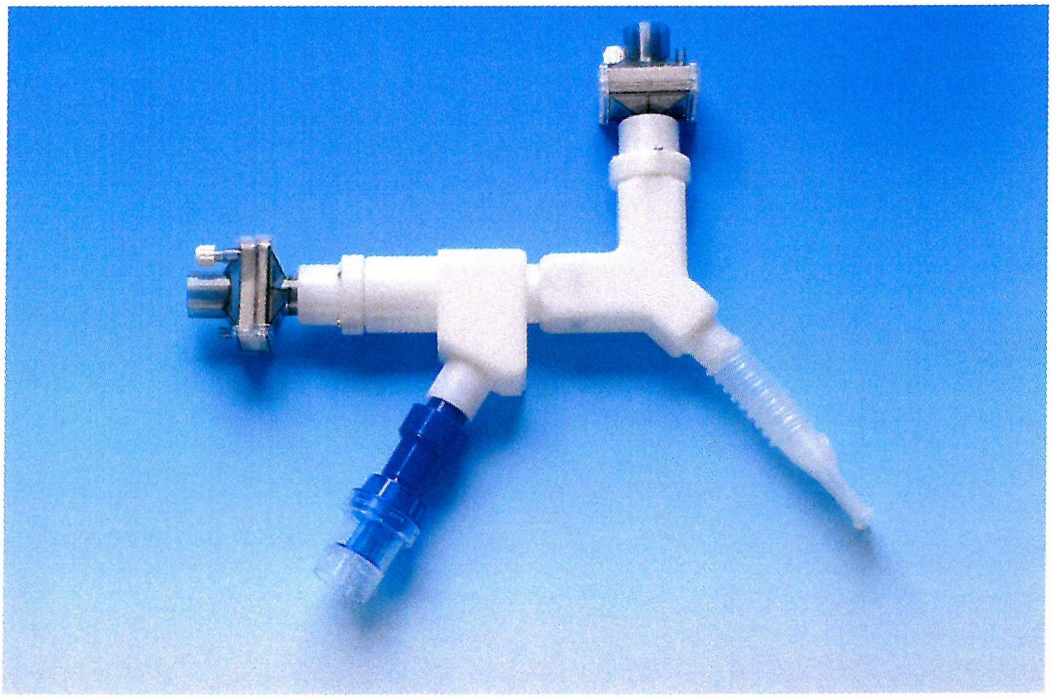

The assembled breathing circuit without pneumotachographs

The circuit consisted of acetyl blocks, which had been turned and milled by the technicians from the Department of Medical Physics at Southampton General hospital for the previous trial (see figure 2.2.1). The acetyl blocks were hollowed out with a smooth circular internal bore of 22 mm and were designed to keep airflow resistance and dead space to a minimum. The nebuliser was introduced to the circuit via an acetyl block "Y" connector. The aerosol was thus entrained into the airflow, which led to the mouthpiece. Exhaled air passed along a second limb of the "Y" connector to an absolute filter.

The circuit contains two minimum resistance one-way valves. The first was required on the inspiratory limb to allow additional air to be entrained without allowing the escape of any of the aerosol. The second was to allow exhaled breath to leave the circuit without mixing with the incoming airflow. An absolute filter (BB25a, Pall breathing systems filter, Pall Newquay Ltd, Cornwall) was placed distil to the inspiratory valve to ensure that no activity leaked from the system. This was a pleated hydrophobic filter which is reported to remove >99.999% of particles [76]. A second filter was placed after the expiratory valve to collect the activity exhaled.

Two pneumotachographs were included to produce two signals relating to the speed and volume of the breathing manoeuvre. These were placed on the inspiratory and expiratory limbs of the circuit, distal to the filter and one-way valves. The pneumotachographs detected changes in pressure that accompanied changes in airflow with breathing manoeuvres. The signal generated was passed through an Analogue to Digital converter and on to a computer running a specifically written programme. The output was displayed as a line on the computer screen, with time on the x – axis and volume on the y – axis.

Once the subject had settled into a regular breathing pattern, the program would repeatedly sample 1 minute of the subjects breathing pattern. From this, mean volumes and rates of breathing could be determined. Having analysed the subjects respiratory

pattern, the program then produced a target rate and volume for the subject to aim for, based on his original breathing pattern. This took the form of two lines corresponding to 10% above and below the target value with vertical columns corresponding to the rate. The subject would then be asked to breath between the two lines (see figure 2.2.2). The circuit was always calibrated with nebuliser of 0.9 % w/vol saline operating at 8 l/min.

There is some evidence that breathing from a circuit will cause a subject to breathe well above Functional Residual Capacity (FRC) and as such potentially changing the deposition pattern of the aerosol [56]. Therefore, the programme required modification to avoid the subjects breathing at higher lung volumes. This took the form of an additional respiratory manoeuvre prior to the delivery of the radioaerosol and data collection. Once the subjects were comfortable breathing on the circuit, they were asked to exhale maximally, then inhale maximally and exhale fully once more before returning to a normal breathing pattern. This effectively measured the subject's vital capacity. This process was repeated three times with the computer recording the highest value. This maximal expiratory manoeuvre forced the subjects to breath at a more normal FRC once they returned to the regulated breathing pattern.

The operating programme was in Basic and sampled data every 0.009 s at a speed of 111 Hz. Data was stored on the hard drive of the Dell 486 computer and final signal was displayed on the computer screen. Mr Frank Clewlow, of the department of Medical Physics at Southampton General Hospital wrote these changes under the direction of the author. He also wrote the original programme.

2.2.2.1 Calibration procedure

The breathing circuit was developed for use when a nebulised aerosol was entering the circuit at 8 l/min with a starting volume of 4 ml of 0.9% w/vol saline. Therefore, the calibration procedure was carried out under those conditions. This formed part

of the original programme and was routinely performed prior to any data collection. The equipment was warmed up for a minimum of 20 minutes. With the nebuliser running at 8 l per minute, the pnuemotachograph was calibrated against a 1l syringe.

Figure 2.2.2
- Screen Display

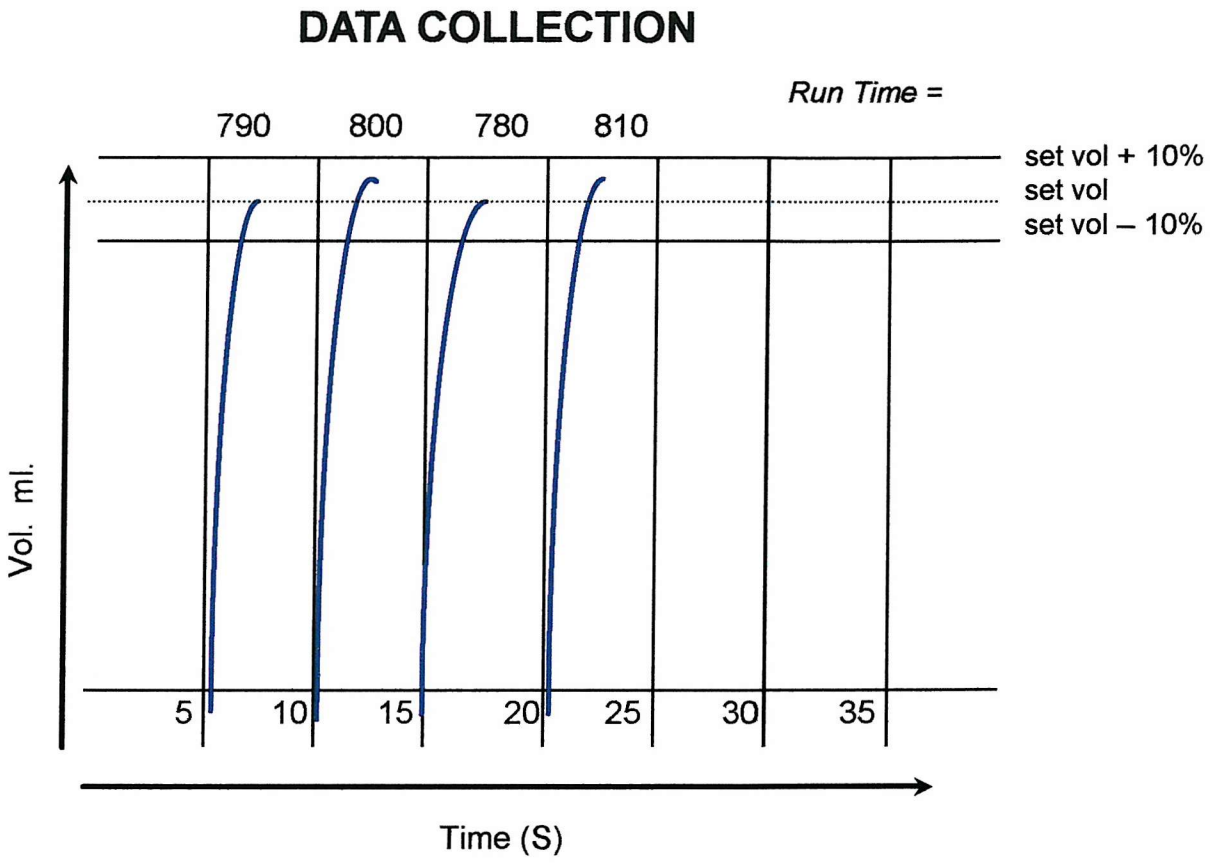

2.2.2.2 Review of the reliability of the breathing circuit

Having added the additional manoeuvre to the programme it was then necessary to review its reliability. This was performed by comparing the output recorded by the computer to that recorded by a bell spirometer. This is a hollow piston containing a known volume of gas sealed by a water trough. As the piston moves up

and down, changes in volume are recorded by a pen trace on a moving paper chart recorder.

There were two phases to this process; phase one compared the volumes produced by a 1l syringe and phase two recorded the tidal volumes and vital capacities of ten healthy volunteers

In both cases, the breathing circuit was directly connected to the spirometer so that simultaneous readings could be made. Prior to data collection, the breathing circuit was set up and allowed to warm up for a twenty-minute period, then calibrated using the standard method. This was then attached, via a closed circuit, to a Godart water spirometer (Godart Corp. Holland). The spirometer was then calibrated to allow for the extra 8l of entrained gas required to drive the nebuliser. With the chart recorder running at 60mm / minute, the spirometer was allowed to fill. This resulted in a gradient from the change in background volume (ΔV_B) over a measured time (ΔT_B) and therefore the background flow rate could be calculated and compensated for in the later calculations (see figure 2.2.3a). As the spirometer only had a limited volume of 8 litres, only short recording traces of about 1 minute were possible before the spirometer needed emptying.

The volumes recorded by the computer could be read directly from the screen but the volumes recorded by the spirometer had to be calculated from measurements taken by hand from the spirometer trace. The start and end points of the manoeuvre were identified and the distance measured for time and volume.

For inspiratory manoeuvres the true volume was equal to the measured flow rate plus the background flow rate multiplied by the time of the manoeuvre (see Figure 2.2.3b).

True inspiratory volume = $a + (V_B / T_B) \times t$

The atmospheric temperature and pressure were recorded to allow for correction in the calculations. Only the inspiratory manoeuvre was used with these subjects, as the pneumotachographs were not heated. A summary of these results is presented in section 3.2.2.

Figures 2.2.3a & b

Calculations from bell spirometer trace

Figure 2.2.3a

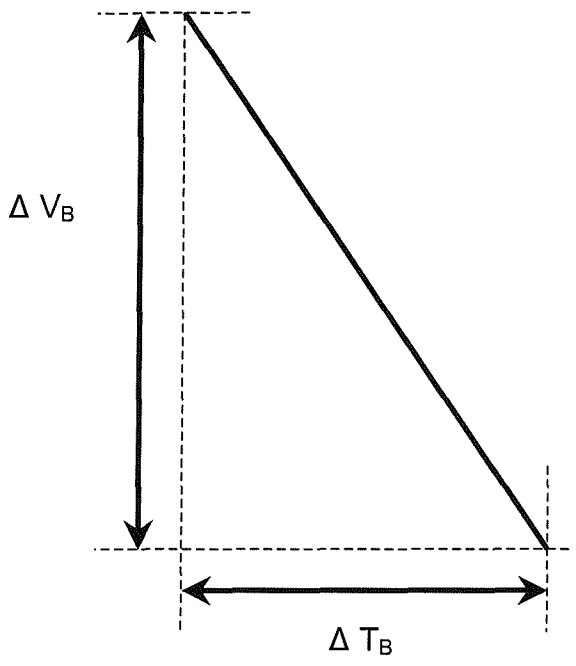

Where:
a = measured volume
t = estimated time (extrapolated from the gradient from the start and end of the breath
V_B = Background Volume
T_B = Background Time
V_B / T_B = Background Flow rate

Tidal volume for each exhaled breath = $a - (V_B / T_B) \times t$

Tidal volume for each inhaled breath = $a + (V_B / T_B) \times t$

Figure 2.2.3b

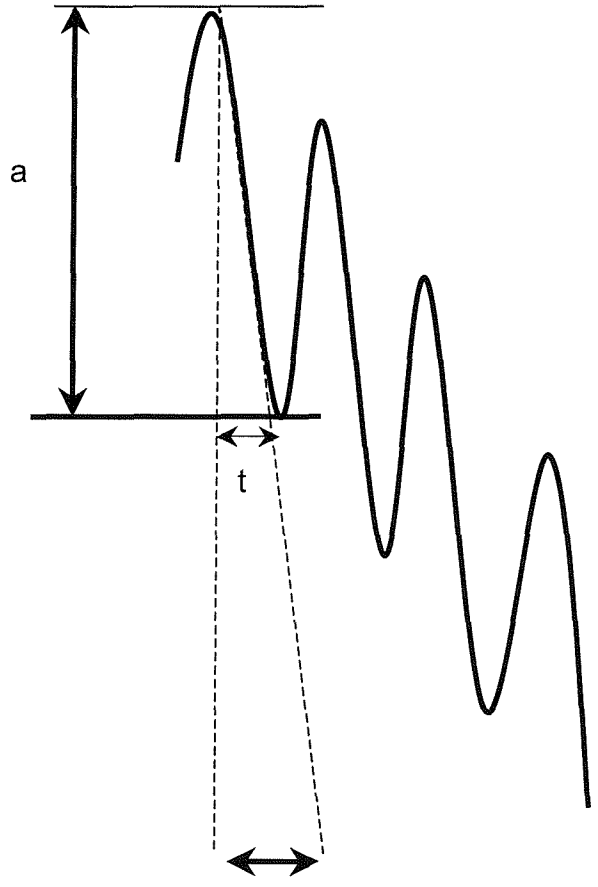

2.2.3 Radiolabelling human serum albumin

Radio-aerosols have long been used to assess the pulmonary deposition of an inhaled aerosol. This work was initially two dimensional (2D) [55], but in recent years, three dimensional (3D) techniques have been developed which also rely on this method [77, 78]. A widely used method involves the incorporation of an isotope Technetium (^{99m}Tc) with a freeze-dried micro-colloid such as Human Serum Albumin (HSA) [79]. The ^{99m}Tc, in the form of pertechnetate (TcO_4^-) rapidly and irreversibly binds with amino acid side chains of the HSA. This ensures that the ^{99m}Tc remains where it was deposited and is only cleared slowly by mucocilary clearance. This movement is not significant for the duration of the image acquisition [80].

The ideal radiolabel should be a gamma emitter, with a short half-life but long enough for the duration of the test. It should be chemically stable and not alter the characteristics or behaviour of the substance to which it is attached. ^{99m}Tc has a half life of only 6.04 hours which makes it optimal for most medical imaging and is quoted as being used in 70% of all medical imaging [81]. The short half-life does require the use of a parent/daughter generator to continually produce the isotope. In this case a ^{99m}Molybdenum/^{99m}Technetium generator (Amersham, Aylesbury, UK) was used. The ^{99m}Mo continually produces ^{99m}Tc, which is eluted by passing isotonic saline through the generator. The saline exchanges the chloride ion to form sodium pertechnetate $Na^+(^{99m}TcO_4^-)$. These generators remain productive for around 1 week.

Technetium administered as sodium pertechnetate to the lungs is rapidly absorbed and cleared by the pulmonary circulation [82]. Whereas, if the ^{99m}Tc is administered as a non-absorbable form such as Tc-colloidal human serum albumin, the deposited activity can remain in the lungs for over 24 hours. The binding of ^{99m}Tc to the HSA is quoted as being as high as 95% [83]. Commercially produced Tc-HSA kits, which only require the

addition of sodium pertechnetate, are widely available. Their ease of use makes them a popular method of producing a radiolabel for lung deposition studies; as such this was the method selected for this study.

The reliability of ^{99m}Tc-HSA as a marker within a nebuliser solution or suspension has been well validated. O'Doherty et al [84] assessed the stability of ^{99m}Tc-HSA by a series of paper chromatography studies comparing radioactivity against drug concentration over a range of conditions. They found ^{99m}Tc-HSA to be stable throughout the nebulisation process and cascade impaction. Other work [79] demonstrated that the addition of the radiolabel has no effect on the particle size of a nebulised solution. As this is such a well recognised method of administration of a radioisotope, the assumption was made that this was a stable system which did not require further validation.

For this thesis, the ^{99m}Tc-HSA was prepared by injecting a known volume and activity of ^{99m}Tc pertechnetate (5ml with an activity of at least 100 MBq/ml) into a sterile vial, containing freeze-dried HSA (nanocoll, Nycomed, Amersham Sorin, Vercelli, Italy). Each vial contained 0.5 mg of human albumin colloidal particles and 0.2 mg of stannous chloride dihydrate. This preparation was formulated to produce very small albumin particles, typically more than 95% below 80 nm. The manufacturer stated that all donors for this product were all non reactive for Hepatitis B, Hepatitis C and Human Immunodeficiency Virus, in accordance with European Union regulation. The pertechnetate was injected into the vial and the vial shaken which rapidly and irreversibly binds with the HSA. Four mls were then withdrawn using a syringe and the activity verified as being around 400 MBq in total. The level of activity was checked using an Amersham Radioisotope Calibrator ARC – 120 (Capintec Inc. New Jersey, USA) and adjusted to that level with the addition of normal saline. The solution was then ready to be injected into the nebuliser for inhalation by the subject. At all times a sterile procedure was used behind lead shielding.

To comply with departmental regulations, the elution of the pertechnetate was performed by a radio-pharmacist and a technician from the Nuclear Medicine Department of Southampton General Hospital performed the mixing of the Tc-HSA kits. The author performed the administration of the aerosol.

The level of binding of the radiolabel to the HSA was reviewed as part of routine the quality control tests within the Department of Nuclear Medicine by the radio-pharmacist. Each batch was tested twice, once on its first use with a second random check at a later stage. The level of disassociation was checked by paper chromatography using Whitman 3mm paper and normal saline as the solute.

2.2.4 Aerosol delivery and analysis of the respiratory pattern

The development of the breathing circuit as described in 2.2.2 allowed close monitoring of the subjects respiratory pattern throughout the aerosol delivery. The program was capable of directly calculating the mean, SEM, minimum and maximum values for the volume and duration of inhalation. In addition the respiratory rate and an estimate of vital capacity were also recorded. Summaries of these data generated are presented in section 3.2.5.

2.2.5 Selection of activity levels for SPECT markers

The alignment of the SPECT image with the MRI required the use of markers on specific soft tissue and bony points. These were the xiphisternum, the supra-sternal notch and the nipples. In the case of the MRI it was straightforward and small oil capsules were used. These have a high density and show up well on the scan[66].

SPECT requires the use of radioactive markers. These require sufficient activity to be clear on the reconstructed image but not so high that they obscure the image or generate any artefacts.

A model of an adult male thorax was used as phantom. This consisted of an acrylic chest wall surrounding a water filled thorax. This would mimic the attenuation of the tissue surrounding the

lungs. The "lungs" themselves were acrylic shell cast in the shape of lungs filled with expanded polystyrene foam beads. These could in turn be filled with water to mimic the lower density of the lung tissue. The foam beads caused the "lungs" to be very buoyant. To avoid them floating to the anterior chest wall when the phantom was positioned in supine during the imaging, the "lungs" were firmly clamped in place within the thorax. This ensured that the lungs mimicked anatomical position in life.

In early trials of the phantom it was found that one of the lungs was cracked and leaking. This could not be repaired and as such precluded any activity being placed within it. So only one lung could have activity placed in it but the leaky lung was retained within the model to maintain the appropriate level of attenuation.

Ten MBq of activity from ^{99m}Technetium as sodium pertechnetate was instilled into the right lung of the model. This was equivalent to half the total dose for both lungs to be used in the trial. The lung was sealed, then shaken to ensure even distribution of the activity before being clamped into the water filled model. Seven markers were injected with pertechnetate and applied to the outside of the model. The level of activities was, 0.06, 0.12, 0.2, 0.8, 1.0, 1.6 and 2.6 MBqs respectively and their distribution on the phantom is demonstrated in Figure 2.2.5. A SPECT acquisition was then performed according to the protocol to be used in the study (see 2.4.5) and the images reviewed. From that data the level of activity to be used in the markers was selected. An example of the images generated is presented in section 3.2.4.

2.3.0 Screening process prior to entry into the trial. Background data on the population

It is accepted that the changes in pulmonary function that disease produces can have significant effects on inhaled aerosol deposition [3, 61, 82]. It was therefore necessary to screen all subjects prior to their entry to the trial to ensure that their lung

function was within normal parameters. The tests used are described in the following sections and were all performed in a laboratory setting either by the author or where stated, by a pulmonary function technician (Mr John Heath) at Southampton General Hospital.

Figure 2.2.5

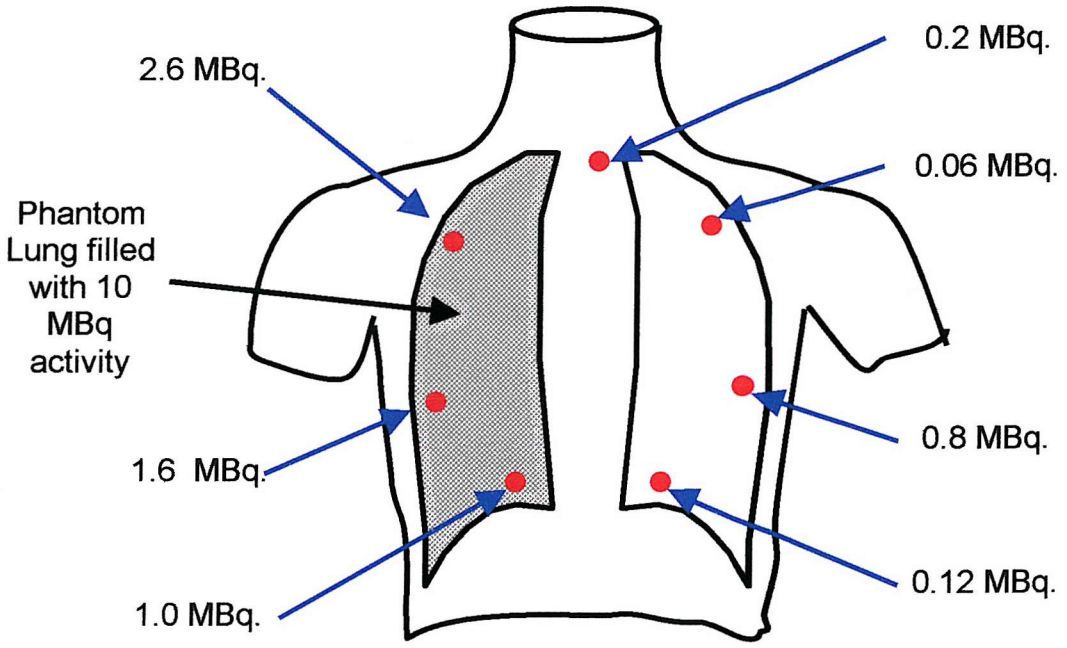

2.3.1 Measurement of airway calibre

One of the most common measurements to detect airflow obstruction is an assessment of the maximal ability to move gas rapidly out of the lungs. This requires a measurement of flow such as the Forced Expiratory Volume in the first second (FEV_1).

This was formally assessed using a Sensomedic (Sensomedic corp. USA) rolling seal spirometer, sampled at 100 Hz by a 10 bit A-D converter. This in turn was connected to an Archimedes computer (Acorn UK) that processed the data to produce the relevant curves and loops. This was performed by the lung function technician. Prior to inhalation of the labelled aerosol, an "on the spot" measurement of lung function was made by the author. This

was performed with a Vitalograph Compact C spirometer (Vitalograph Ltd., Buckinghamshire, UK), which operates on the principal of measuring a pressure drop across a Fleisch type pneumotachograph and interpreting that pressure drop as flow. The spirometer was calibrated, at the measured room temperature, with a half litre syringe, to a volume of ten litres each study day. The best of three technically correct manoeuvres performed in sitting were recorded. A summary of the data is presented in section 3.3.

2.3.2 FEV_1

FEV1 is the volume of air a subject can exhale in the first second of a maximal expiration, following a maximal inspiration. The result is expressed in litres [85].

2.3.2 Forced Vital Capacity

Forced Vital Capacity (FVC) is the volume expired when the FEV_1 manoeuvre is continued until no more air can be expelled. Again, the result is expressed in litres [85].

In a clinical situation these two tests tend to be the first choice when investigating diseases of the lung and response to bronchodilation, as they are simple to perform and are reproducible. However, they are relatively insensitive to small airway changes [85].

2.3.3 FEV_1/FVC

FEV_1 is dependent on the vital capacity. This can be corrected for by expressing the result as a ratio with FVC. This normally takes the form of a percentage with the FEV_1 being approximately 80% of the FVC but is also dependent on age and height. Any lower can reflect airflow obstruction, but can also indicate a change in vital capacity. In obstructive lung disease this can be overestimated as a result of air trapping during the forced expiratory manoeuvre.

2.3.4 Flow-Volume Loop / Curve

Assessment of small airways can be achieved by dynamic measurement of lung volumes and flow. This is referred to as a flow-volume curve or loop. This procedure starts from maximal inspiration, from there the subject performs a maximal expiration, followed by a maximal inspiration. The curve is then plotted from flow rates at specific volumes.

The inspiratory portion of the curve is sometimes used to assess the response to exercise, respiratory muscle weakness and can give information on patency of large airways.

The expiratory parts of the curve are widely measured as they are thought to reflect the flow characteristics of the small airways. It is thought that the large airways determine the flow in the early parts of expiration while the small airways influence flow in the later phases. The inspiratory portion of the curve was not considered in this thesis, and only the expiratory portion was used.

2.3.5 Helium Rebreathing Lung Volumes

Inspiratory and expiratory manoeuvres cannot measure volumes beyond vital capacity. To achieve this either whole body plethysmography or a gas dilution method may be used. In subjects with impaired lung function a gas dilution method is likely to underestimate the residual volume when compared to plethysmographic methods, but there is good agreement between the two methods in healthy subjects. As only healthy subjects were to be used in this study, the gas dilution method as previously described [86] was selected for use in this thesis. Figure 2.3.5 describes these lung volumes.

Figure 2.3.5 - Static Lung Volumes

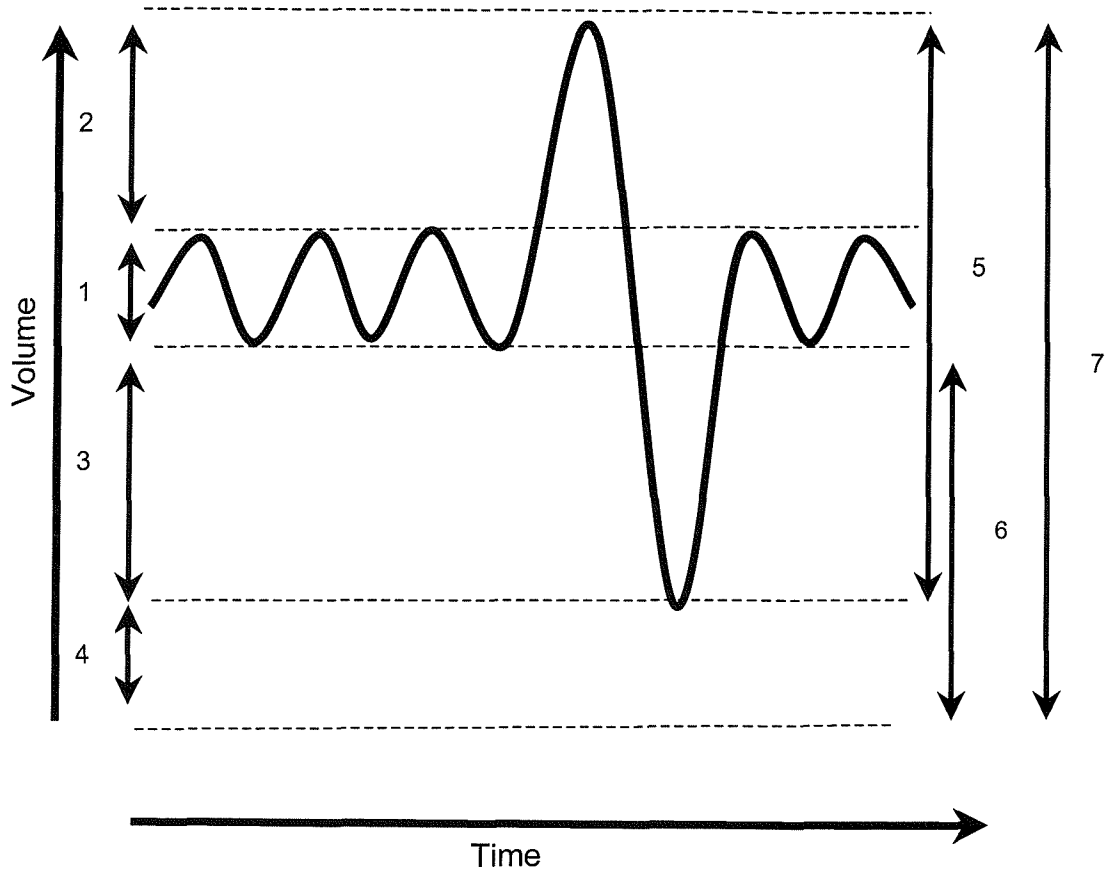

The curve above represents the spirogram or trace from a closed circuit bell spirometer. As the subject inhales, the trace is deflected upwards and as he exhales, the trace moves down. From this trace the lung volumes can be measured. In this case the subject has made a maximal inspiratory manoeuvre followed by a full exhalation. The subdivisions of total lung volumes are labelled as follows

1 = Tidal Volume
2 = Inspiratory Reserve Volume
3 = Expiratory Reserve Volume
4 = Residual Volume
5 = Vital Capacity
6 = Functional Residual Capacity
7 = Total Lung Capacity

2.3.6 Skin sensitivity testing.

The use of HSA in aerosol studies is a well-established technique with no side affects. However, there have been some anecdotal reports of individuals having a degree of sensitivity to HSA aerosol solutions. As such it was felt necessary to screen all subjects for sensitivity to HSA prior to entry into the trial.

Skin prick testing was selected as the method to screen the subjects. This is a standard method of assessing atopy (a tendency to express an allergic response), is safe, quick, and easy to perform having been described in detail previously [87].

The solutions used in this study were histamine and 0.9% normal saline as positive and negative controls, pollens (grass and tree mix), house dust mite, cat, dog and feather (ALK Abello UK, Hungerford, Berkshire) and HSA solution at a concentration twice that to be used during the aerosol delivery.

2.4.0 Clinical Imaging

Once through the screening process the subjects entered the imaging portion of the study. This consisted of three stages: the Magnetic Resonance Imaging (MRI) to provide the attenuation mapping then the SPECT imaging to review the distribution of the aerosol followed by the image analysis.

2.4.1 Introduction

SPECT relies on gamma cameras to detect the distribution of the gamma-emitting isotope. The camera consists of an array of scintillation crystals, a collimator and photomultiplier tubes, which transpond the gamma rays into flashes of light. The collimator acts as a lens, only allowing gamma rays to approach the detector from one direction. The light generated is then converted into an electronic signal, which can be processed to produce the final image.

Once acquired, the data from the gamma camera requires correction for the attenuation of the gamma rays by body tissue.

Attenuation is the reduction of the number of primary photons in a beam of radiation caused by scattering and absorption [81]. This is dependent on both the density of tissue and the distance that the photon beam has to travel through the tissue. If no attempt at correction is made, superficial structures will be emphasised at the expense of deep structures. There are three main methods for calculating attenuation correction. A "phantom" is a structure designed to mimic that part of the body being imaged, in to which a source of radiation is placed. Studies using this method have been reported as underestimating the dose within the lung [79, 88] which does not account for the anatomical differences between subjects. A degree of regional correction specific to individuals can be achieved by the use of a "flood source". A source of radioactivity (usually ^{99m}Tc) is placed in front of the gamma camera and the resulting image is compared to one produced when the subject sits between the source and the camera. The attenuation factor is calculated from the difference in counts between the two images. While this method also allows correction specific to the individual and gives definition of the lung outline, it does expose the subject to an additional, however small, dose of radiation. As SPECT began to be used as a tool for aerosol studies it became necessary to refine the attenuation pattern in more detail on a transverse view by transverse view basis. To fulfil this need Perring *et al* [77] used Computed Tomography (CT). This gave the tissue densities and anatomical detail but involved a significant radiation dose to the subject. This was later replaced by MRI [78], which had the advantage of no radiation dose while providing similar information. The correction factors were calculated by defining tissue as bone, soft tissue or lung thus generating an "attenuation" map for each 8mm transverse view. This was the form of analysis used in this thesis.

All images reported in this thesis were acquired using a dual-head Sopha DSTXL gamma camera (Sopha Medical Vision, Buk, Paris France), (Fig2.4.1) in the Department of Nuclear Medicine at

Southampton General Hospital. This was fitted with 128 x 128 matrix, low energy, high resolution collimators in 180-degree configuration. Mr Julian Williams, a medical technician within the department, manipulated the cameras with all other work performed by the author unless otherwise stated.

Figure 2.4.1, the Gamma Camera

The dual-head Sopha DSTXL gamma camera used for data collection in the Department of Nuclear Medicine at Southampton General Hospital. Here, it is fitted with 128 x 128 matrix, low energy, high resolution collimators in 180 degree configuration.

2.4.2. Single Photon Emission Computed Tomography

Single Photon Emission Computed Tomography (SPECT) is a form of imagining which results in three-dimensional data on the distribution of a radioisotope, by using rotating gamma cameras. A series of planar images are acquired at set angles around the subject. A backprojection is then performed by the SPECT system's digital computer which results in the reconstructed images. The data can then be viewed tomographically in sagittal, coronal or transverse planes. The use of a dual headed gamma

camera with an elliptical orbit cuts down imaging time and improves resolution down to 10 mm.

2.4.3 Protocol for planar total deposition

Immediately following the inhalation of the radio-aerosol the subject rinsed his mouth and swallowed 100mls water to clear the oropharynx of activity. A further 100mls were gargled and spat out. This water was retained along with any tissues to quantify any remaining activity present.

Before and after the SPECT image acquisition, dual planar static images (anterior and posterior) were acquired. For this, the subject undressed to the waist and lay supine with his arms by his side on the gamma camera couch. The acquisition time was 30 seconds and the images included the lungs, stomach and oropharynx. These images could then be combined to produce a geometric mean image [89].

To account for all the activity used within each imaging session, planar images were acquired of the mouthwash and any tissues used by the subject and the aerosol equipment. The mouthwash used an acquisition time of 60 seconds and was performed immediately after the SPECT. The aerosol equipment was imaged the next day with an acquisition time of 100 seconds. The difference in timing and acquisition times resulted from the different activity levels expected. The aerosol equipment had a comparatively high activity concentrated in a small area, therefore the activity was allowed to decay prior to imaging.

An additional planar image was acquired 24 hours after the inhalation of the isotope in the sitting position. On these occasions the acquisition time required was 5 minutes as a result of the isotope decaying. This provided a means of monitoring the mucocilary clearance of the inhaled HSA. These results are presented in 3.4.1

2.4.4 SPECT protocol for acquiring activity map

Once the initial planar image had been acquired, the subjects were required to lie supine with both arms above their head. For comfort their arms were supported. With the arms raised, the soft tissue markers were applied to mark the nipples, supra-sternal notch and the xiphisternum. The SPECT study was then performed, using a dual-head camera and an elliptical orbit. Thirty-two pairs of opposing views were acquired in a 360° arc around the subject. An acquisition time of 30 seconds per frame 128 x 128 matrix was used, giving a total acquisition time of 16 minutes. The markers were then removed for the subsequent planar image. After the final planar image, the subject left the department.

2.4.5 Magnetic resonance imaging

Magnetic resonance imaging (MRI) uses uniform magnetic fields and magnetic field gradients applied to the body to produce images. MRI has the advantage of not using ionising radiation and produces high contrast sensitivity for imaging soft tissue. The technique has the disadvantages of complex image acquisition, hence longer acquisition times, image artefacts and patient claustrophobia [81].

MRI of the thorax was used in this thesis to provide anatomical information and to generate a map of attenuation to be aligned with the SPECT data [90].

2.4.6 Protocol for magnetic resonance imaging

The MR imaging for this thesis was performed in the MRI suite of the Wessex Neurological Centre (located within Southampton General Hospital). The image acquisition was supervised by the author and Angela Darekar (medical physicist) and performed by members of the radiography department of the Wessex Neurological Centre. The scanner used was a Signa Advantage (IGE Medical Systems, Milwaukee, USA) operating at 0.5 Tesla. The imaging was performed a few days prior to the first SPECT.

The subjects were required to undress to the waist and lie supine with both arms above their head for the duration of the imaging. This was the same position assumed for the SPECT. Oil capsules were applied to the subject with tape to mark the nipples, supra-sternal notch and the xiphisternum. All images were acquired during tidal breathing. After a coronal localiser, axial T_1 weighted images were acquired from apex to base of the lungs. The slices were 8mm thick and contiguous with an in-plane resolution of 1.7 mm x 1.7 mm. Respiratory and cardiac gating were used to reduce motion artefacts. The respiratory gating re-orders the acquired data such that the most motion sensitive data is related to the mid-point of the respiratory cycle. Respiratory motion was monitored with a Respitrace (this is an expansive wire coil with sensors to detect thoracic movement). In a similar way, the ECG gating is aimed at avoiding image acquisition at the extremes of cardiac motion. Cardiac function was recorded with a 4 lead ECG, recorded from the posterior thoracic wall. The data acquisition is triggered by the recognition of the R wave of the ECG with the image acquisition occurring between the S-T segment of one cardiac cycle and the initiation of the P wave of the next. All data was archived on to optical discs.

2.5 Image analysis

2.5.1 Image reconstruction

The SPECT and planar image reconstruction was performed on a network of RISC workstations using the Southampton General Hospital Nuclear Medicine Department PICS general medical image processing software [91]. The MRI segmentation was performed using Analyze software (Mayo Clinic, Rochester, Minnesota, USA). Livia Bolt (medical physicist) and the author performed this task using the protocol as published by Fleming *et al* [78].

A variety of techniques for the quantitative planar analysis of aerosol images use a ventilation image to assist in the definition of regions of interest and to act as a reference against which the

aerosol images can be compared. In this study the MRI data were used to generate simulated anterior and posterior ventilation images as previously described [92, 93]. The lung was identified on the workstation by drawing Regions of Interest (ROIs) by hand. This was refined by the application of a threshold technique that identified all pixels (picture elements) with a value of 10% or more of the maximum value within the RIO. From this the maximal pixels count can be derived. The lung edge is then defined as areas with a pixel count of 10% of the maximum identified within the manually drawn area. The aerosol images were then aligned with the simulated ventilation images. This process allowed the application of the attenuation map to the data. The activity in the lung could then be calculated from number of counts recorded in ROI with the appropriate correct for absorption of activity by the surrounding tissue. The planar images were corrected for radioactive decay and tissue attenuation according to the method previously described [89].

The geometric mean images of the thorax (including head and stomach) mouthwash and equipment were displayed separately on screen. Regions of interest were defined corresponding to the oro-pharynx, the mediastinum, the stomach, the right and left lungs and the mouthwash. The activity in the oropharynx was estimated from the anterior image. As it is difficult to generate an accurate attenuation map for the area, an estimation of a 15% reduction was applied. The mediastinal region of interest equates to the activity within the trachea and oesophagus. These two structures overlie one another and cannot be separately distinguished. As all subjects had swallowed 100mls of water after inhalation of the radioaerosol, activity within the mediastinum was assumed to be in the trachea. The counts per region could then be described as a percentage of the total counts within: the right lung, the left lung, the gastrointestinal tract (oropharynx, mouth wash and stomach) and the equipment.

The SPECT images were initially reconstruction using a simple backprojection technique. Filtered backprojection is a mathematical image reconstruction used in CT and SPECT [81]. Backprojection refers to the method used by the computer to build up the image. Essentially the computer reverses the acquisition steps. Artefacts are reduced by the application of filters (mathematical operations) to the profiles prior to backprojection. The images were corrected for radioactive decay [94].

This initial reconstruction does not take attenuation of the gamma-rays by the thoracic tissue into account. If this is not corrected, superficial structures are emphasised at the expense of deeper ones. In order to correct for this the MR images were used. These were segmented to produce binary images of the lungs, bone and soft tissue. Each 8 mm transverse slice is divided into lung, soft tissue and bone within the whole body outline (See Figure 2.5.0). This process was carried out by hand in conjunction with Dr Steve Harden (Radiologist). These areas are then multiplied by attenuation correction factors appropriate to the gamma-ray energy used in the SPECT. This could then be recombined to produce an attenuation map [90].

The attenuation map was then interpolated to have cubic voxels with the same dimensions as the SPECT images. The chest wall markers were segmented into separate volume with the same cubic voxels. The pixel co-ordinates for the chest wall markers were located for both the SPECT and MR images. A transformation matrix calculated for translation and rotation using a least squares approach then aligned the SPECT and MR images. The attenuation map was then aligned using the calculated transformation matrix. Finally, the second reconstruction was completed employing specially written software [95], which used the attenuation map to correct for the attenuation of the thoracic tissue and performed subtraction of malpositioned scattered photons. The completed reconstruction consisted of a 3D data set of the

distribution of the activity, which allowed transverse, coronal and sagittal views to be produced.

Figure 2.5.0

The generation of attenuation map for Subject 1, MRI Slice 15

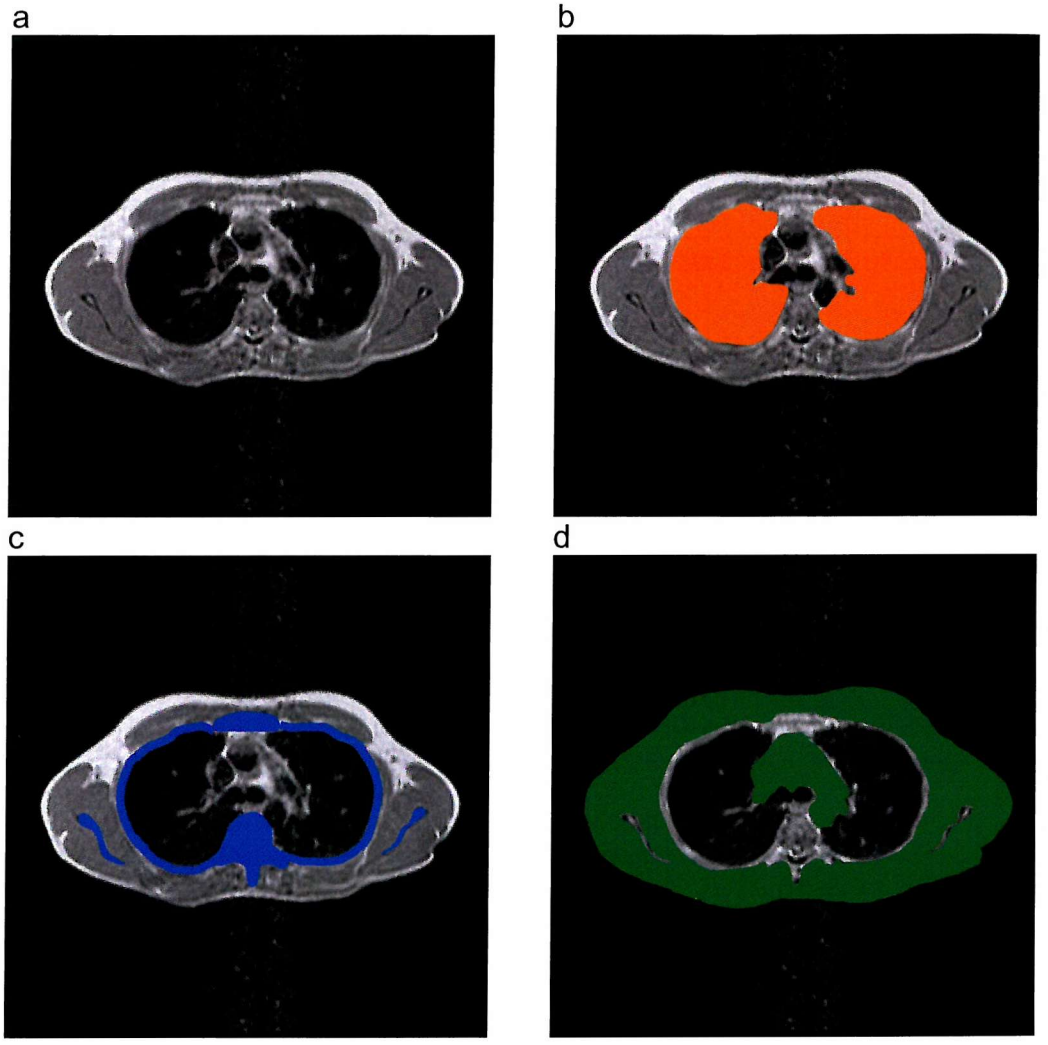

Section "a" demonstrates the transverse MRI slice prior to the attenuation mapping process.

Section "b" demonstrates the mapping process the areas in orange defined as lung.

Section "c" demonstrates the mapping of the of bone highlighted in blue.

Section "d" demonstrates the mapping the soft tissue mapping in green.

2.5.3 Shell analysis

The lung outline was defined as a 3D volume of interest using the aligned MR images. Using successive MR transverse slices a voxel (unit of volume in a 3D map) was identified which defined the lung hilum. This voxel identified the point at which the upper lobe bronchus branched away from the main bronchus for both left and right lungs (see figure 2.5.3). This was performed in conjunction with Dr Steve Harden (radiologist). The hilum and lung outline were then used to construct a series of ten, hemispherical concentric shells. This process was first described by Perring *et al* [77] and was performed by taking each voxel within the lung and expressing its 3D position as a percentage distance from the hilum to the periphery. The voxel could then be assigned to one of a series of the ten concentric shells on the basis of its distance from the hilum in the spherically transformed space. This allowed the activity to be described as a percentage of the total in the lung, per shell. The shell volume increases dramatically from the centre to the periphery at a rate of the shell number squared. This could potentially mask useful information. Activity can also be described as a percentage of the deposition normalised to shell volume. This is referred to as activity concentration.

Using this shell analysis, deposition was therefore described in terms of;

- *Percentage activity* – The percentage of the total activity per shell
- *Activity concentration* – The volume corrected activity expressed as a percentage of total activity per shell.

To gain an impression of the *volumetric* penetration of the aerosol the activity concentration was expressed as a ration of the peripheral to central region activity in this case:

- Activity concentration in the inner 5 and outer 2 shells.

This was referred to as the *Penetration Index (PI).*

These results are presented in 3.4.2.

Figure 2.5.3

Subject 1,Slice 16
The level of the division of the right main stem bronchus

This demonstrates the point at which the bronchus to the right upper lobe branches away from the right main stem bronchus.

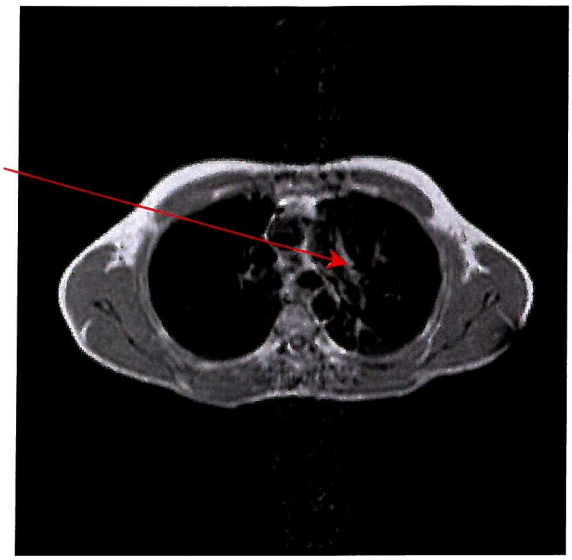

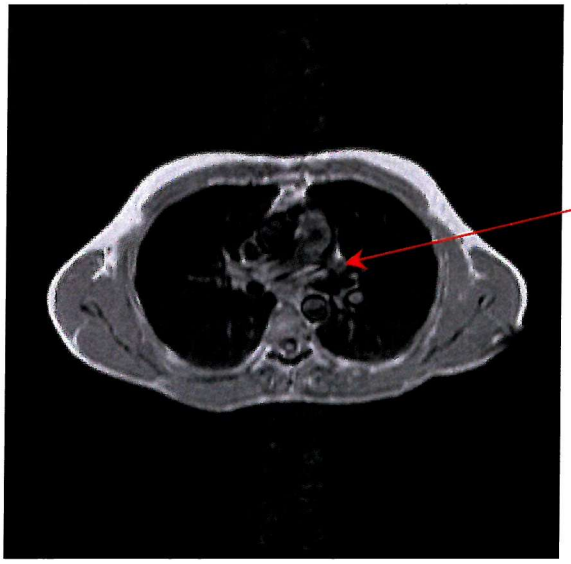

Subject 1, Slice 18
The level of the division of the left main bronchus

This demonstrates the point at which the bronchus to the left upper lobe branches away from the left main stem bronchus.

2.5.4 Segmental and lobar analysis

While the shell analysis is valuable and gives some information as to the regional distribution of the aerosol within the lung, it does not relate to the anatomical regions of the lung, namely the lobes and segments.

A segmental model of the lung has been developed based on the lung shape of a male subject with normal lung function and a

near average value of lung size as adjudged from the functional residual capacity (FRC)[96]. MR images of the subject's thorax were segmented to obtain the lung outline and then each voxel in the lung assigned a value according to the lung segment to which it belonged; there are classically ten segments in each lung. This was achieved by digitising photographs of cast of the lung airway in which the different segments in the lung were denoted by different colours and registering them to the outline of the standard lung model. Figure 2.5.4.1 shows an example slice through the model.

Figure 2.5.4 .1
Example slice through the segmental model showing different segments by their grey shades

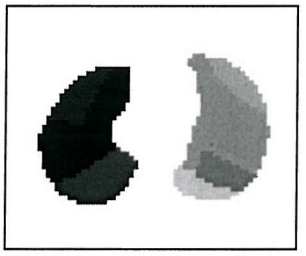

The elastic transformation of the SPECT imaging data to a standard template was achieved using a spherical transform based on knowledge of the lung outline of the subject under investigation and that of the standard segmental lung template. It was also necessary to define a single common anatomical location in both the subject and template. The hilum of the lung where the main bronchus enters the lung space is in many ways a natural choice for the centre of a spherical transform as both airways and blood vessels branch out approximately radially from that point. However this position is either on, or close to, the edge of the lung and therefore cannot be used, as nearly half the radii from this point have a very short or zero length within the lung. Therefore a point

in the centre of the lung (c_x, c_y, c_z) is chosen related to the hilum position (h_x, h_y, h_z) such that:

$$c_x = (h_x + e_x)/2, \quad c_y = h_y, \quad c_z = h_z \qquad [97]$$

where x, y and z represent the left/right, anterior/posterior and superior/inferior directions respectively. e_x represents the lateral edge point on the lung at the same y and z co-ordinates as the hilum. The transform is illustrated in Figure 2.5.4.2. Each voxel t in the template shape is characterised by its direction cosines and the fractional radial distance ($f_t = VO_t / VO_e$) from the centre of the image (O_t) to the equivalent extrapolated position on the edge (O_t). The voxel, s, in the subject image along the line starting at O_s with the same direction cosines as $\mathbf{VO_t}$, which has the nearest fractional distance to f_t, is found. The SPECT data from this voxel transferred to voxel, t, in the template shape. This process is repeated for all the template voxels. These results are presented in 3.4.3

Figure 2.5.4.2

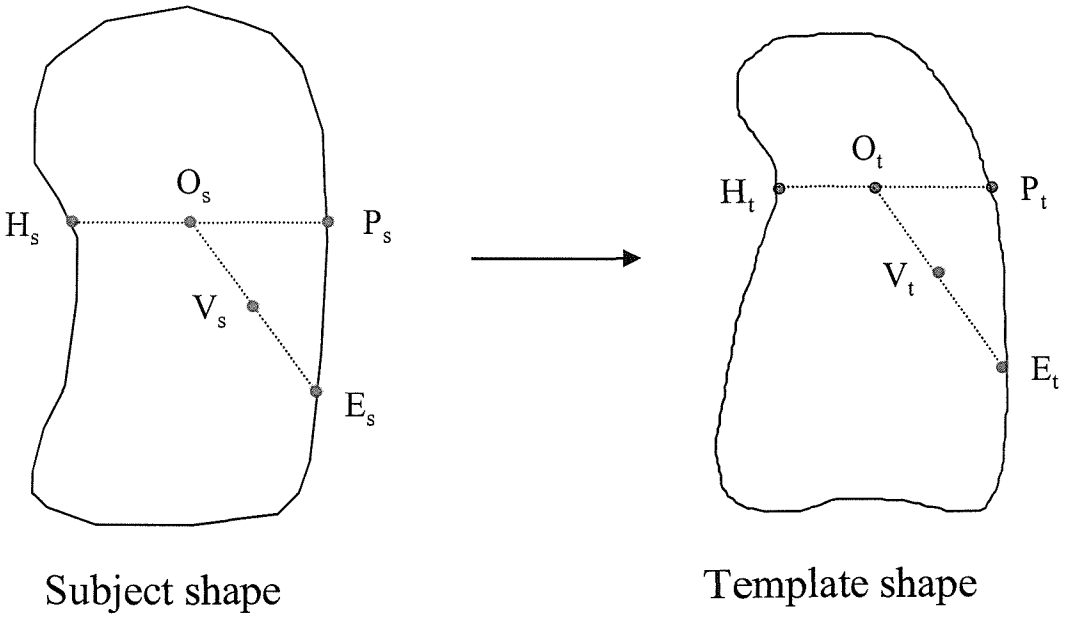

Schematic diagram illustrating the principle of the registration

Chapter 3 Results

3.1.0 Introduction

This chapter reports the data collected using the methodology described in Chapter 2. It will follow a similar pattern, first reviewing the pre clinical testing to evaluate the techniques and equipment to be used. This will encompass the nebuliser output, a review of the reliability of the breathing circuit and the selection of the soft tissue and bony point markers used for the Single Photon Emission Computer Tomography (SPECT) imaging.

This will be followed by a lung function data used to screen the subjects prior to entry into the study and the respiratory pattern on the delivery of the radio-aerosol. Finally the deposition data will be in terms of the overall deposition and regional patterns using the shell, segmental and lobar models.

3.2.1 Nebuliser output

The output from the nebulisers was measured using the laser diffraction technique described in section 2.2.1. There were two principal reasons for this work before embarking on the full study. The first was to ensure that the addition of, human serum albumin (HSA) did not increase the particle size generated by the nebuliser. The previous experience from the Southampton group suggested that there would be no change in the particle size with the addition of HSA [66]. In that work a freeze-dried HSA produced by Incstar Ltd, (Wokingham, Berkshire, UK) was used. The Nuclear Medicine Department had since then changed the supplier of HSA to nanocoll, (Nycomed, Amersham Sorin, Vercelli, Italy). Therefore it was felt necessary to review the output of the nebulisers with the addition of this new preparation of the micro colloid. Second, as a number of nebulisers were to be used within the study there was a need to ensure that there was limited variability between them and all produced an output within the respirable range.

Figure 3.2.1

Particle size generated by the nebulisers over time with normal saline and Human Serum Albumin

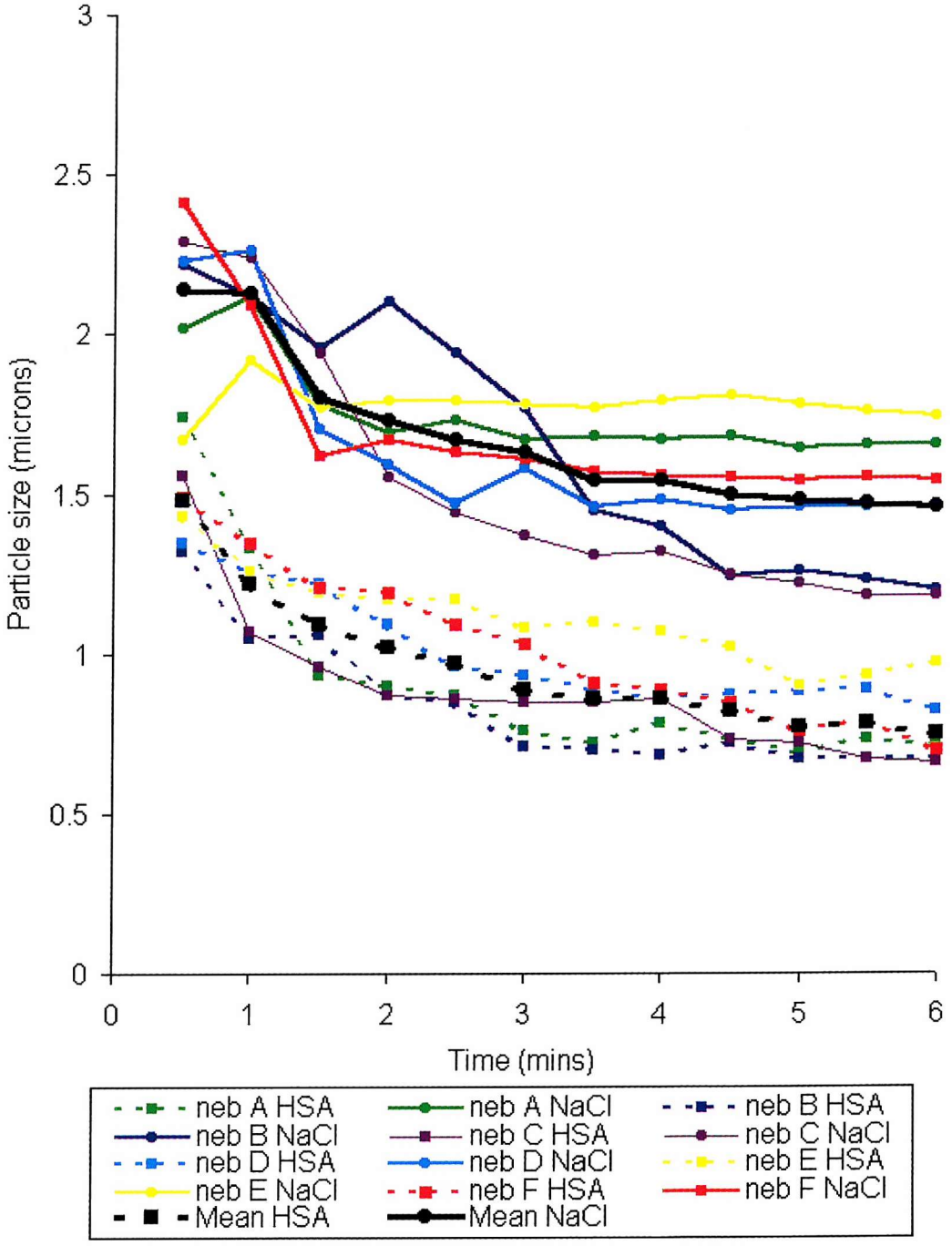

Neb = nebuliser
NaCl = Saline
HSA = Human Serum Albumin

The particle size generated over six minutes of output for the nebulisers with both normal saline (0.9%) and the HSA solution are described in figure 3.2.1. The data for each nebuliser are the mean of three separate determinations. The broken lines represent the output with the normal saline, while the solid line represent the HSA solution. The addition of the HSA certainly did not increase the particle size generated. Indeed the opposite appeared to occur with an obvious reduction particle size on the addition of the colloid. This difference was statistically significant when the data sets for each nebuliser are paired and tested by a t-test ($p<0.01$). While these findings were unexpected and are contrary to the previous experience of the Southampton group [66], there had not been an increase in the particle size generated by the nebulisers with the addition of HSA and the output was still within the respirable range (< 5 μm). There was a small range of difference in particle size generated by each nebulisers with the choice of the solution to be aerosolised having more impact on the particle size generated that the choice of which nebuliser was to be used. Therefore, these nebulisers were deemed acceptable for the purpose of this study.

3.2.2 Development of the breathing circuit and pneumotachograph validation

Within this section the data recorded simultaneously by the pneumotachograph and the bell spirometer are presented. This follows the methodology described in 2.2.2. Previous work using the same circuit [66] had demonstrated a linearity of within 3.5%, or 70 – 100 ml. This was consistent with ERS guidelines [86] but having added the vital capacity manoeuvre into the original computer programme (2.2.2), it was felt appropriate to review the output of the circuit again. The aim of this work was ensure that there was a degree of consistency in the tidal volumes when delivering the aerosol. The comparison of the volumes recorded with a bell spirometer and the pneumotachograph was not ideal. While the spirometer was the accepted standard it is a variable

measure. The figures obtained were derived from calculations using measures taken from a pen trace on paper chart recorder. The results required correction for atmospheric temperature and pressure, plus the background flow rate of the entrained airflow to drive the nebuliser. Each of these stages in the calculation potentially added an error. The disadvantage of using pneumotachographs to measure gas flow is that is difficult to correct for variations in temperature, pressure and humidity. While the calibration process is normally considered adequate to compensate for this, it is not ideal and does add another potential source of variation.

A statistical method was required which tested the level of agreement between the two data sets. The Bland Altman plot [98] provided such a test. This approach is based on graphical techniques and simple calculations. In this case the two measurement of volume produced by the different methods are combined and divided by two in order to produce a mean value for each measure. This is then plotted against the difference between the original two values, with the mean value on the horizontal axis and the difference on the vertical axis.

Graphical representations of this technique are demonstrated in Figures 3.2.2.1 and 3.2.2.2. The first is a simple plot of the tidal volumes produced by the two different techniques and demonstrates a linear correlation in the results over a 600 ml range (from 412 to 1030 ml). Figure 3.2.2.1 provides an example of the Bland Altman plot. This demonstrates no systematic error and a maximum difference of 60ml. At this point the question of how far apart measurements can be without causing difficulties needs to be asked. This is a question of judgement. The majority of the data points lie between the d ± (1.96) lines with only two outliers. This would suggest a reasonable level of agreement between the two forms of measurement but there are differences of up to 60 ml. Is that difference in measurements acceptable? The original aim of this work was look for some equivalence between two measures

not for close agreement. It was accepted that the true value would not be known and there were a number of sources of error within both techniques. The larger differences occur in the larger tidal volumes (of up to 1litre) and a difference of 60 ml, in this case, is not of concern. As such the circuit was accepted as appropriate for the study.

Figure 3.2.2.1 Tidal Volume of the pneumotachograph vs. the spirometer

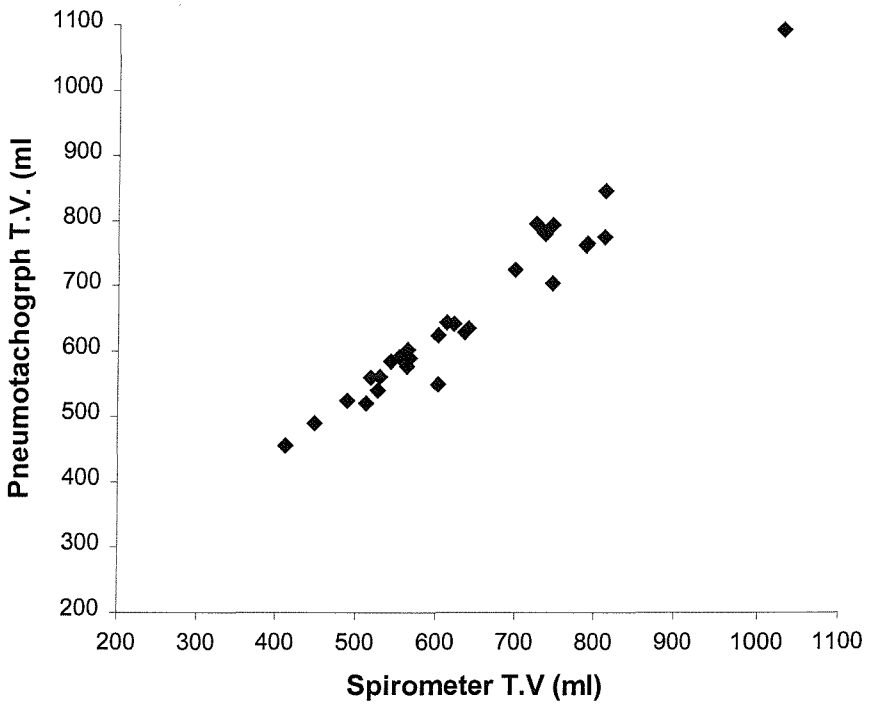

3.2.3 Radiolabelling human serum albumin

The use of Technetium (^{99m}Tc) bound with a freeze-dried micro-colloid such as human serum albumin (HSA) is widely used as described in section 2.2.3. Therefore it was not felt necessary to perform checks on the level of binding of the radiolabel to the colloid other than those routinely performed in line departmental protocols. This involved a process of paper chromatography and is

described in section 2.2.5. No disassociation of the label from the colloid was highlighted by these tests.

Figure 3.2.2.2. The mean of pneumotachograph and the spirometer inspired tidal volumes vs. the difference in volume.

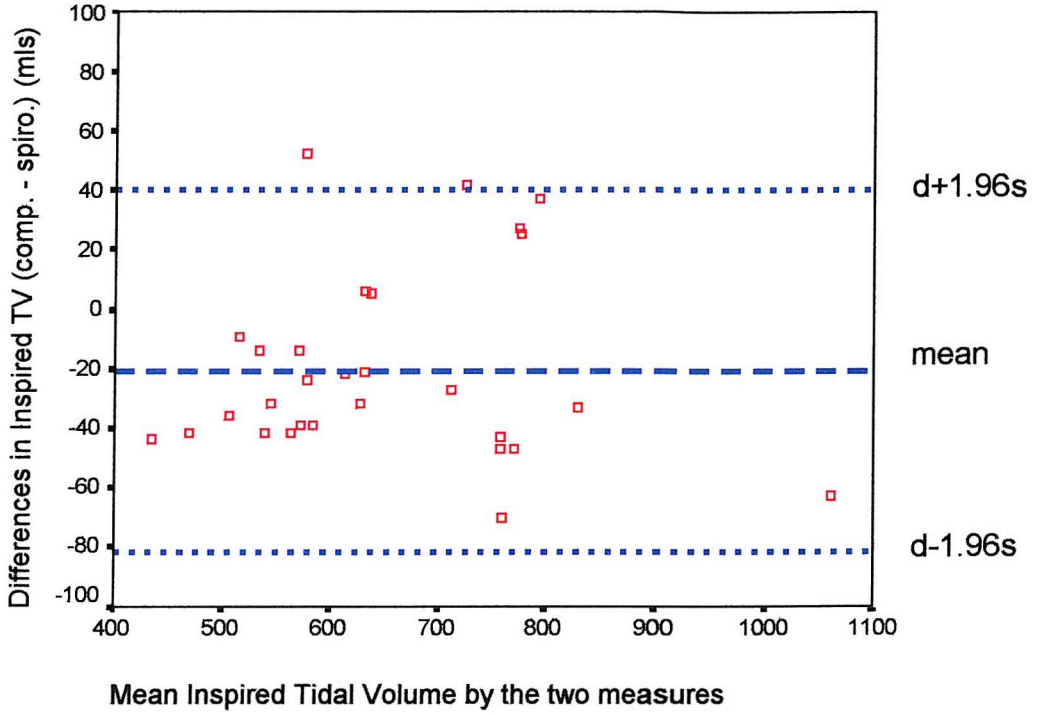

3.2.4 Analysis of the respiratory pattern during aerosol delivery

The computer recorded a variety of ventilatory parameters before and during the delivery of the aerosol. In part, this was a by-product of the programming to regulate and pace the subject's respiratory pattern as described in sections 2.2.2 and 2.2.2.1. It also allowed retrospective comparison of the individual subjects breathing pattern between visits and comparisons between subjects.

Prior to the aerosol delivery, the subject practiced to become accustomed to the regulated breathing pattern. During this period the programming calculated a predicted tidal volume and

respiratory rate. This would form the basis of the paced pattern. In addition, a vital capacity manoeuvre was performed in an attempt to correct the respiratory pattern to functional residual capacity. Once established on the regulated pattern the aerosol delivery would start. During the six minutes of administration of the radioaerosol, the actual respiratory rate, tidal volume, inspiratory and expiratory times were recorded.

A degree of variation in the respiratory pattern within the subjects is not surprising. The variation in the set tidal volume and rate was small but on the actual delivery there was wider variation. In part this variation is a product of the breathing circuit's sensitivity as some pauses in the respiratory pattern or occasions when the subject swallowed were recorded as breaths. It also underlines the difficulty in training subjects to breathe in a regulated fashion.

The data are summarised in Table 3.2.4 with the mean and standard deviation (in brackets) of each parameter recorded over the three separate deliveries of the aerosol for each subject.

Examples of variations in respiratory parameters.

Over the three visits, subject three had a mean total number of breaths of 111.5 with a standard deviation of 11.33 instead of the predicted 68. In contrast, subject 10 took a mean total of 65 breaths with a standard deviation of 1.73. This agrees well with a predicted rate of 10 breaths per minute over the six minutes that would give a total of 60.

Table 3.2.4 Ventilation parameters over the three visits during aerosol delivery

Subject no	VC (ml)	Predicted TV (ml)	TV (ml)	Resp Rate (Breaths / min)	No. of breaths (total)	Insp. Time (s)	Total Insp Time (s)	Total Exp Time (s)
1	6493 (915)	856 (22.3)	860.5 (117)	9.33 (1.15)	67.67 (6.66)	2.64 (0.59)	147 (36.3)	213 (36.3)
2	4418.7 (390.2)	686 (25.7)	657 (7.6)	10.67 (1.15)	86.33 (12.66)	2.19 (0.12)	140 (17.2)	220 (17.2)
3	5131.7 (104)	755.5 (24.8)	745 (38.2)	11.33 (0.58)	111.5 (16.26)	1.67 (0.25)	113 (7.9)	247 (7.9)
4	4333.7 (194.2)	646.7 (62.7)	618.5 (72.8)	12.33 (1.53)	92.5 (10.61)	1.5 (0.13)	110 (10)	250 (10)
5	5982.7 (458.4)	781.7 (55.8)	744.3 (77.7)	10.33 (0.58)	71.33 (0.58)	1.96 (0.27)	121 (16.8)	239 (16.8)
6	4008 (364.4)	610.3 (63.4)	572.3 (81)	8.67 (1.53)	68.67 (7.37)	2.27 (0.54)	121) (47.5)	239 (47.5)
7	4750.7 (341.2)	847 (35.7)	832.3 (90)	8 (1)	52 (7.55)	2.14 (0.34)	103 (25.6)	257 (25.6)
8	4889.3 (346.7)	774.3 (53.9)	765 (75.7)	8.33 (1.53)	51.67 (7.09)	2.16 (0.57)	106 (19.8)	254 (19.8)
9	4356 (308.4)	576.3 (56)	578 (48.5)	11.67 (2.08)	81.33 (9.81)	1.5 (0.07)	105 (17.5)	255 (17.5)
10	4222.7 (89.8)	572.7 (44.9)	561.3 (45.5)	10 (0)	65 (1.73)	1.59 (0.19)	95.4 (11.5)	265 (11.5)

VC (ml)	Vital Capacity
No. of breaths (total)	Total number of breaths
TV (ml)	Tidal Volume
Insp. Time (s)	Inspiratory time for each breath
Total Insp Time (s)	Total time of inspiration
Total Exp Time (s)	Total time of expiration

3.2.5 Selection of activity levels for SPECT markers

Prior to imaging the subjects, there was a need to select the level of radioactivity in the soft tissue and bony point markers used during the SPECT image acquisition. A selection of markers were injected with varying levels of activity and then placed on a acrylic water filled model of the thorax. This "phantom" was then imaged using the same SPECT protocol as the subjects. This is described in more detail in section 2.2.5. A simple review of the images generated indicated the level of the activity required. Too little would not be visible and too much would produce an artefact that could obscure activity in surrounding structures. Figure 3.2.5 demonstrates two examples of the SPECT data obtained. These two plates are transverse cuts and should be viewed as if facing the phantom with the right lung on the left of the plate. In figure 3.2.5.a the higher level of activity in the marker on the left (in this case 1.6MBq) can be seen to cause a streaking artefact making it unsuitable for use in the imaging. In comparison, there is no such artefact visible in figure 3.2.5.b with an activity in the marker of 0.2MBq. This demonstrates that 0.2MBq is a suitable level of activity to use in the markers for the SPECT protocol.

Figure 3.2.5.

a

a. A "streaking" artefact can clearly be seen as a result of the high level of activity in the marker on the left of the field. This could potentially obscure activity in the tissue underlying the marker.

b

b. With a lower activity level there is no streaking artefact visible.

3.3. Screening process prior to entry into the trial. Background data on the population measurement of airway calibre

The entry criteria for this study were based on clinical grounds, namely healthy male subjects with no history of airway disease. Two years previously, subject six had an episode of pneumonia but reported no limitation following this and required no ongoing medication and so was entered into the study.

In total, ten healthy male subjects with no smoking history were recruited and completed the study, with a mean (SD) age 28.7 (6.15) yrs, a mean height of 1.78 (0.08) m and a weight of 78.7 (5.35) Kg. Simple spirometry demonstrated normal pulmonary function with a mean FEV_1 of 4.60 (0.79) l. and a mean FVC of 5.63 (0.83) l. There was no evidence of airflow obstruction with a mean FEV_1 / FVC of 81.55 (6.7) %. Full data for airflow are presented in table 3.3.1.

As part of the image analysis it was necessary to know the functional residual capacity (FRC) of the subjects. This was calculated by helium dilution with the other figures of vital capacity (VC) residual volume (RV) and total lung capacity (TLC) being calculated at the same time. These figures are presented in table 3.3.2.

Having based the entry criteria on simple spirometry, it was of note that there was a wide degree of variation in some of the other parameters recorded, in particular MEF_{25} and MEF_{50}. It has been suggested that these measures may be of value in screening patients for mild airflow obstruction. MEF_{50} is not as reproducible as FEV_1 and so is not recommended for use in the clinical management of patients. In contrast, MEF_{25} can provide some evidence of airway narrowing but is not in routine clinical use [85]. So while these data suggest there may have been some small

airway obstruction in these subjects they were included as they met the clinically based entry criteria.

The lung volumes recorded for the subjects were within the normal range. The only exception for this was the ratio of residual volume (RV) and total lung capacity (TLC), which tended to be lower than predicted. This ratio will increase with the presence of airflow obstruction as the RV increases as a result of air trapping and therefore becomes a higher proportion of the TLC. A low figure is consistent with the healthy population recruited to this study and so these results would not exclude any subject from the study.

3.3.3 Skin sensitivity testing.

None of the subjects entered into the trial demonstrated any degree of sensitivity to the HSA or other allergens used in the skin testing. As such they were deemed suitable to continue onto the aerosol delivery phase of the study.

Table 3.3.1 Measurements of airway calibre by spirometry for the subjects entered into the study.

pt no	FEV_1 (l)		FVC (l)		FEV_1/FVC (%)		MEF_{50} (l)		MEF_{25} (l)		PEFR (l/min)	
	obs	pred	obs	pred	obs	pred	obs	pred	obs	pred	obs	pred
1	5.26	4.70	7.00	5.74	75.1	80.80	4.75	8.22	1.72	2.72	846	623
2	4.23	4.59	4.93	5.53	85.8	81.70	4.89	7.74	2.27	2.69	716	613
3	4.68	4.18	5.23	4.91	89.5	82.70	7.13	6.67	2.87	2.49	813	579
4	4.93	4.13	5.78	4.85	85.3	82.60	6.01	6.63	2.73	2.46	618	575
5	5.94	4.51	6.88	5.34	86.3	82.90	7.66	7.22	3.41	2.70	748	607
6	3.68	4.51	5.31	5.41	69.3	81.80	2.82	7.54	1.31	2.65	603	607
7	4.59	4.66	5.84	5.54	78.6	82.90	4.18	7.50	2.08	2.79	618	620
8	5.28	4.55	5.92	5.39	89.2	82.90	5.98	7.30	3.12	2.73	813	611
9	3.43	3.92	4.47	4.64	76.7	81.70	3.29	6.51	1.14	2.29	618	556
10	3.93	3.49	4.93	4.13	79.7	80.60	3.59	6.03	1.48	1.97	716	519
Mean	**4.60**	**4.32**	**5.63**	**5.15**	**81.55**	**82.06**	**5.03**	**7.14**	**2.21**	**2.55**	**710.90**	**591**
SD	**0.79**	**0.39**	**0.83**	**0.50**	**6.70**	**0.87**	**1.63**	**0.66**	**0.80**	**0.26**	**93.13**	**33.45**

FEV_1	Force Expiratory Volume in 1 second	**FEV_1/FVC (%)**	Ratio of FEV_1 & FVC as a percentage	**MEF_{25}**	Maximal Expiratory Flow at 25 % of lung volume	**l**	Litres
FVC	Force Vital Capacity	**MEF_{50}**	Maximal Expiratory Flow at 50 % of lung volume	**PEFR (l/min)**	Peak Expiratory Flow Rate	**l/min**	Litres per minute
obs	observed	**pred**	predicted				

Table 3.3.2 Lung volume data for the subjects entered into the study measured by helium dilution.

pt no	FRC (l)		VC (l)		RV (l)		TLC (l)		RV/TLC (%)		Age (yr)	Height (m)	Weight (Kg)
	obs	pred	obs	pred	obs	pred	obs	pred	obs	pred			
1	4.13	3.73	7.14	6.03	2.49	2.07	9.63	8.22	25.90	27.70	36.00	1.92	84.20
2	3.67	3.54	5.14	5.80	1.80	1.88	6.94	7.74	25.90	25.80	31.00	1.86	86.50
3	2.69	3.17	5.51	5.14	0.99	1.57	6.50	6.67	15.20	23.40	25.00	1.72	79.70
4	3.22	3.17	5.63	5.08	1.30	1.59	6.93	6.63	18.80	23.80	26.00	1.72	77.50
5	3.25	3.33	6.80	5.60	1.20	1.64	8.00	7.22	15.00	23.00	21.00	1.79	85.30
6	3.60	3.47	5.07	5.67	1.77	1.83	6.84	7.54	25.90	25.40	30.00	1.83	74.10
7	3.98	3.41	5.50	5.81	2.04	1.69	7.74	7.50	27.10	23.00	23.00	1.83	72.30
8	3.30	3.35	5.66	5.66	1.40	1.65	7.06	7.30	19.80	23.00	22.00	1.80	79.50
9	2.36	3.18	4.60	4.85	1.39	1.68	5.99	6.51	23.20	25.80	36.00	1.70	76.30
10	2.58	3.09	5.04	4.32	1.25	1.73	6.29	6.03	19.90	28.10	37.00	1.64	71.50
Mean	3.28	3.34	5.61	5.40	1.56	1.73	7.19	7.14	21.67	24.90	28.70	1.78	78.69
SD	0.59	0.20	0.79	0.53	0.46	0.15	1.05	0.66	4.55	1.95	6.15	0.08	5.35

FRC	Functional Residual Capacity	**RV**	Residual Volume	**RV/TLC**	Ratio of RV to TLC	**l**	Litres
VC	Vital Capacity	**TLC**	Total lung Capacity	**obs**	observed	**pred**	predicted

3.4 Image Analysis

The preceding section of this chapter described the results of the preparatory work to ensure the reproducible delivery of the aerosol in terms of particle size and respiratory manoeuvre to a clearly defined population. The remaining section will present the imaging and analysis required to describe the regional distribution of the radiolabelled aerosol within the lung.

This process involves several stages. Firstly the planar, two dimensional (2D) images give the total deposition and allow some limited analysis of the left and right lungs. Traditionally these images would also be used to provide some indication of the regional deposition in the form of a penetration index (PI), a ratio comparing the activity in the central lung to the periphery. This has approach has been superseded by a more sensitive three dimensional (3D) technique which divided the lung into 10 concentric shells around the hilum [66] [78]. This approach was used rather than the 2D technique to generate the PI. Finally the activity map for each study was fitted to a standard template in which the individual lobes and segments of the lung were defined. Both the segmental and shell analysis provide information on the regional distribution of the inhaled aerosol within the lung. As such a comparison of that distribution can be made between the positions the subject was in at the time of inhalation.

3.4.1 Total deposition and planar images

Table 3.4.1 presents the mean and standard deviation planar deposition data for the three positions in which the subjects inhaled the aerosol. The deposition data are presented in terms of the activity detected, both in absolute values and relative to the total activity emitted from the nebuliser.

It is of note that the total activity emitted from the nebulisers was consistent between the positions used. While this was not unexpected it was reassuring as these finding supported the earlier

results of the nebuliser output. The percentage of the generated aerosol deposited in the lungs was remarkably consistent between the three postures and there was no statistically significant difference in the total activity deposited in the lungs. The large standard deviation of the absolute activity in the right lung in right side lying is of note. This is the result of a particularly high value recorded in subject 6 (18.09 MBq). If this value were excluded from the analysis the SD would be in line with the figures recorded at 1.24

In contrast to the total deposition, there were obvious differences in the distribution of activity between the right and left lungs. To a degree this would be expected as the right lung with its three lobes has a larger volume than the left lung with two lobes. This should equate to higher ventilation and therefore improved deposition. These differences were increased by the changes in posture, particularly when the aerosol was inhaled in right side lying. When compared with both sitting and supine lying using a repeated measures analysis of variance the changes in activity achieved in side lying were significant ($p=0.001$). A similar comparison of sitting and supine lying did not reach a significant level ($p < 0.05$).

Table 3.4.1.1 The mean and (standard deviation) for all subjects of the activity deposited in the lungs in the three postures use

	Absolute activity MBq				**% of deposited activity in the right lung**	**% of generated aerosol deposited in lungs**
	Right lung	Left lung	Total activity in lungs	Total activity Emitted		
Sitting	6.70 (1.25)	5.83 (0.97)	12.53 (2.15)	57.30 (9.29)	53.35 (2.18)	22.99 (3.24)
Supine	7.53 (1.29)	6.26 (1.31)	13.79 (2.46)	56.74 (6.46)	54.69 (3.16)	24.40 (3.85)
Side lying	8.42 (3.6)	5.00 (1.59)	13.41 (4.93)	57.47 (14.80)	62.13 (6.34)	23.10 (3.53)

These results are visually presented in Figure 3.4.1. These are the planar images from subject 1 in the three positions. Areas of high activity and therefore deposition correspond to the bright colours and the darker areas with lower activity. A marked reduction in activity is visible in the left lung when the subject was in right side lying.

Figure 3.4.1

a. Sitting b. Supine lying c. Right side lying

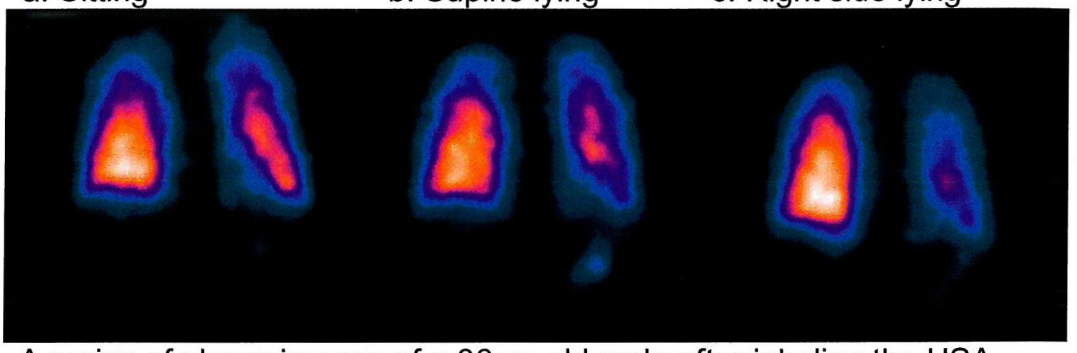

A series of planar images of a 36 yr. old male after inhaling the HSA radiolabelled with ^{99m}Tc in the three postures of sitting, supine lying and right side lying. They should be viewed as if facing the subject with the right lung on the left of the image, the head at the top and feet at the bottom. The small area of activity in the bottom left of the field is activity within the stomach. The bright areas correspond to areas of high activity.

3.4.2 Three dimensional analysis

The use of SPECT allows the distribution of the radioaerosol to be viewed in three-dimensions by a process of backprojection and mathematical modelling. These reconstructed images can then be viewed tomographically in sagittal, coronal or transverse planes. Examples of the images generated can be seen in figure 3.4.2 and do give an impression of differences in the distribution of the aerosol. While these are useful, to objectively review the data it needs to be applied to a model. In this case there were two available, shell or segmental analysis.

Figure 3.4.2

	Apical	Basal
These two plates were acquired after the subject inhaled in **sitting** and demonstrates increased deposition in the postero-inferior segments of the lung.	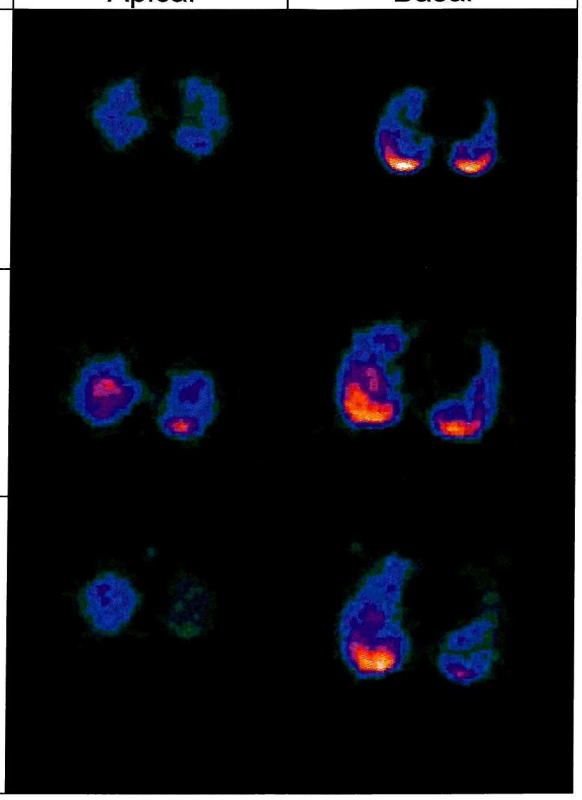	
These two plates were acquired after inhalation in **supine lying** and demonstrates a more even deposition throughout the lung.		
The above two plates were acquired after inhalation in **right side lying** and clearly demonstrates a marked difference in deposition with more activity in the right lung		

Each figure above demonstrates two examples of transverse, tomographic views, from a data set of a 34 year old male subject who inhaled a radiolabelled aerosol of HSA with a MMD of 1.5 µm. These images have been fully analysed, corrected for tissue attenuation and volume changes with image artefact removed. They should be viewed as if taken from below with the subject's right lung on the left of each image. The areas with the brightest colours are those with the most activity and therefore deposition. The slice on the left is taken from an apical section, around the level of the sternal notch and the one on the right from a basal section of the lung just below the nipples.

3.4.2.1 Shell analysis

The shell analysis is a technique that converts the spatial distribution of the radioaerosol into hemispherical shape divided into 10 concentric shells centred around the hilum of the lung. There was the possibility of some activity being present in the stomach as a result of the mouthwash to clear the oropharynx and oesophagus

of activity. This may have increased the apparent level of activity on the base of the left lung as this is located directly above the stomach. To avoid this occurring, the majority of the analysis was performed on the right lung only.

The data are presented in three forms:

- As a percentage of the total activity in the lung per shell.
- The activity concentration per shell.
- A penetration index calculated as a ratio from the inner five shells and the outer two.

The SPECT image acquisition results in a data set composed of volume elements or "voxels" measuring 0.467 cm^3. With the relatively small volumes of the inner shells this is a crude tool but becomes relatively more sensitive in the outer shell with larger volume. This change in sensitivity is reflected in the variability of the data with large variation in the central shell compared to the outer shells. Shell 10 also demonstrates wider variation. This can be attributed to the volume effect resulting from the resolution of the imaging technique. Other contributions to this variability results from the analysis technique itself, which adapts the data to fit an artificial model and the natural variations in the anatomy of the subjects. A larger sample size would have reduced the later but this was not possible. These data are the mean results from the subjects.

3.4.2.1 Percentage of total activity per shell

These data have been tabulated (Table 3.4.2.1) and then plotted in Figure 3.2.4.1 (this data has been off set to better show the error bars). In both presentations, the increase in the proportion of the inhaled activity within any shell increases the further away it is from the hilum is demonstrated. This is primarily a volume effect. The shells nearer the hilum have considerably smaller volume than those towards the periphery of the lung. Therefore a higher proportion of the total activity can be deposited in the outer shells. It

should be noted that the shell analysis corrects the results to a standard lung volume.

Posture appears to have little impact on the distribution of the activity between the shells. This is clearly demonstrated in Figure 3.4.2.1 with the lines for the three postures are all very similar. There was no statistically significant difference ($p > 0.05$) between shells as a result of posture.

Table 3.4.2.1 The mean percentage of the total deposited activity in the lung per shell for all subjects

Shell	Posture		
	Sitting Mean% (SD)	Supine Mean% (SD)	Side Lying Mean% (SD)
1	0.07 (0.03)	0.09 (0.05)	0.08 (0.03)
2	0.59 (0.12)	0.77 (0.34)	0.68 (0.24)
3	1.70 (0.21)	2.09 (0.61)	1.92 (0.47)
4	3.43 (0.44)	3.91 (0.82)	3.75 (0.55)
5	5.86 (0.77)	6.40 (1.13)	6.23 (0.71)
6	9.12 (1.26)	9.75 (1.58)	9.55 (0.97)
7	13.11 (1.92)	13.56 (1.79)	13.49 (1.25)
8	17.52 (1.83)	17.34 (1.41)	17.55 (1.02)
9	21.93 (0.81)	21.00 (1.71)	21.40 (1.06)
10	26.66 (5.49)	25.09 (5.39)	25.35 (3.51)

Figure 3.4.2.1

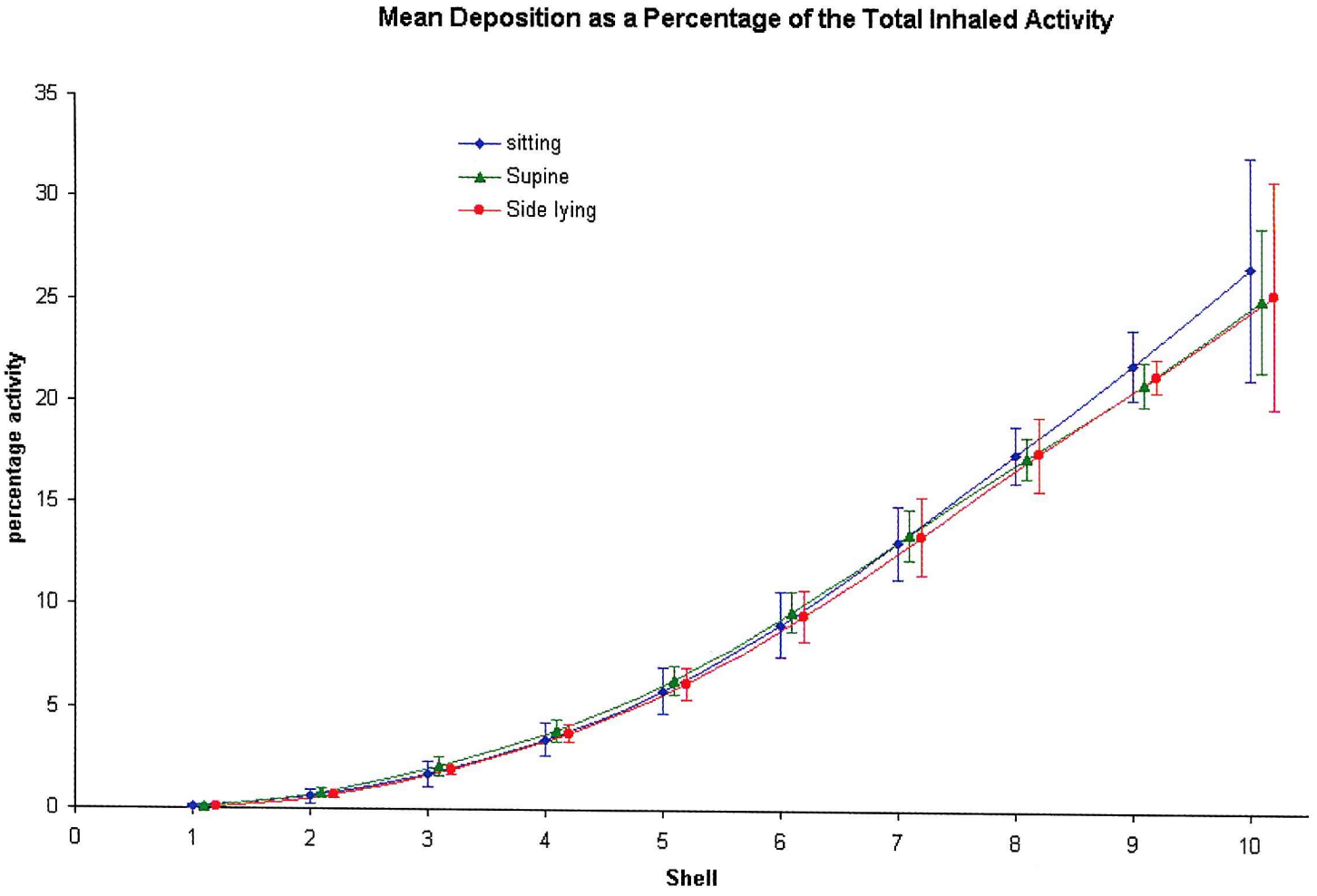
Mean Deposition as a Percentage of the Total Inhaled Activity
sitting
Supine
Side lying
percentage activity
Shell
0
5
10
15
20
25
30
35
0
1
2
3
4
5
6
7
8
9
10

3.4.2.2 Activity concentration per shell

This volume corrected figure is an expression of the percentage of the total inhaled activity per unit volume, in this case the percentage of the total inhaled activity per millilitre of lung volume. These data have been tabulated (Table 3.4.2.2) and then plotted as a graph in figure 3.4.2.2 (slightly off set to better demonstrate the error bars). As might be expected, with the volume differences between shells accounted for, a higher concentration of activity is seen in the inner shells. This would be

Table 3.4.2.2 Mean and standard deviation of the activity concentration per shell (% of total concentration /ml (normalized to the standard lung volume).

	Posture		
Shell	Sitting Mean %/ml (SD)	Supine Mean %/ml (SD)	Side lying Mean %/ml (SD)
1	0.055 (0.021)	0.070 (0.040)	0.062 (0.024)
2	0.053 (0.011)	0.070 (0.030)	0.062 (0.022)
3	0.053 (0.006)	0.065 (0.019)	0.060 (0.015)
4	0.053 (0.007)	0.060 (0.013)	0.058 (0.009)
5	0.054 (0.007)	0.058 (0.010)	0.057 (0.006)
6	0.055 (0.008)	0.058 (0.009)	0.057 (0.006)
7	0.056 (0.008)	0.057 (0.008)	0.057 (0.005)
8	0.054 (0.006)	0.054 (0.004)	0.054 (0.003)
9	0.052 (0.002)	0.050 (0.004)	0.050 (0.002)
10	0.049 (0.010)	0.046 (0.010)	0.046 (0.006)

Figure 3.4.2.2

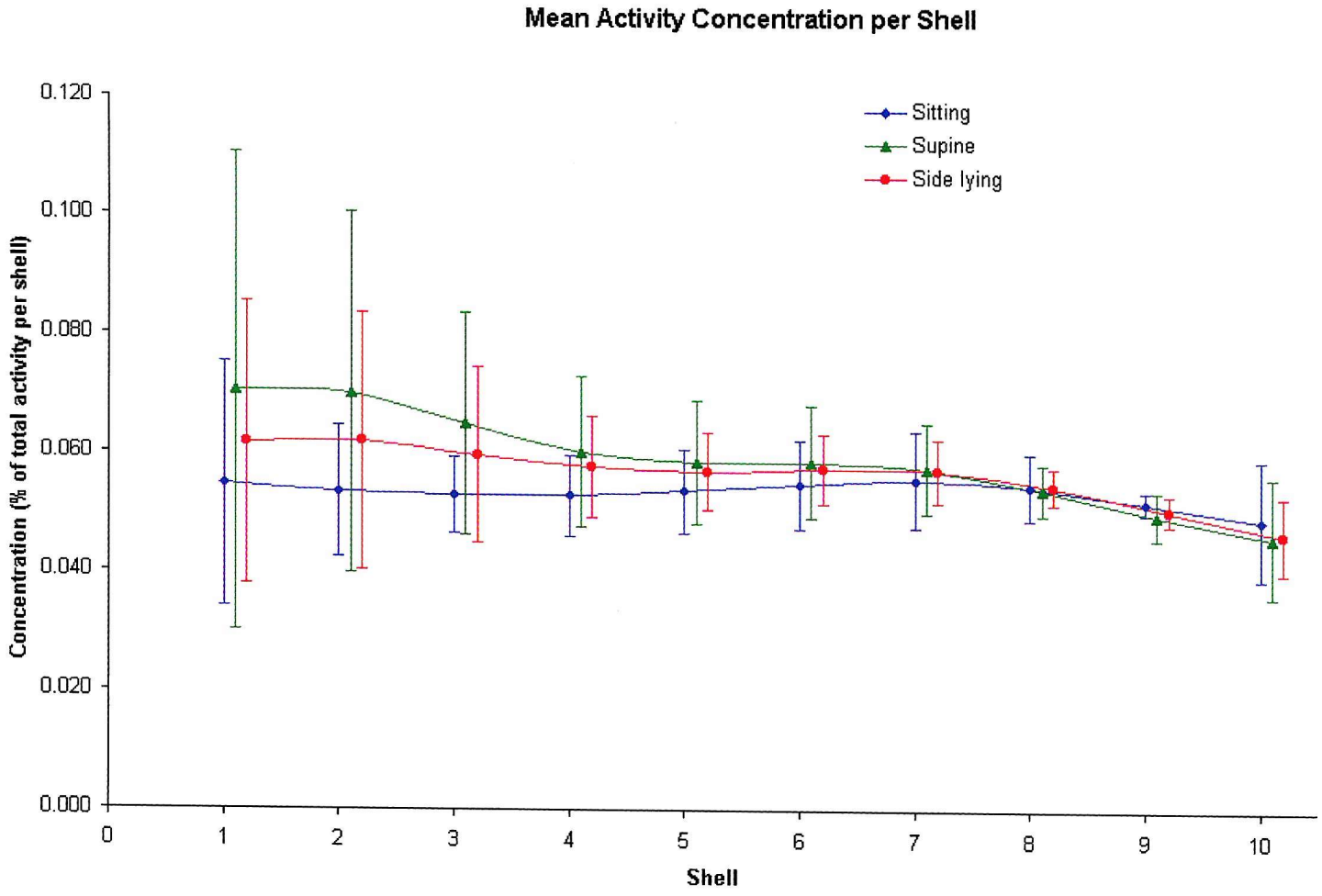
Mean Activity Concentration per Shell
Sitting
Supine
Side lying
Concentration (% of total activity per shell)
0.120
0.100
0.080
0.060
0.040
0.020
0.000
0
1
2
3
4
5
6
7
8
9
10
Shell

consistent with the impaction of larger particles within the central airways. Within any set posture, the data demonstrated a wide degree of variation between subjects for individual shells. There was no statistically significant ($p > 0.05$) difference in the activity concentrations of any shells with posture.

3.4.2.3 Penetration index

The Penetration Index, a technique that provided a comparison of the central to peripheral distribution of the activity, demonstrated no significant difference ($p> 0.05$) between the postures adopted for inhalation within the right lung. A full data set is presented in Table 3.4.2.3. To a degree, this may be surprising, especially on referring back to the planar images with the marked changes in the global distribution of the activity. This may well be as a result of shell analysis itself, which averages out the total activity for that entire shell. So while there may be localised areas of increased activity these are averaged out over the entire shell and lost in the analysis. Interestingly, some statistical significance was achieved by comparing the penetration index (PI) for left and right lungs in the same subject in different postures. These data were paired and tested with a T-test. This demonstrated a significant difference in the PI of the two lungs in the side lying position ($p = 0.002$). This was achieved despite the potential increase in the activity of within the left lung from the presence of the radioisotope swallowed into the stomach.

Table 3.4.2.3

	Sitting		Supine		Side lying	
Subject	Right lung	Left lung	Right lung	Left lung	Right lung	Left lung
1	0.67	1.13	0.55	0.93	0.59	0.98
2	1.35	1.37	0.87	0.7	1.07	1.43
3	0.68	1.01	0.37	0.45	0.62	1.01
4	1.03	1.12	1.07	0.78	1.02	0.97
5	0.76	1.32	0.92	1.4	0.9	1.22
6	0.9	0.79	1.09	0.85	0.79	0.87
7	0.93	0.73	0.89	1.03	1.01	1.04
8	1.09	1.11	0.96	1.02	0.74	0.96
9	0.93	0.87	0.95	0.96	1.13	1.3
10	1.34	1.29	0.62	0.81	0.72	0.96
Comparison of the Lungs in each posture ($p < 0.05$ **significant**)	0.218		0.45		**0.002**	

3.4.3 Segmental and lobar analysis

The segmental model translates the SPECT data set in a similar way to the shell analysis but instead of a series of concentric hemispheres, the data is fitted to a model that reflects the anatomical structures of the lung, namely the segments. This model moves away from describing the lung in terms of central and peripheral airways, but is also subject to some of the same limitations as the shell model. Those lung segments with a smaller volume show a relatively larger range in values reflected in a higher standard deviation than the segments with a higher volume. This is the result of the level of resolution of the SPECT data set with voxels of 0.467 cm^3. To a degree, this is compensated for when the segments are combined into the larger anatomical units of the lobes.

The data is presented in two forms:

- As a percentage of the total activity in the lung per segment.
- The activity concentration per segment. This is a volume corrected figure.

Statistical comparison was made using a Repeated Measures Analysis of Variance

3.4.3.1 Percentage of total activity per segment

These data are presented in two forms. The mean and standard deviation of the total activity in terms of a percentage of the total inhaled activity along with the volume of the individual lung segments are shown in Table 3.4.3.1. This data has also presented graphically in Figure 3.4.3.1.

These data demonstrate two sources of variation. Firstly there is the impact of volume. For example, it is by no means surprising that the Right Posterior Basal segment with a volume of 379.6 ml contained a mean of 12% of the total inhaled activity in the sitting position, whereas the Right Apical segment with a volume of 16ml only contained a mean of 0.74% of the activity. Second, it is of note that the posture does impact on the total amount of activity in each lung segment. This effect is not uniform throughout the lungs with some segments increasing and others reducing their proportion of the total inhaled activity. The Right Anterior Basal segment increases its proportion of activity from 10.02% in sitting to 11.05% in side lying, whereas the Left Posterior Basal segment drops from 13.42% in sitting to 9.57% in the right side lying posture. These changes would seem to suggest a redistribution of the inhaled activity.

Table 3.4.3.1 **Mean and (Standard Deviation) of the percentage of the total activity inhaled per lung segment**

Lung Segments	Volume (mls)	Sitting (S.D.)	Supine (S.D.)	Right Side Lying (S.D.)
R Hilum	15.79	0.42 (0.05)	0.49 (0.07)	0.54 (0.14)
R Apical	16.50	0.74 (0.14)	0.93 (0.19)	0.98 (0.27)
R Anterior	193.51	4.65 (0.69)	4.96 (0.46)	5.82 (1.09)
R Posterior	126.70	2.78 (0.47)	3.47 (0.61)	4.10 (1.02)
R Apical superior	189.74	8.27 (1.93)	7.91 (1.10)	11.02 (2.34)
R Lateral	38.60	1.30 (0.11)	1.46 (0.16)	1.63 (0.24)
R Medial	136.27	3.71 (0.60)	3.52 (0.53)	4.04 (0.72)
R Anterior basal	391.81	10.02 (0.58)	10.34 (1.23)	11.05 (1.12)
R Medial basal	147.88	5.83 (0.64)	5.83 (0.84)	6.52 (0.92)
R Lateral basal	67.52	2.83 (0.55)	2.51 (0.53)	3.30 (0.44)
R Posterior basal	379.59	12.16 (2.38)	12.12 (1.70)	13.35 (2.70)
L Hilum	8.76	0.21 (0.07)	0.26 (0.08)	0.18 (0.06)
L Apical	48.99	1.08 (0.34)	1.36 (0.28)	1.19 (0.49)
L Anterior	171.82	4.02 (0.70)	4.34 (0.64)	3.79 (0.96)
L Posterior	32.59	0.82 (0.15)	0.97 (0.18)	0.85 (0.23)
L Apical superior	226.92	7.93 (0.83)	8.04 (0.86)	7.12 (1.22)
L Superior Lingular	145.23	4.20 (0.52)	4.24 (0.48)	3.73 (0.63)
L Inferior	135.56	2.92 (0.42)	2.81 (0.53)	2.40 (0.52)
L Ant medial basal	386.51	10.23 (1.08)	10.50 (2.02)	7.32 (1.45)
L Lateral basal	120.08	2.46 (0.55)	2.42 (0.57)	1.51 (0.63)
L Posterior basal	357.59	13.42 (1.05)	11.51 (1.33)	9.57 (2.00)

Figure 3.4.3.1

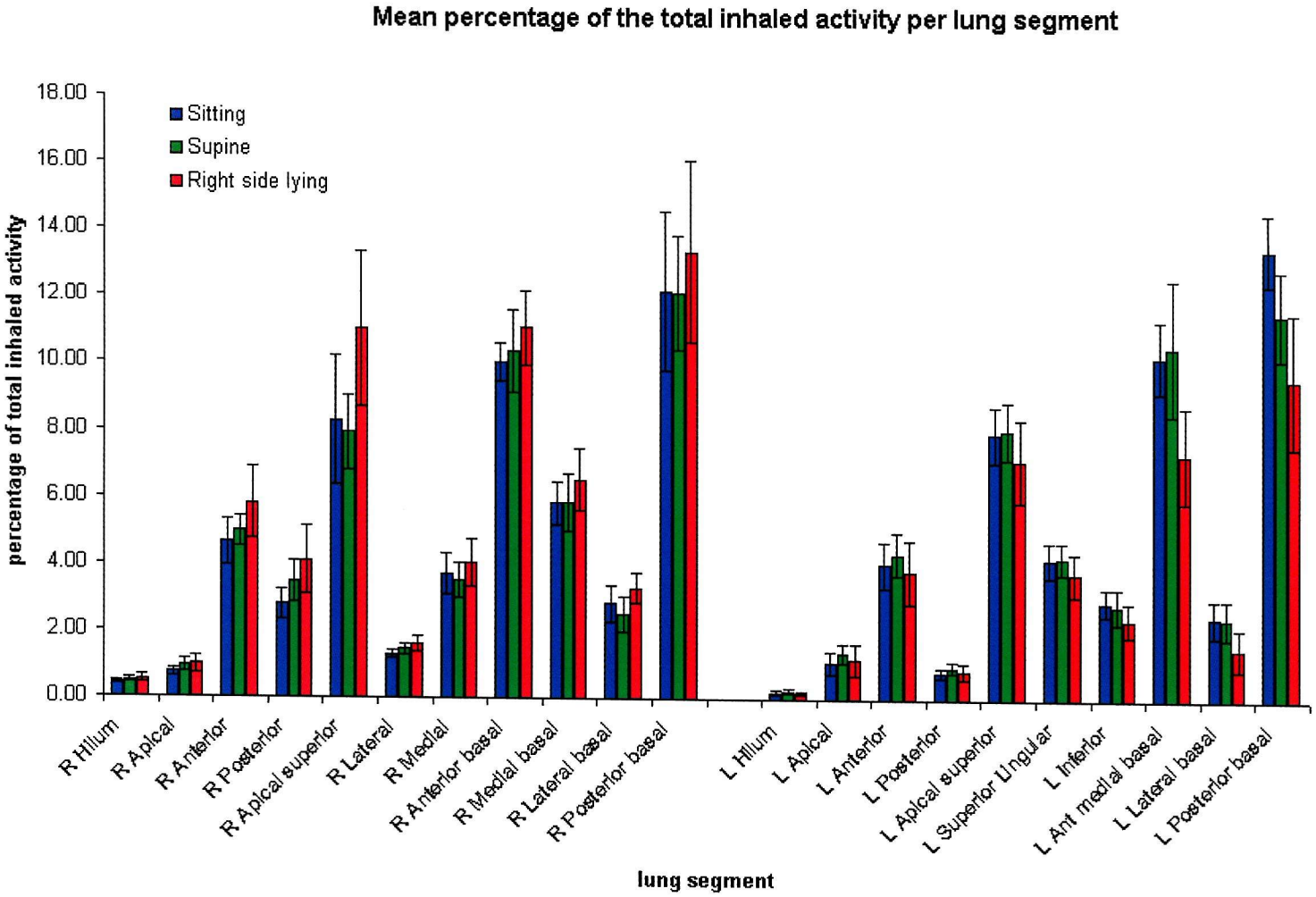
Mean percentage of the total inhaled activity per lung segment
Sitting
Supine
Right side lying
percentage of total inhaled activity
18.00
16.00
14.00
12.00
10.00
8.00
6.00
4.00
2.00
0.00
R Hilum
R Apical
R Anterior
R Posterior
R Apical superior
R Lateral
R Medial
R Anterior basal
R Medial basal
R Lateral basal
R Posterior basal
L Hilum
L Apical
L Anterior
L Posterior
L Apical superior
L Superior Lingular
L Inferior
L Ant medial basal
L Lateral basal
L Posterior basal
lung segment

3.4.3.2 Activity concentration per segment

While statistical analysis of the absolute levels of activity within the segments is possible it would seem logical to correct for the effect of volume before carrying out these calculations. This was achieved by dividing the percentage of the total inhaled activity by the volume of the segment. The results, in terms of percentage of total inhaled activity per ml of lung volume, have been plotted in figure 3.4.3.2. Having accounted for the effect of volume, there are clear differences in the concentrations of activity in individual segments between postures, with the concentration in some segments increasing and decreasing in others. Taking the sitting position as the standard it can be seen how the distribution of the aerosol is by no means even, with some segments having much higher activity concentrations than other. For example the apical segment of the upper lobe has a concentration of activity around twice that of the other two segments. Unsurprisingly a statistical comparison of the apical segment with the other two using the repeated measures analysis of variance (ANOVA) produced a highly significant result ($p<0.001$). In contrast the comparison of the other two segments did not approach significance ($p=0.176$).

The postural differences were tested statistically in a similar manner by a repeated measures (ANOVA), with a p value of less than 0.05 being considered significant. The results are presented in table 3.4.3.2. The comparison between sitting and supine lying produced six lung segments out of the twenty-one that achieved significance. Supine versus right side lying produced nine significant results but the comparison of sitting to side lying produced fifteen significant results.

Figure 3.4.3.2

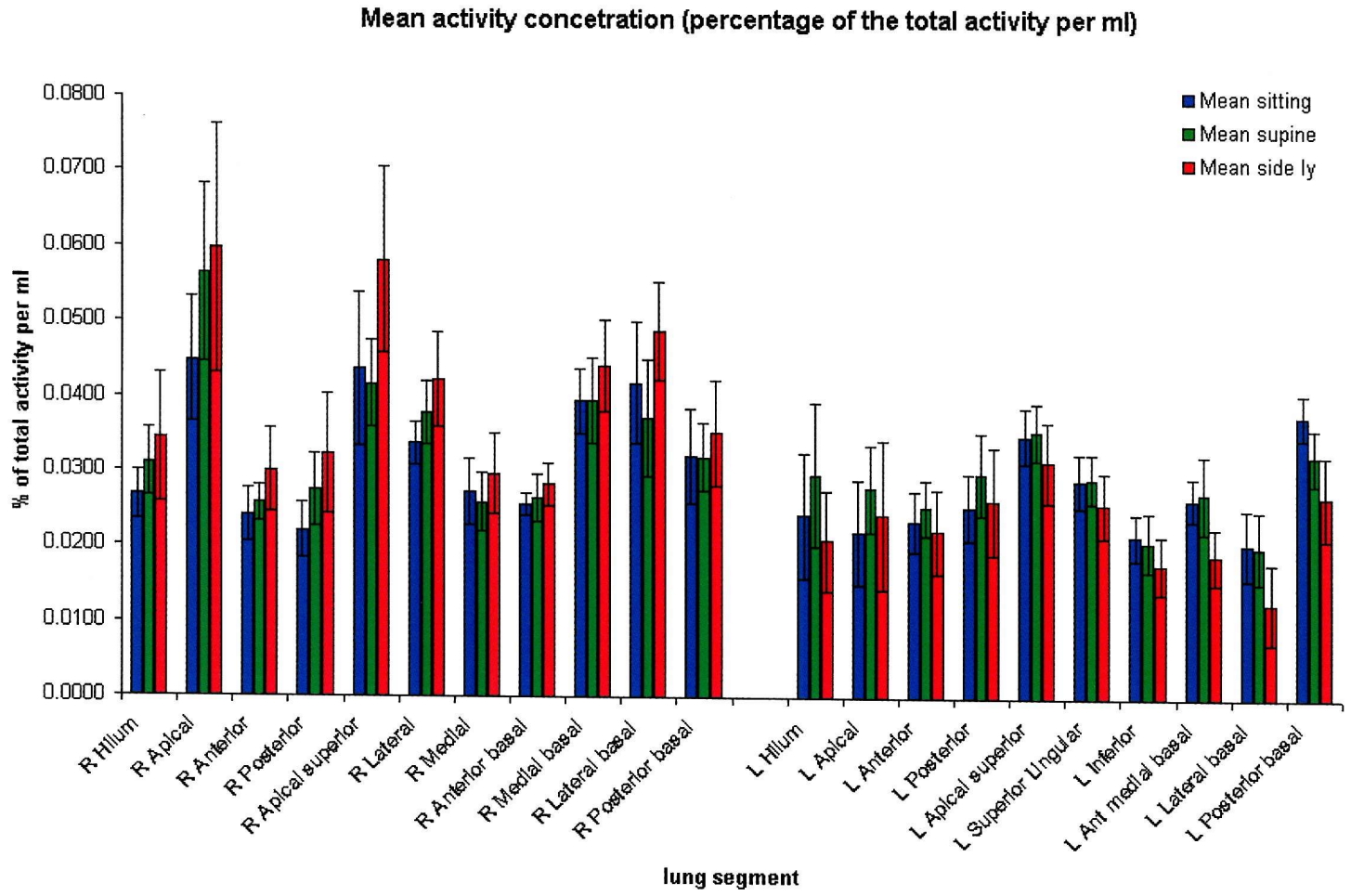
Mean activity concetration (percentage of the total activity per ml)
Mean sitting
Mean supine
Mean side ly
% of total activity per ml
0.0800
0.0700
0.0600
0.0500
0.0400
0.0300
0.0200
0.0100
0.0000
R Hilum
R Apical
R Anterior
R Posterior
R Apical superior
R Lateral
R Medial
R Anterior basal
R Medial basal
R Lateral basal
R Posterior basal
L Hilum
L Apical
L Anterior
L Posterior
L Apical superior
L Superior Lingular
L Inferior
L Ant medial basal
L Lateral basal
L Posterior basal
lung segment

Table 3.4.3.2 A Comparison of the activity concentration lung per segment in the three postures

	Comparison ($p < 0.05$ **significant**)		
Lung Segment	Sitting vs. Supine	Sitting vs. Right Side Lying	Supine vs. Right Side Lying
R Hilum	**0.018**	**0.05**	0.289
R Apical	**0.003**	**0.002**	0.549
R Anterior	0.104	**0.001**	**0.013**
R Posterior	**0.011**	**‹0.001**	0.061
R Apical superior	0.551	**‹0.001**	**0.001**
R Lateral	**0.021**	**0.001**	0.080
R Medial	0.509	**0.028**	0.167
R Anterior basal	0.373	**0.014**	0.074
R Medial basal	0.992	**0.049**	0.081
R Lateral basal	0.207	**0.010**	**0.001**
R Posterior basal	0.958	0.110	0.239
L Hilum	0.091	0.072	**0.015**
L Apical	**0.032**	0.243	0.186
L Anterior	0.078	0.224	**0.022**
L Posterior	0.075	0.631	0.146
L Apical superior	0.774	0.054	0.097
L Superior Lingular	0.727	**0.004**	**0.004**
L Inferior	0.454	**‹0.001**	**0.003**
L Ant medial basal	0.648	**‹0.001**	**‹0.001**
L Lateral basal	0.845	**‹0.001**	**‹0.001**
L Posterior basal	**0.006**	**‹0.001**	**0.017**

3.4.3.3 Activity concentration per lobe

By combining the data of the relevant lung segments together the concentration of activity in each lobe can be calculated. These results have been plotted in Figure 3.4.3.3 and the statistical comparisons are presented in table 3.4.3.3.

Figure 3.4.3.3 demonstrates the variation in activity concentration with posture. In the sitting position (in blue) the upper lobe in both the left and right lungs have a low concentration when compared with the dependant lower lobes. In the supine position (in green) the posterior sections of the upper lobes become

dependent and this is reflected by a small increase in the activity concentration. The lower lobes which are principally located in the posterior portion of the thoracic cavity remain dependent and the activity concentration changes little. In the right side lying position (in red) the entire right lung becomes dependent with an increase in activity whereas the left lung is now superficial and has a marked reduction in the activity concentration.

Table3.4.3.3 summarises the statistical analysis of the lobar concentration with significant results ($p < 0.05$) in **bold** type. A repeated measures analysis of variance was used to compare the activity concentration of each lobe for each subject in each of the three positions. The movement from sitting to supine lying produced an increase in concentration in the right upper lobe that was significant, as was the reduction in activity in the left lower lobe. The increases in the concentration for the right lung and decreases for the left on moving from sitting to side lying were all significant. The movement from supine to side lying bought an increase in the activity in the right lung, but this did not achieve significance in the middle lobe. The accompanying reduction in activity in the lobes of the left lung did, however, reach significance.

The lobar analysis with only five rather than twenty-one lung regions to compare, provides an easier model in which to observe the changes which arise as a result of the changes in posture. This is probably best seen in figure 3.4.3.4, which combines a schematic lateral view of the lungs demonstrating the positions of the lobes with figure 3.4.3.3 and the statistical analysis of table 3.4.3.3 In the centre of the diagram are the lateral view of the left and right lung divided into the five lobes. An arrow leads away from each lobe to a bar graph of the activity concentration and the p value for each comparison of posture. When a region of the lungs becomes dependent as the subject changes position, the concentration of activity increases. At the same time the regions which become non-dependent have a reduction in their activity concentration. .

Figure 3.4.3.3

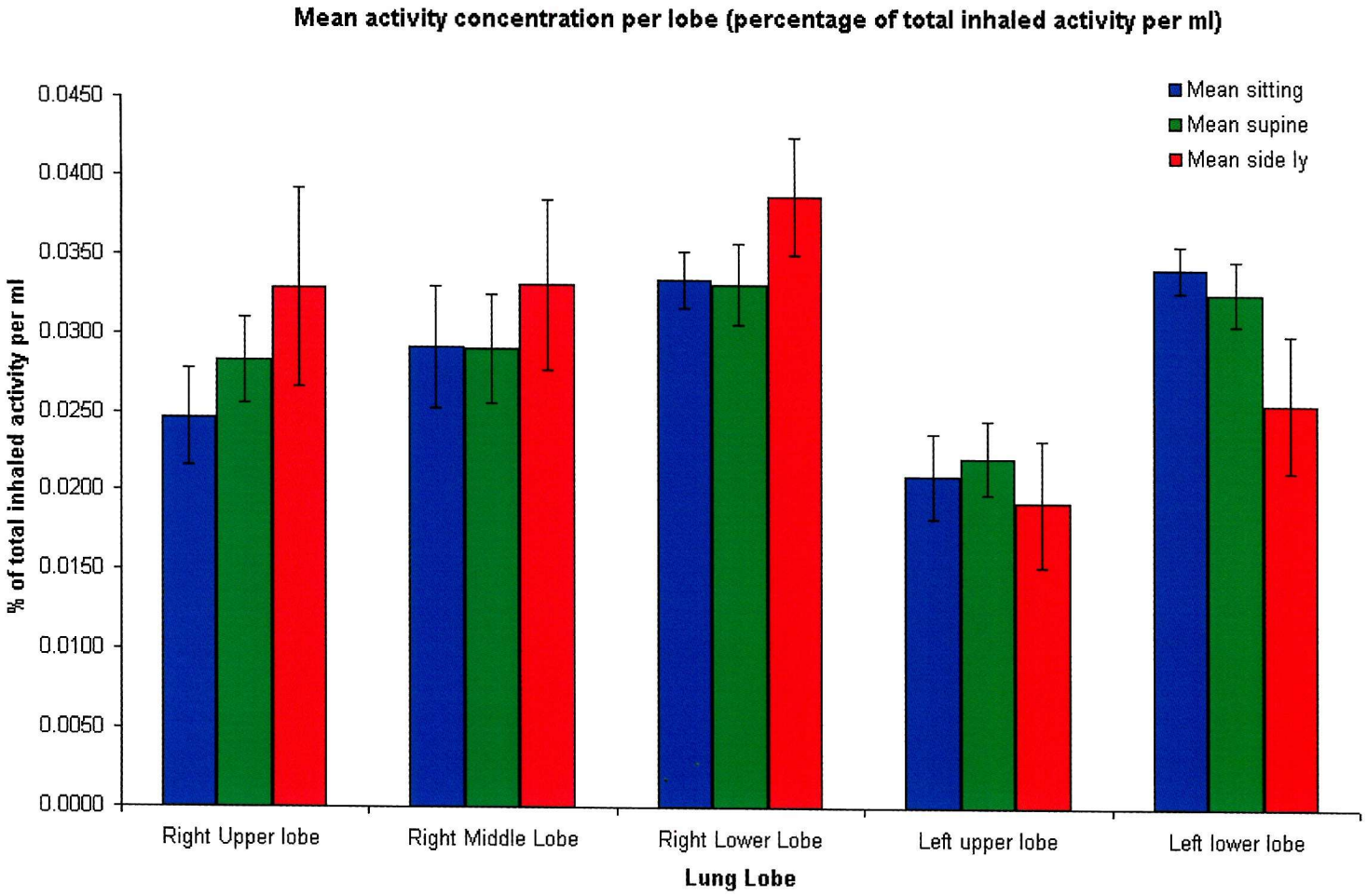
Mean activity concentration per lobe (percentage of total inhaled activity per ml)
Mean sitting
Mean supine
Mean side ly
% of total inhaled activity per ml
0.0450
0.0400
0.0350
0.0300
0.0250
0.0200
0.0150
0.0100
0.0050
0.0000
Right Upper lobe
Right Middle Lobe
Right Lower Lobe
Left upper lobe
Left lower lobe
Lung Lobe

Table 3.4.3.3 A Comparison of the concentration of the deposited activity in each lobe of the lung in the three postures

	Comparison ($p < 0.05$ **significant**)		
Lung Lobe	Sitting vs. Supine	Sitting vs. Right Side Lying	Supine vs. Right Side Lying
Right Upper Lobe	**0.002**	**‹0.001**	**0.031**
Right Middle Lobe	0.955	**0.006**	0.130
Right Lower Lobe	0.692	**0.001**	**0.001**
Left Upper Lobe	0.052	**0.034**	**0.005**
Left Lower Lobe	**0.021**	**‹0.001**	**‹0.001**

Figure 3.4.3.4

An Illustration of the lobar activity concentration and it change with posture

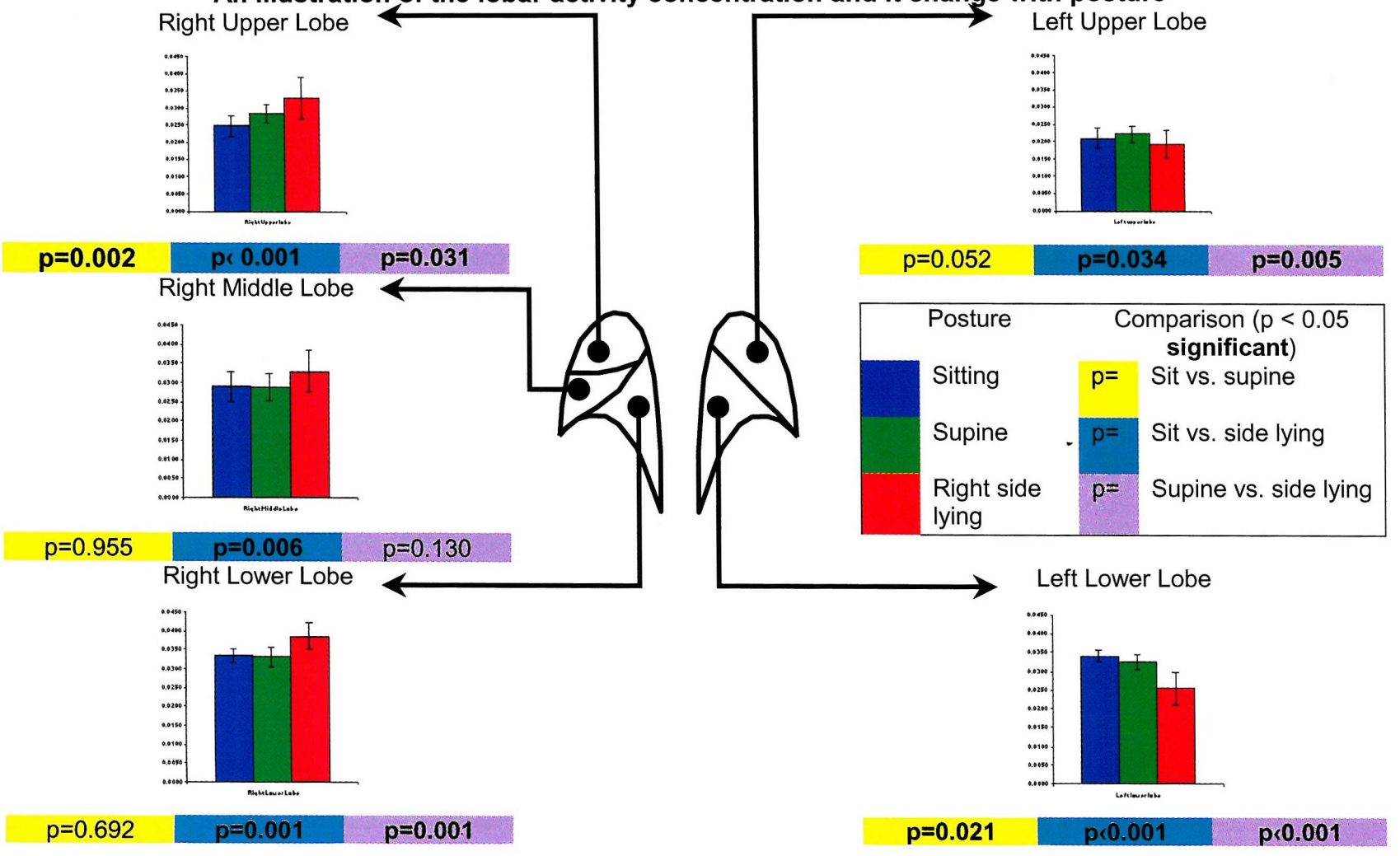

In summary the planar analysis demonstrated similar total deposition of the aerosol but a significant difference in activity in the right and left lungs when sitting or supine lying were compared to the side lying posture ($p=0.001$). The Shell Analysis did not show any significant difference in aerosol distribution with posture in the right lung but when the penetration indices of the two lungs were compared in the different postures, side lying produced a significantly higher result ($p=0.002$). The segmental model demonstrated clear differences in the activity concentration with posture. This effect was not uniform throughout the lung.

Chapter 4 Discussion.

There remains a fundamental difference in the literature describing the distribution of an inhaled aerosol within the lung. The majority of the aerosol science work divides the lungs into central and peripheral regions. This stems from the current, accepted standard of imaging to assess the distribution of an inhaled aerosol, namely planar radioisotope studies. This technique is two dimensional (2D) in nature and as such, has a limited resolution. This has some obvious limitations, as this form of imaging projects a three dimensional (3D) structure in 2D. Structures that are overlying one another are effectively indistinguishable. The image analysis has been developed to attempt to address this problem by identifying regions of interest, namely the central or peripheral regions of the lung. The central regions principally equate to the main airways, while the peripheral regions relate to the distal airways and alveolar region. Whilst these methods formed the basis of the current understanding of aerosol behaviour within the lung, the division into only two regions does not reflect the anatomy or dynamic nature of the lungs.

In contrast, the clinician would tend to describe the lung in terms of its anatomical structures, the lobes and segments. A network of airways and blood vessels supplies the gas exchange units within these regions of the lungs. The lobes are physically separated from each other by the fissures of the lung that are lined by the pleura and this allows each lobe to function as an independent unit. In essence, the lung is not a uniform structure but has different regions with varying levels of ventilation. This is consistent with the current understanding of the ventilation gradients within the lung from apex to base. It has been suggested that these ventilation gradients change as the body position changes. Assuming that deposition will follow ventilation as suggested by Chamberlain et al [99], it would seem logical that the variations that occur in ventilation with posture would be reflected in the aerosol deposition patterns. Areas with more ventilation, more

deposition and areas of less ventilation, lower deposition. It was on this basis that the hypothesis was formulated that.....

the posture of an individual, at the time of inhalation of an aerosol, has an effect on the final destination of the aerosol within the lung.

The principal aims of the study were to:

1. To assess the in vivo, three-dimensional (3D) intra-pulmonary regional deposition of an inhaled, radiolabelled aerosol using single photon emission computed tomography (SPECT) aligned with magnetic resonance imaging (MRI).

2. To establish if the intra-pulmonary deposition of an inhaled particle is affected by the postural position of a healthy subject.

To test the hypothesis and achieve the stated aims, several clear stages needed to be completed. Prior to the imaging, systems needed to be in place to ensure that the aerosol was delivered in a reproducible manner to a controlled population. The output of the nebulisers needed to be reviewed to ensure they were consistent over the delivery time and on separate visits. There needed to be a system in place to regulate and control the subject's respiratory pattern on inhalation of the aerosol over the three separate visits, despite the changes in posture. Finally, there was a need to screen the subjects to ensure that they all met the entry criteria. These were all achieved satisfactorily and so the imaging could proceed.

The planar imaging demonstrated no difference in the total deposition between the postures used, but there was a significant difference in the distribution of this activity between the right and left lungs when the side lying posture was compared to sitting or supine lying ($p=0.001$).

With such highly significant results generated by the planar data and images (see Fig 3.4.1), it cold be argued that there was little additional value in the 3D data. It is more time consuming than 2D in terms of image acquisition and analysis, plus exposes the subject to comparatively higher levels of ionising radiation. This would certainly be the case if the distribution was being investigated in terms of total dose or response to a pharmacological agent as previously suggested [4]. However, it should be remembered that the structure that was imaged (the thorax) is 3D in nature, and so 2D techniques results in images where structures overlying one another. So while it may be possible to discriminate central to peripheral distribution, it is not possible to be more discriminating. As such, the use of a 3D technique is not only more sensitive than 2D techniques to calculate the central to peripheral ratio [100] but also allows quantification of aerosol deposition in the "geographical" terms of lobes and segments. With these areas defined, the impact of posture can be more clearly demonstrated as the activity concentration and hence deposition pattern can be seen to rise and fall with posture.

Two forms of analysis were used to review the 3D data sets generated following the delivery of the radioaerosol. Shell analysis gave an impression of the central to peripheral distribution of the aerosol. There was no significant difference in the penetration of the aerosol into the right lung between postures. Interestingly, when the data for right and left lung were paired for each posture, this produced a significant result for the side lying posture. The application of a segmental model to the data gave a different impression of the distribution of the aerosol. This was more in keeping with "geographical" regions of the lung. In contrast, with the shell analysis, this did produce a variety of results some of which reached significance ($p<0.05$) and others that did not as the activity levels rose and fell in the different postures. This suggested that effects of changing posture were not uniform throughout the lung.

Effective nebuliser therapy requires a device that repeatedly and quickly delivers sufficient drug to the site of action [101] and therefore, the performance of the nebuliser selected is vital. In the case of this work, not only was there the need for reliable and consistent aerosol delivery but also a sound understanding of the output of the nebuliser, as this directly related to the delivered dose of radioactivity

The choice of the optimist, a nebuliser that is no longer in commercial production, may be surprising but there were sound reasons behind this decision. This nebuliser was well known to the Southampton Aerosol Group. Its output had been described in detail previously by other members of the team [66] and so it was felt that further, detailed investigations would not be required. Had a different nebuliser been selected, this detailed characterisation work would have been repeated on all of the chambers to be used prior to the clinical imaging. Even with this consideration taken into account, it was important to review the output of the nebulisers to be used in terms of particle size, as wide variation in the particle size generated by nebulisers, even from the same batch, have been reported [102]. This would ensure their output and performance was both comparable and consistent.

The results from the laser diffraction measurements did demonstrate that the particle size generated by individual nebulisers was comparable with a range of 0.5μm but it was of note that the particle size was reduced by the addition of the human serum albumin (HSA). This was contrary to the previous experience of the Southampton Group [66] and other published work [84]. The preparation of HSA used in this study was different from that previously used, so this may provide an explanation. Also, a degree of foaming was noted in the nebuliser chamber when the aerosol was being generated. This suggests that there may have been some reduction in the surface tension of the solution. Recent work has suggested that this would have an impact on the nebuliser output [103]. While this is certainly of

interest it was not central to the thesis and therefore was not pursued.

Having controlled the generation of the aerosol to be delivered to the subjects within the study, it was also necessary to attempt to control another of the key determinants of deposition, that is the respiratory manoeuvre. It is widely accepted that changes in both the flow rate and respiratory cycle will influence the deposition of inhaled aerosols. The challenge was to develop a system that, as far as possible, encouraged and regulated the subject to breathe at a normal tidal volume from functional residual capacity (FRC) during the aerosol delivery. In addition, there was a need to monitor and record the respiratory pattern to allow comparisons between visits.

With no suitable commercial system readily available, there was a need to modify equipment that had been developed "in house". Previous work had produced a partial solution to this problem [66], a closed circuit breathing system, consisting of milled blocks, minimal resistance valves and pneumotachographs, attached to a computer running a specific programme to produce a self-regulated breathing pattern. This pattern was selected to mirror the delivery of aerosols to patients clinically. After a training period, the computer programme would analyse the subject's respiratory pattern to produce a target rate and volume for them to follow.

The system had been developed to control a subject's respiratory pattern on two separate visits during the delivery of aerosols with two different particle sizes. While it did control and regulate the breathing pattern very well, it did not address the problem of changes in background lung volumes (principally FRC) as a result of either breathing from a circuit or from changes in posture. So before it could be used within this study, there needed to be some modifications made to the programming. This took the form of a vital capacity manoeuvre, similar to the approach of Chan et al [56] but with the aim of the subjects breathing from FRC and not one litre above that value. The changes to the programme

were completed by the original programmer (Mr Frank Anderson) under the supervision of the author. With this addition to the programming in place, it was felt necessary to review the reliability of the system against the accepted standard for measurement of lung volumes, in this case a bell spirometer. The two systems were connected in series, to allow simultaneous measurements.

The spirometer recorded volume change directly by tracing a pen line on to a chart recorder moving at 60 mm/ min. This limited its accuracy, as all measures needed to be taken from this trace by hand, using a rule to measure the displacement of the line. It also had a limited volume of 8 litres. As the aerosol circuit would run with 8l per minute of air driving the nebuliser this caused two problems: one, the spirometer need to be calibrated for this flow rate; and two, it only allowed for short runs of data collection before the spirometer would need to be emptied. In addition, all volumes taken from the spirometer needed to be corrected for changes on temperature and atmospheric pressure. So, in essence, while the bell spirometer was accepted as the "gold" standard for volume measurement, with a number of potential sources of error, it was not the most accurate means of recording volume. The pneumotachographs in the aerosol deliver circuit once calibrated recorded volume as a result of the pressure drop. Therefore, the comparison of the two techniques was of a measure of volume of limited accuracy (the spirometer) against a measure of volume of uncertain accuracy (the aerosol circuit). With the true value of the volume not known, there was a need to look for a level of agreement between the two data sets. This was achieved by applying a Bland Altman plot [98] to the data, an approach based on graphical techniques and simple calculations. The results of this analysis on the data produced by the two techniques prior to the imaging portion of the study demonstrated an acceptable level of agreement for both tidal volumes and vital capacity and, therefore, the system was deemed appropriate for use within the study.

With the system to regulate and record the respiratory pattern of the subjects in place the delivery of the aerosol was possible. The subjects found the system relatively easy to use and became accustomed to the regulated respiratory pattern relatively quickly. However the results demonstrated a wider degree of variation than had been expected or previously experienced. For example, while subject two produced a mean tidal volume of 657 ml, with a standard deviation of 7.55 over the three visits, subject one's mean tidal volume was 860 ml, with a standard deviation of 117. This did not appear to be related to a training effect nor was this variability related to the posture in which the subjects were positioned. All subjects were allowed to breathe on the circuit until they felt entirely comfortable, before the aerosol delivery and data collection. One explanation of this wider variation than expected comes from the sensitivity of the circuit. If the patient were to swallow or pause during the delivery, a small tidal volume would be recorded. This would skew the results for individual sessions and result in wider variation in tidal volumes.

A similar variation in the inspiratory to expiratory (I:E) ratio of the respiratory pattern was also noted, with some subjects varying more than others. This was important as while the nebuliser was producing an aerosol throughout the six minutes of the delivery, deposition could only occur during the inspiratory phase of the respiratory cycle. These findings were also counter to the previous experience and would have influenced the deposition of the aerosol.

In addition, there was also a discrepancy between the vital capacity measured by the breathing circuit prior to aerosol delivery and that measured by Helium dilution, with the value produced by the circuit being consistently lower. This is not as unexpected as the other variations in the respiratory parameters and there are a variety of explanations for this. These measurements were not made simultaneously under the same conditions nor did the same individual supervise them. Therefore the degree of encouragement

will have been different. The subjects could have had a full lung function screening prior to each delivery of aerosol. This may have allowed a better comparison but was not practical. It should be remembered that the primary aim of the manoeuvre within the aerosol delivery was not to provide an accurate measure of volume but an attempt to ensure the individual was breathing from FRC. In that respect, the actual value was irrelevant. What was important, was that the subject had gone through the process of a maximal expiratory manoeuvre to reduced the possibility of them breathing at an artificially high lung volume. In this respect, the manoeuvre appeared to be successful, although the only sure method of ensuring that the individuals were breathing from FRC would have been to measure the value simultaneously. As has been stated, this was not possible.

For the subjects to work well with the regulated breathing pattern, they needed a clear view of the computer screen. This was relatively easy in the sitting or side lying positions but was more of a challenge in the supine lying position, where they would need to turn their heads to one side. There is some evidence, from MRI studies, that the lateral dimensions of the upper airway are reduced when the head is rotated [104]. This change in the architecture of the upper airway would have had some impact on airflow and therefore the deposition pattern. A simple solution to this problem was the use of a small mirror held by the subject. This maintained head alignment and allowed a clear view of the screen. The fact that the mirror reversed the screen display did not prove to be a problem for any of the subjects. A more straightforward solution would have been to move the screen to above the subjects' head. This was not practical, as no suitable support was available for the computer monitor within the clinical area where the aerosol was delivered.

The control of the respiratory pattern while delivering an aerosol is not straightforward and some subjects managed this better than others. No particular pattern with posture or in the order

of the delivery was noted. In comparison to the previous use of this circuit [66], there appeared to be a wider range in values obtained between and within subjects. There is no obvious reason why this should be the case. In many respects, this finding underlines the difficulty of delivering an aerosol in a controlled and reproducible manner. In retrospect, there may have been some value in reviewing subjects' compliance with the delivery equipment, prior to admission to the trial, rather than using a screening process based past medical history and the results of their lung function tests. This may have produced a more consistent delivery of aerosol.

The aims of the screening process were two fold: first to ensure the safety of the subjects who volunteered to participate; and secondly to make certain the aerosol was delivered to a controlled healthy population with comparable lung function. This was achieved by recording a clear medical history, the use of skin sensitivity and pulmonary function tests. There are clearly accepted standards and guidelines that apply to the protocols and equipment to be used for tests of both pulmonary function [86] and skin sensitivity [87]. These standards were applied in the screening of the subjects. No subjects had a positive skin test to the HSA, all had pulmonary function within normal ranges and there was no reduction in airway calibre after the administration of the aerosol. While the MEF_{25-50} results were suggestive of a small degree of airflow obstruction, these figures are not routinely used in clinical practice and so did not exclude the subjects from the study. As such, the aims of safety and controlling the population were achieved.

Having discussed how the aerosol was delivered to a controlled population, the techniques used to image its distribution will now be discussed. The current accepted standard of imaging to assess total lung and oropharyngeal deposition of aerosols labelled with gamma- ray emitting radionucliotides such as ^{99m}Technetium is two-dimensional, planar, gamma scintigraphy with estimates of regional lung deposition being made by drawing

"regions of interest" on the images acquired. This is dependent on appropriately validated and suitable corrections being made for attenuation of the gamma rays by body tissue [3]. It should be remembered that in any gamma scintigraphy, the distribution of the aerosol is imaged and not the anatomy of the lung.

In this study planar images were acquired of the subjects to calculate the total deposition to provide a basis for the later 3D analysis. This simple data could easily be reviewed to test the hypothesis. First impressions simply by examining the images generated suggest that there were marked differences in the distribution of the total activity between the lungs in different postures. This was confirmed when the activity between the lungs was quantified with the most significant results produced by the comparison of right side lying and sitting postures ($p=0.001$). These results would appear to support the hypothesis and are consistent with current thinking, namely that dependant lung units will be better ventilated. Improved ventilation will result in improved aerosol deposition. The next logical question is what additional information does the 3D over the 2D analysis give regarding the regional and geographical distribution of the aerosol?

As has already been stated, any gamma scintigraphy data, even when corrected for attenuation, will only give the distribution of the radioisotope and is not related to the anatomy. So the challenge is to find a method that will allow the scintigraphy data to be matched to the anatomy.

This was first attempted with the shell analysis. The SPECT data is fitted to a model of the lung that converts the lung into 10 hemispherical shells centred on the hilum. The hilum and lung edge are identified, then each voxel (volume element) assigned to the relevant shell dependent on how far away it is from the hilum or lung edge. This has been demonstrated to be more sensitive than planar imaging when assessing the penetration of the aerosol into the peripheral lung [105], it does, however, still compare the central lung as a unit to the peripheral lung.

This model was applied to the right lung of this data set in order to avoid any chance of swallowed activity in the stomach affecting the results. When statistically analysed the results did not show any significant differences as posture changed ($p < 0.05$). This was somewhat surprising bearing in mind the planar data. It was only when the Penetration Index for left and right lungs of each subject were paired and compared in the different positions that any significant differences were noted in the side lying position ($p = 0.002$). Why should this be, especially when one looks at the initial planar data that supported the hypothesis?

The shell analysis was designed to investigate the penetration into the peripheral lung as a whole and so does not differentiate between geographical areas. A useful analogy would be a bowl with a small volume of water at the bottom. The shell analysis creates a mean value for the entire internal surface of the bowl and so the small area of high concentration, namely where the water has pooled at the bottom, is lost as the mean value for the entire internal surface is generated. So while shell analysis is a more sensitive tool for measuring the penetration of an aerosol into the lungs than planar imaging, it does not add to the understanding of the geographical distribution between lung segments and lobes. To achieve this required a means of relating the SPECT data with the airway morphometry.

The anatomical details of each subject were obtained using Magnetic Resonance Imaging (MRI) and matched to the SPECT data by markers on soft tissue structure (the nipples) and boney points (Sternal notch and xiphisternum). MRI does have the advantage of not increasing the exposure to ionising radiation but the 0.5 Tesla magnet used in this study, lacked the definition of the airways that high resolution Computer Tomography (CT) would provide. So while the bone and soft tissue could be distinguished well enough to allow the construction of the attenuation map, it was not possible to generate detailed information regarding the individuals' bronchial or segmental anatomy. In the future this may

be possible with the use of hyperpolarized Helium. The gas is inhaled during the image acquisition, acting as a contrast agent and allows clear views of the airways to be generated. This technique is in the early stages of development and requires some complicated equipment that is not widely available. So while this technique is promising it has yet to prove its value [106, 107]. Therefore, as a result of the poor definition of the current system, if any inferences were to be made regarding geographical distribution of the aerosol the SPECT data would need to be fitted to a standard model rather the specific anatomy of the individual.

The segmental model had been developed by taking measurements from a cast taken from the airways of a cadaver [96]. This is not ideal. While the anatomy will reflect the branching tree of the cadaver, there will have been changes after death and so the dynamic and flexible nature of the human airways in health will not be presented. There is also no way of knowing what the position of the cadaver was in when the cast was taken. One would assume that it was in a supine position. As we have already stated that posture will affect the airway structure in health and it would not be unreasonable to assume that similar processes will occur with the cadaveric lung. As such there may be an inherent errors in this model.

The SPECT data was "stretched" to fit the model in a similar manner to the construction of the shell analysis with each voxel being assigned a position in x, y and z planes relative to the hilum but instead of being allocated to a shell, each voxel was assigned to a lung segment according to the model of the anatomy as described. So while this did not reflect the true anatomy of the subject, it was more representative of the geographical distribution and moved away from the central to peripheral concept.

Despite the assumptions made by this approach to the data, it revealed wider variations in the distribution of the aerosol. These results underline the non-homogeneous nature of the lung with "hot" and "cold" spots that are more in keeping with the

tomographic data that was demonstrated in figure 3.4.2. This would not have been possible with the 2D planar imaging. Taking the sitting position as the control to which the others are compared there is a tendency towards a higher activity concentration in the lower lobes. But within these there are segments that produce a higher concentration of activity. For example, within the right upper lobe, the apical segment has one of the highest activity concentrations where as the anterior and posterior segments have comparatively much lower concentrations. The result is that when combined together to form the upper lobe the overall concentration is lower. This raises the question of why a segment in the upper portion of the lung would receive such a high proportion of the aerosol? This would appear to be contrary to the principals of compliance and its effect on ventilation discussed in chapter 1.

So how can the changes in activity concentration that occur with changes in posture be explained? It is probably easiest to review the effect of changes in posture by examining the changes in activity concentration in entire lobes initially rather than isolated segments. While the segments may suggest interesting trends, their smaller volume produces a larger potential for error. Focusing on the lobes reduces this. The most striking comparison is between the sitting position and the right side lying position. Here all the lobes of the right lung on becoming dependent show an increase in activity concentration where as the lobes of the left lung demonstrate a corresponding drop in activity. These results achieve significance with p values ranging from 0.034 to ‹0.001 and so support the original hypothesis.

Interestingly, an examination of the changes in deposition within the lung segments reveal that this is not a simple process. The right apical superior segment or the right lower lobe provides a good example. In the sitting posture it is comparatively non-dependent being located at to the posterior aspect of the lungs at the top of the lower lobe. If the principals of lung compliance and ventilation were rigidly applied, on moving to the supine position

this segment would become dependent and so the activity concentration should rise. In reality there was no significant change (p=0.551) whereas the comparison of the same segment between sitting and side lying was highly significant (‹0.001). How can this be explained?

These findings would support the concept of ventilation and thus deposition being determined by a variety of factors. The architecture of the airways will significantly influence the ventilation and deposition pattern with the deposition being enhanced where airways branch, at the dividing spur of the airway and on the inner sides of the daughter airways [108]. This may provide some explanation of the geographical differences of deposition in one position but changes in posture are unlikely to change architecture of the large airways with their support cartilaginous rings. There may be some change in the small airways without this support but this cannot be confirmed by the imaging techniques currently available as they lack the appropriate level of resolution. So having suggested that there are limits to the effect that changes in compliance have on ventilation and thus deposition there are no alternative explanations which challenge the current thinking, which would suggest that the changes in pleural pressures and the shift in perfusion would change the lung compliance and hence the ventilation [109]. Based on the evidence presented in this thesis, there is no reason to challenge this thinking.

It is worth attempting to compare the results from this study to the mathematical models of aerosol deposition. This is not a simple task as the models rely on certain assumptions that do not necessarily match the conditions of this study and apply to the tidal volume, flow rates, background lung volumes, particle size and density and a simplification of the anatomy. Most models still use the symmetrical scheme of Weibel [20]. The data is also presented in a different manner with the use of deposition efficiency defined as the ratio of particles deposited in a particular zone to those that entered that zone and deposition fraction defined as the ratio of

particles deposited in a particular zone to the those entering the respiratory tract [110]. One must also assume that all the modelling work was performed with the subject in an upright position. It would be extremely interesting what results these models would produce with the subjects in the positions used in this observational study. The National Council on Radiological Protection and Measurement (NRCP [111] and the International Commission on Radiation Protection (ICRP) [112] produced two such models. These both divide the lung into regions such as the oropharynx, tracheo-bronchial or pulmonary regions. This is in part a result of the methods used to validate them, namely planar imaging, which lacks the resolution to discriminate between areas. While these models are widely accepted, they cannot easily be used as a comparison with this study.

There are, however, some models that do reflect this asymmetrical structure. Yeh and Schum [113] developed a five-lobe model with uneven compliance. More recently this work has been developed by the use of more accurate formulae for particle behaviour [114]. This produced some interesting results but detailed comparisons of the data sets are difficult because of the different forms of presentation of the data. Firstly the lung deposition fraction, which they calculated for particles of 2.6 μm, was 0.26 ±0.08. This compared well to other experimental data [115] but the mean figures from this study were considerably higher. The sitting posture produced a mean figure of 0.67 (SD 0.13) with supine and side lying both producing a figure of 0.75. This is a remarkably high figure.

The modelling data did show a higher deposition fraction in the lower lobes and hence greater deposition than the upper lobes, which agrees with the observed data from this study, but they also demonstrated the lowest level of deposition in the middle lobe. This was contrary to the finding of this work. In addition there was a lack of agreement between the modelled deposition per surface area and volume concentration data of the observed study. These are

very different measures, with surface area increasing dramatically in comparison to volume but one would expect the two data sets to demonstrate similar trends. They do not. The observed data gives the highest deposition in the lower lobes followed by the middle lobe and then the upper lobes. The modelled data suggests the highest deposition in the bronchi of the upper lobes with considerably lower deposition in the lower lobes and minimal deposition in the middle lobe. It is difficult to resolve these differences in the data sets and it is unclear whether they are in part a result variation in the means of presenting the data or if there are more fundamental differences.

As the image resolution improves with 3D techniques such as SPECT and Positron Emission Tomography (PET) gaining wider acceptance there will be greater opportunities to improve the mathematical models by comparison with observed data. This will add to the understanding of the processes that influence deposition, which will be of value in aerosol medicine and inhalation toxicology. This study will contribute to this process.

There is increasing interest in the use of the inhaled route to treat systemic disease that requires an improved understanding of what influences the distribution of inhaled aerosols within the lung. Many challenges and unanswered questions remain in this field to enable the delivery of a consistent dose to the relevant part of the lung to give effective treatment regardless of the technique of the patient or the condition in which they inhale. Posture may have a role to play in this process to enable to drug to be delivered to the areas of maximum perfusion but is more likely that the delivery systems will have more influence in this field.

Having demonstrated that posture influences the deposition of aerosols in health, the next obvious step is to see if this effect extends into disease states. There is a large population of patients with chronic respiratory diseases who are dependent on their inhaled medication. Improving the understanding of the influence of airflow obstruction, be it the result of bronchospasm or sputum

and airflow restriction can only improve drug delivery. If the efficiency were improved a similar clinical effect might be observed with a smaller dose of active agent. Primarily this would be better for the patient but with the increasing use of expensive agents, there may be cost benefits. Alternatively, if changes in posture can influence deposition it may be possible to target specific lungs or regions with active agent. Two potential cases are the use of inhaled topical chemotherapy agents to directly treat alveolar cell carcinoma or the delivery of cyclosporine to lung transplant patients, particularly those with single lung transplants.

Treatment using conventional chemotherapy agents, particularly cytotoxic drugs, is a balance between achieving an effective dose but minimising the damage to surrounding tissue and unpleasant side effects. A recent review [116] demonstrated that these agents could be safely delivered to the lung and improve the clinical outcome. If the aim of using the inhaled route is to reduce the total dose of agent delivered to the patient and maintain efficacy, then the use of targeting specific regions of the lung by the use of posture would seem a logical progression of this thinking maintaining the dose to one region of the lung where the agent is required and reducing it elsewhere.

Cyclosporin is the treatment of choice for the treatment of organ rejection after transplant. Its use as an inhaled agent was summarised well by Burckart *et al* [117] in the treatment of lung allograft rejection. Essentially, as an immunosupressant, it slows the inflammatory process that leads to organ failure but this is not without side effects as cyclosporine is hepatic and renal toxic. Topical treatment reduces these side effects and while maintaining efficacy. Further focusing this treatment on to the in the case of single lung transplant would intuitively make sense.

In conclusion, in this small population of healthy male subjects, the posture in which they inhaled an aerosol had an effect on its the final destination within the lung. While this work was carried out in a disease free population, there may be some

implications for drug delivery to the lungs, be it for topical treatment or delivery of systemically active agents. With an improved understanding of the behaviour of aerosols in the lung, it may be possible to target specific segments, lobes or whole lungs for topical treatment as opposed to assuming an even distribution throughout the lung fields. These changes in deposition are consistent with the current understanding of the distribution of ventilation within the lung. Indeed, this is the first time that these changes with posture have been demonstrated by imaging in three dimensions.

Abbreviations

ANOVA	Analysis of Variance
ARSAC	Administration of Radioactive Substances Advisory Committee
COPD	Chronic Obstructive Pulmonary Disease
CT	Computed Tomography
DPI	Dry Powder Inhaler
FEV_1	Forced Expiratory Volume in 1 second
FRC	Functional Residual Volume
FVC	Forced Vital Capacity
GSD	Geometric Standard Deviation
HSA	Human Serum Albumin
I:E	Inspiratory to Expiratory Ratio
ICRP	International Commission on Radiological Protection
l	Litres
MBq	Mega Becquerels
MDI	Metered Dose Inhaler
Min	Minute
MEF_{25}	Maximal Expiratory Flow at 25 % of lung volume
MEF_{50}	Maximal Expiratory Flow at 50 % of lung volume
MMAD	Mass Median Aerodynamic Diameter
MMD	Mass Median Diameter
MRI	Magnetic Resonance Imaging
NRCPM	National Council on Radiation Protection and Measurement
PI	Penetration Index
Re	Reynolds Number
ROI	Regions of Interest
RV	Residual Volume
SD	Standard Deviation
SPECT	Single Photon Emission Computer Tomography
TLC	Total Lung Capacity
V/Q	Ventilation to Perfusion ratio

Glossary

Aerosol

An aerosol is a dispersion of fine solid particles or liquid droplets in a gas. These are produced both in nature and by man intentionally and incidentally and have a wide range of particle sizes from 0.001μm to 100μm although 5 μm or less is the particle size used for drug delivery to the lungs [34].

Attenuation

The reduction in the number of primary photons in a beam of radiation. This is caused by the absorption and scattering of the primary photons [81].

Computed Tomography (CT)

A CT machine consists of an X-ray source and an array of detectors that surround the patient. An X-ray source rotates around the patient and the resulting attenuated beam is measured by the detectors. The signals from the detectors are used to construct an image by a mathematical technique. The reconstructed images are transverse (axial) cross-sections of the patient and are viewed as if from the feet of the patient. It has the disadvantage of relatively high cost and the increased radiation exposure [118].

Gamma Rays

Electromagnetic radiation emitted from a nuclide as it decays to a more stable lower energy state are described as gamma rays [81]

Isotope.

Elements or atoms with the same atomic number but different atomic weights [81].

Lung Compliance

This refers to the distensibility of the lungs and results from the interaction of the respiratory muscles and chest wall pulling outwards by generating a negative pleural presure against the inward force of the elastic tissue within the lung and the surface tension at the air tissue interface.

Magnetic Resonance Imaging

A magnetic resonance image is obtained by placing an individual in a strong magnetic field that polarizes some of the hydrogen protons in the body so that they have the same alignment. The application of radiofrequency wave pulses of specified lengths and repetition (pulse sequences) displaces the protons, and some of this transmitted energy is absorbed by them. With the cessation of the radiofrequency pulse, the protons return to their initial alignment and in so doing they emit, as a weak signal, some of the energy that they have absorbed; this signal is received, amplified and handled in digital form, and subsequently reconstructed into an image [118].

Radioactivity

Atomic nuclei are composed of protons and neutrons and there are some combinations of which are not stable. Stability is achieved by the conversion of a neutron to a proton or vice versa. When this occurs there is an emission of energy and it is this process of transformation that is referred to as radioactive decay. The SI unit for radioactivity is the becquerel (Bq) and is defined as one disintegration per second [81].

Single Photon Emission Computed Tomography (SPECT)

SPECT is a form of imagining which results in three-dimensional data on the distribution of a radioisotope, by using rotating gamma cameras. A series of planar images are acquired at set angles around the subject. A backprojection is then

performed by the SPECT system's digital computer which results in the reconstructed images. The data can then be viewed tomographically in sagittal, coronal or transverse planes.

Voxel

A volume element of set dimensions in a three dimensional map of activity.

References

1. Dalby, R.N., Hickey, A.J. and Tiano, S.L.,, *Medical devices for the delivery of therapeutic aerosols to the lungs.*, in *Inhalation aerosols. Physical and Biological Basis for Therapy*, A.J. Hickey, Editor. 1996, Marcel Dekker: New York. p. 441-473.
2. Hubbard, R.C., *Alpha-1 Antitrypsin*, in *Inhalational Delivery of Therapeutic Peptides and Protiens*, A.L.a.G. Adjei, P.K., Editor. 1997, Marcel Dekker: New York. p. 315-329.
3. Snell, N.J. and D. Ganderton, *Assessing lung deposition of inhaled medications. Consensus statement from a workshop of the British Association for Lung Research, held at the Institute of Biology, London, U.K. on 17 April 1998.* Respir Med, 1999. **93**(2): p. 123-33.
4. Smaldone, G.C., *Radionuclide Scanning, Respiratory Physiology and Pharmacokinetics.* Journal of Aerosol Medicne, 2001. **14**(2): p. 135 - 137.
5. Ewart, W., *The treatment of bronchiectasis and of chronic bronchial affections by posture and respiratory exercise.* Lancet, 1901. **2**: p. 70-2.
6. Chopra, S.K., et al., *Effects of hydration and physical therapy on tracheal transport velocity.* Am Rev Respir Dis, 1977. **115**(6): p. 1009-14.
7. Jenkins SC, S.S., Moxam J., *The effect of posture in lung volumes in normal subjects and in patients pre- and post-coranary artery surgery.* Physiotherapy, 1988. **74**: p. 492-496.
8. Hurewitz, A.N., H. Susskind, and W.H. Harold, *Obesity alters regional ventilation in lateral decubitus position.* J Appl Physiol, 1985. **59**(3): p. 774-83.

9. Hofmann, W., *Modeling techniques for inhaled particle deposition: the state of the art.* J Aerosol Med, 1996. **9**(3): p. 369-88.
10. Balashazy, I. and W. Hofmann, *Quantification of local deposition patterns of inhaled radon decay products in human bronchial airway bifurcations.* Health Phys, 2000. **78**(2): p. 147-58.
11. Martonen, T.B., *Deposition patterns of cigarette smoke in human airways.* Am Ind Hyg Assoc J, 1992. **53**(1): p. 6-18.
12. Myojo, T. and M. Takaya, *Estimation of fibrous aerosol deposition in upper bronchi based on experimental data with model bifurcation.* Ind Health, 2001. **39**(2): p. 141-9.
13. Zhang, L., B. Asgharian, and S. Anjilvel, *Inertial and interceptional deposition of fibers in a bifurcating airway.* J Aerosol Med, 1996. **9**(3): p. 419-30.
14. Toogood, J.H., et al., *Bioequivalent doses of budesonide and prednisone in moderate and severe asthma.* J Allergy Clin Immunol, 1989. **84**(5 Pt 1): p. 688-700.
15. *The effect of intensive treatmentof diabetes on the development and progression of long term complications in insulin dependant diabetes.The Diabetic Control and Complications Trial Group.* New England Joulrnal of Medicine, 1993. **329**(14): p. 977- 986.
16. Laube, B.L., Georgopoulos, A., Adams, G.K.III,, *Preliminary study of the efficacy of insulin aerosol delivered by oral inhalation in diabetic patients.* J A M A, 1993. **269**: p. 2106-2109.
17. Farr, S.J.a.T., G., *Insulin Inhalation. Its Potential as a Nonparenteral Method of Administration*, in *Inhalation Delivery of Therapeutic Peptides and Protiens*, A.L.a.G. Adjei, P.K., Editor. 1997, Marcel Dekker: New York.
18. Weibel, E.R., *Morphometry of the Human Lung*. 1963, Heidelberg: Springer- Verlag.
19. Reid, L., *Visceral cartilage.* J Anat, 1976. **122**(2): p. 349-55.

20. Schreider, J.P. and O.G. Raabe, *Structure of the human respiratory acinus.* Am J Anat, 1981. **162**(3): p. 221-32.
21. Engel, L.A., *Gas mixing within the acinus of the lung.* J Appl Physiol, 1983. **54**(3): p. 609-18.
22. Leith, D.E., *Cough.* Physical Therapy, 1968. **48**: p. 439 - 447.
23. Sleigh, M.A., J.R. Blake, and N. Liron, *The propulsion of mucus by cilia.* Am Rev Respir Dis, 1988. **137**(3): p. 726-41.
24. Morrow, P.E., *Clearance kinetics of inhaled particles*, in *Respiratory Defence Mechanisms*, J.D. Brain, Proctor, D.F. and Reid, L.M., Editor. 1977, Marcel Dekker: New York. p. 491 - 543.
25. Ultman, J.S., *Gas Transport in the Conducting Airways*, in *Gas mixing and Distribution in the Lung*, A.E.a.P. Engle, M., Editor. 1985, Marcel Dekker: New York. p. 63-136.
26. Simone, A.F. and J.S. Ultman, *Longitudinal mixing of oxygen with air during steady flow through the larynx.* Bull Eur Physiopathol Respir, 1982. **18**(2): p. 389-93.
27. Dekker, E., *Transition between laminar and turbulent flow in the human trachea.* J Appl Physiol, 1961. **22**: p. 1060-1064.
28. Tsuda, A., Y. Otani, and J.P. Butler, *Acinar flow irreversibility caused by perturbations in reversible alveolar wall motion.* J Appl Physiol, 1999. **86**(3): p. 977-84.
29. Butler, J.P. and A. Tsuda, *Effect of convective stretching and folding on aerosol mixing deep in the lung, assessed by approximate entropy.* J Appl Physiol, 1997. **83**(3): p. 800-9.
30. Engel, L.A., et al., *Gas mixing during breath holding studied by intrapulmonary gas sampling.* J Appl Physiol, 1973. **35**(1): p. 9-17.
31. West, J., and Hugh-Jones, P., *Pulsatile gas flow in bronchi caused by the heart beat.* J Appl Physiol, 1961. **16**: p. 697-702.

32. Colbeck, I., *Introduction to Aerosol Science*, in *Physical and Chemical Properties of Aerosols*, I. Colbeck, Editor. 1998, Blackie Academic and Professional: London. p. 1-30.
33. Smith, J.a.J., ML., *Mathematical and graphical interpretation of the log-normal law for particle size distribution.* J Colloid Sci, 1964. **19**: p. 549-559.
34. Conway, J. *Nebuliser Design: Advances to Improve Therapy and Patient Acceptability.* in *Respiratory Drug Delivery VIII.* 2002. The Westin La Paloma, Tuscon, Arizona, USA: Amy Davis Biggs.
35. Nerbrink, O., M. Dahlback, and H.C. Hansson, *Why do medical nebulizers differ in their output and particle size characteristics?* J Aerosol Med, 1994. **7**(3): p. 259-76.
36. Phipps, P.R. and I. Gonda, *Evaporation of aqueous aerosols produced by jet nebulizers: effects on particle size and concentration of solution in the droplets.* J Aerosol Med, 1994. **7**(3): p. 239-58.
37. Martonen, T.B., and Yang, Y, *Depostition Mechanisms of Pharmaceutical Particles in Human Airways*, in *Inhalation Aerosols Physical and Biological Basis for Therapy*, A.J. Hickey, Editor. 1996, Marcel Dekker: New York.
38. Annapragada, A.V., Swanson, P.S. and Muzzio, F., *Biophysics of Inhaled Drug Particles*, in *Inhalation Delivery of Therapeutic Peptides and Protiens*, A.L.a.G. Adjei, P.K., Editor. 1997, Marcel Dekker, Inc.: New York. p. 27-58.
39. Gerrity, T.R., *Pathophysiological and disease constraints on aerosol delivery.*, in *Respiratory drug delivery*, P.R. Byron, Editor. 1990, CRC Press inc: Boca Raton, Florida, USA. p. 1-38.
40. Love, R.G. and D.C. Muir, *Aerosol deposition and airway obstruction.* Am Rev Respir Dis, 1976. **114**(5): p. 891-7.
41. Tsuda, A., et al., *Aerosol transport and deposition in the rhythmically expanding pulmonary acinus.* J Aerosol Med, 1996. **9**(3): p. 389-408.

42. Tsuda, A., J.P. Butler, and J.J. Fredberg, *Effects of alveolated duct structure on aerosol kinetics. I. Diffusional deposition in the absence of gravity.* J Appl Physiol, 1994. **76**(6): p. 2497-509.
43. Waller, R., *Non-Biological Particles and Health*, C.o.t.M.E.o.A. Pollutants, Editor. 1995, HMSO.
44. Bisgaard, H., Anhoj, J., and Wildhaber, J.H., *Spacer Devices*, in *Drug Delivery to the Lung*, H. Bisgaard, O'Callaghan, C., and Smaldone, G., Editor. 2002, Marcel Dekker: New York.
45. Hickey, A.J. and T.B. Martonen, *Behavior of hygroscopic pharmaceutical aerosols and the influence of hydrophobic additives.* Pharm Res, 1993. **10**(1): p. 1-7.
46. Morrow, P.E., *Factors determining hygroscopic aerosol deposition in airways.* Physiol Rev, 1986. **66**(2): p. 330-76.
47. Phipps, P.R., et al., *Regional deposition of saline aerosols of different tonicities in normal and asthmatic subjects.* Eur Respir J, 1994. **7**(8): p. 1474-82.
48. Chan, H.K., et al., *Regional deposition of nebulized hypodense nonisotonic solutions in the human respiratory tract.* Eur Respir J, 1994. **7**(8): p. 1483-9.
49. Laube, B.L., et al., *The effect of inspiratory flow rate regulation on nebulizer output and on human airway response to methacholine aerosol.* J Allergy Clin Immunol, 1985. **76**(5): p. 708-13.
50. Anderson, M., Svartengren, M., Philipson, K., Camner, P., *Deposition in man of particles inhaled in air or helium-oxygen mixture at different flow rates.* J. Aerosol Med, 1990. **3**: p. 209-216.
51. Newman, S.P., Pavia, D., Moren, F., and Clarke, S.W., *Improving the bronchial deposition of pressurised aerosols.* Chest, 1981. **80 (Suppl)**: p. 909-911.
52. Brown, J., Zeman, KL, Bennett, WD., *Regional deposition of coarse particles and ventilation distribution in healthy*

subjects and patients with cystic fibrosis. Journal of Aerosol Medicne, 2001. **14**(4): p. 443-454.

53. O'Riordan, T.G. and G.C. Smaldone, *Regional deposition and regional ventilation during inhalation of pentamidine.* Chest, 1994. **105**(2): p. 396-401.
54. Chan, H.K., et al., *Deposition of aqueous aerosol of technetium-99m diethylene triamine penta-acetic acid generated and delivered by a novel system (AERx) in healthy subjects.* Eur J Nucl Med, 1999. **26**(4): p. 320-7.
55. Kim, C.S., et al., *Enhanced aerosol deposition in the lung with mild airways obstruction.* Am Rev Respir Dis, 1989. **139**(2): p. 422-6.
56. Kim, C.S., et al., *Persistence of enhanced aerosol deposition in the lung after recovery from carbachol-induced airway obstruction.* J Appl Physiol, 1990. **69**(6): p. 2104-12.
57. Yanai, M., et al., *Deposition and clearance of inhaled 18FDG powder in patients with chronic obstructive pulmonary disease.* Eur Respir J, 1998. **11**(6): p. 1342-8.
58. Kim, C.S. and M.A. Eldridge, *Aerosol deposition in the airway model with excessive mucus secretions.* J Appl Physiol, 1985. **59**(6): p. 1766-72.
59. Olseni, L., J. Palmer, and P. Wollmer, *Quantitative evaluation of aerosol deposition pattern in the lung in patients with chronic bronchitis.* Physiol Meas, 1994. **15**(1): p. 41-8.
60. Kim, C.S. and S.C. Hu, *Regional deposition of inhaled particles in human lungs: comparison between men and women.* J Appl Physiol, 1998. **84**(6): p. 1834-44.
61. O'Riordan, T.G., Smaldone, G. C., *Aerosols as Indicies of Regional Ventilation.* J Aerosol Med, 1994. **7**(2): p. 111 - 117.
62. Cabahug, C.J., et al., *Utility of technetium-99m-DTPA in determining regional ventilation.* J Nucl Med, 1996. **37**(2): p. 239-44.

63. Laube BL, B.G., Dobs AS., *Time to peak insulin level, relative bioavailability, and effect of site of deposition of nebulized insulin in patients with noninsulin-dependent diabetes mellitus.* J Aerosol Med, 1998. **11**(3): p. 153-73.

64. Conway, J.H., *The assesment of intra-pulmonary deposition of aerosols using multi-modality imaging*, in *Faculty of Medicine*. 1996, University of Southampton: Southampton.

65. Saari, S.M., et al., *Regional lung deposition and clearance of 99mTc-labeled beclomethasone- DLPC liposomes in mild and severe asthma.* Chest, 1998. **113**(6): p. 1573-9.

66. Denyer, J., and Nikander, K. *HaloLite - A novel liquid drug aerosol delivery system.* in *Drug Delivery to the Lungs VIII.* 1997. Church House Conference Centre, Westminster, London: The Aerosol Society.

67. Mullinger, B., Meyer, T., Sommerer, K., Weber, N., Beckmann, H., Bernhardt, T. and Scheuch, G. *Patient individualised inhalation optimises peripheral lung deposition.* in *Drug Delivery to the Lungs XII.* 2001. Church House Conference Centre, Westminster, London: The Aerosol Society.

68. Clark, A., *The use of laser diffraction for the evaluation of the aerosol clouds generated by medical nebulisers.* Int J Pharm., 1992. **115**: p. 69-78.

69. Dennis, J.H., *A review of issues relating to nebulizer standards.* J Aerosol Med, 1998. **11**(Suppl 1): p. S73-9.

70. Kwong, W.T., S.L. Ho, and A.L. Coates, *Comparison of nebulized particle size distribution with Malvern laser diffraction analyzer versus Andersen cascade impactor and low-flow Marple personal cascade impactor.* J Aerosol Med, 2000. **13**(4): p. 303-14.

71. Agnew, J.E., et al., *Radionuclide demonstration of ventilatory abnormalities in mild asthma.* Clin Sci (Colch), 1984. **66**(5): p. 525-31.

72. Ryan, G., et al., *Standardization of inhalation provocation tests: influence of nebulizer output, particle size, and method of inhalation.* J Allergy Clin Immunol, 1981. **67**(2): p. 156-61.
73. L. Pan, G.H., H. Nomura, V. Matkovich, *Filtration Properties of Pall Breathing Circuit Filters (Models BB50T, HME-15-22M, and BB25A).* 1995, Pall Technical Report.
74. Perring, S., et al., *A new method of quantification of the pulmonary regional distribution of aerosols using combined CT and SPECT and its application to nedocromil sodium administered by metered dose inhaler.* Br J Radiol, 1994. **67**(793): p. 46-53.
75. Fleming, J.S., et al., *Three-dimensional description of pulmonary deposition of inhaled aerosol using data from multimodality imaging.* J Nucl Med, 1996. **37**(5): p. 873-7.
76. Thomas, S.H., et al., *Variability in the measurement of nebulized aerosol deposition in man.* Clin Sci (Colch), 1991. **81**(6): p. 767-75.
77. Fleming, J.S., et al., *Assessment of deposition of inhaled aerosol in the respiratory tract of man using three-dimensional multimodality imaging and mathematical modeling.* J Aerosol Med, 1996. **9**(3): p. 317-27.
78. Bushberg, J.T., Seibert, J.A., Leidholdt, E.M., Boone, J.M., *The essential physics of medical imaging.* 1994, London: Williams and Wilkins.
79. Melchor, R., et al., *Lung deposition patterns of directly labelled salbutamol in normal subjects and in patients with reversible airflow obstruction.* Thorax, 1993. **48**(5): p. 506-11.
80. Baskin, M.I., A.G. Abd, and J.S. Ilowite, *Regional deposition of aerosolized pentamidine. Effects of body position and breathing pattern.* Ann Intern Med, 1990. **113**(9): p. 677-83.
81. O'Doherty, M., Thomas, S.H.L., Page, C., Clark, A.R., Mitchell, D., Heduan., Nunan, T.O., and Bateman, N.T., *Does 99mTc human serum albumin alter the charecteristics*

of nebulised pentamidine isethionate? Nucl Med Commun, 1989. **10**: p. 523-529.

82. Cotes, J.E., *Assesment of the bellows and mechanical attributes of the lung*, in *Lung Function assesment and application to medicine*. 1993, Blackwell Scientific publications: Oxford. p. 131-179.
83. Quanjer, P.H., et al., *Lung volumes and forced ventilatory flows. Report Working Party Standardization of Lung Function Tests, European Community for Steel and Coal. Official Statement of the European Respiratory Society.* Eur Respir J Suppl, 1993. **16**: p. 5-40.
84. Peat, J.K., C.M. Salome, and A.J. Woolcock, *Longitudinal changes in atopy during a 4-year period: relation to bronchial hyperresponsiveness and respiratory symptoms in a population sample of Australian schoolchildren.* J Allergy Clin Immunol, 1990. **85**(1 Pt 1): p. 65-74.
85. Forge, N.I., P.J. Mountford, and M.J. O'Doherty, *Quantification of technetium-99m lung radioactivity from planar images.* Eur J Nucl Med, 1993. **20**(1): p. 10-5.
86. Fleming, J.S., *A technique for the absolute measurement of activity using a gamma camera and computer.* Phys Med Biol, 1979. **24**(1): p. 176-80.
87. Fleming, J.S., *Technique for the use of standard outlines for attenuation correction and quantification in SPECT.* Nucl Med Commun, 1990. **11**(10): p. 685-96.
88. Fleming, J.S., Britten, A.J., and Perring, S., *A general software package for the handling of medical images.* J Med Eng Technol, 1991. **15**: p. 162-169.
89. Fleming, J.S., Conway, J.H., Bolt, L., Holgate, S.T., *A comparison of planar scintigraphy and SPECT measurement of total lung deposition of inhaled aerosol.* Journal of Aerosol Medicne, 2003. **16**(1): p. 9-19.
90. Fleming, J.S., Hashish, A.H., Conway, J.H., Hartley-Davies R, Nassim,, G. M.A., M.J., Coupe, J, Holgate, S.T., Moore,

E.A., Bailey, A.G.,, and T.B. Martonen, *A technique for simulating radionuclide images from the aerosol deposition pattern in the airway tree.* Journal of Aerosol Medicne, 1997. **10**(3): p. 199-212.

91. Sorenson, J.A.a.P., M.E., *Physicis in Nuclear Medicine.* 1980, London: Grune and Stratton. 32-49.
92. Fleming, J.S., *A technique for using CT images in attenuation correction and quantification in SPECT.* Nucl Med Commun, 1989. **10**(2): p. 83-97.
93. Fleming, J.S., Conway J.H., Bolt L., Quint, M., Salam, A.A. *Template Matching in Radionuclide Imaging of the Lung.* in *Medical Image Understanding and Analysis,.* 2002. University of Portsmouth.
94. K Friston, A.H., K Worsley, J Poline, C Frith, R Frackowiak R, *Statistical parametric maps in functional imaging.* Human Brain Mapping, 1995. **2**: p. 189-210.
95. Bland JM, A.D., *Statistical methods for assessing agreement between two methods of clinical measurement.* Lancet, 1986. **Feb 8;1(8476):**: p. 307-10.
96. Chamberlain, M., Morgan, WKC and Vinitski, S., *Factors influencing the regional deposition of inhaled particle in man.* Clin Sci (Colch), 1983. **64**: p. 69-78.
97. O'Callaghan, C. and P.W. Barry, *The science of nebulised drug delivery.* Thorax, 1997. **52 Suppl 2**: p. S31-44.
98. Alvine GF, R.P., Fitzsimmonds KM, Ahrens RC., *Disposable nebulisers. How reliable are they?* Chest, 1992. **101**: p. 316-319.
99. Steckel, H.a.E., F. *Factors affecting the mean droplet size during nebulisation.* in *Drug Delivery to the Lungs XIII.* 2002. Church House Conference Centre, Westminster, London.: The Aerosol Society.
100. Ono, T., Otsuka R., Kuroda T., Honda E., Sasaki T., *Effects of head and body position on two and three-dimensional*

configurations of the upper airway. J Dent Res, 2000. **79**(11): p. 1879-1884.

101. Fleming, J.S., Sauret, V., Conway, J.H., Holgate, S.T., Bailey, A.G., Martonen, T.B., *Evaluation of the accuracy and precision of lung aerosol deposition measurements from single photon emission tomography using simulation.* Journal of Aerosol Medicne, 2000. **13**(3): p. 187-98.
102. Kauczor HU, E.M., Kreitner KF, Nilgens H, Surkau R, Heil W, Hofmann D, Otten EW, Thelen M., *Imaging of the lungs using 3He MRI: preliminary clinical experience in 18 patients with and without lung disease.* J Magn Reson Imaging, 1997. **7**(3): p. 538-43.
103. Kauczor HU, H.A., Van Beek EJ., *Assessment of lung ventilation by MR imaging: current status and future perspectives.* Eur Radiol, 2002. **12**(8): p. 1962-70.
104. Martonen, T.B., Hofmann, W., Lowe, J.E., *Cigarette smoke and lung cancer.* Health Phys, 1987. **52**: p. 213-217.
105. West, J.B., *Respiratory Physiology, the essentials.* 6th ed. 1999, London: Lippincott Williams and Wilkins.
106. Swift, D., *Mathematical Aerosol deposition models*, in *Inhalation Aerosols,* A.J. Hickey, Editor. 1996, Marcel Dekker: New York. p. 51-78.
107. Phalan, R., Cuddihy, RG., Fisher, GL., Moss, OR., Schlesinger, RB., Swift, DL., Yeh, HC., *Main features of the proposed NRCP respiratory Tract model.* Rad Prot Dos, 1991. **38**: p. 179-184.
108. Bair, W., *Overview of ICRP respiratory tract model.* Rad Prot Dos, 1991. **38**: p. 147-152.
109. Yeh, H., Shum, GM., *Models of human lung airways and their application to inhaled particle deposition.* Bull Math Biol, 1980. **42**: p. 461-480.
110. Subramaniam, R.A., B., *Analysis of differances in the particle deposition in the human lung.* Inhalation Toxicology, 2003. **15**: p. 1-15.

111. Bennett, W.D., Messina, M.S., Smalldone, G.C., *Effect of exercise on deposition in a multipath model of the human lung.* Journal of Applied Physiology, 1985. **59**: p. 1046-1054.
112. Placke, M.E., Zimlich, W.C., Ding, J.Y., Westaway, D.J., Imondi, A.R. *Targeted aerosol therapy for the treatment of lung cancer.* in *Respiratory Drug Delivery VIII,*. 2002. Tuscon, Arizona.
113. Burckart, G.J., Keenan, R., Griffith, B.P., Iacono,, A.T., *Cyclosporine*, in *Inhalation of therapeutic peptides and protiens*, A.L.a.G. Adjei, P.K., Editor. 1997, Marcel Dekker: New York. p. 281-299.
114. Hansel, D., *Thoracic Imaging*, in *The Oxford Tesxtbook of Medicine*, D. Weatherall, Ledingham, JGG, and Warrel, DA., Editor. 1995, Oxford University Press: Oxford.